Tagging Efficiency Measurements at High Intensities

B. Sc. Thesis

Ulrika Forsberg
Division of Nuclear Physics
Department of Physics, Lund University

June 2010

Supervisor: Lennart Isaksson

Abstract

The Swedish National Laboratory MAX-lab contains a facility for production of bremsstrahlung photons for photonuclear experiments. A so called "tagging technique" allows for a determination of the energy of the individual photons via a spectrometric measurement of the energy of the corresponding electron. Some of these photons are lost in a collimation process. The fraction of photons in the collimated beam divided by the number of particles that are detected in the spectrometer is called the *tagging efficiency* and is used to determine the photon flux that impinges on the target, which is a parameter that is needed in order to determine absolute cross sections.

The tagging efficiency depends on various factors, such as radiator thickness, steering of the beam and collimator size, and is measured approximately once a day to make sure that the experimental setup does not change in time. The measurements are usually made at an intensity that is several orders of magnitude lower than during production runs, due to the fact that a detector has to be placed directly in the photon beam. It is assumed that the measured tagging efficiency is the same as the tagging efficiency at high intensities, but this has not been verified before for the upgraded facility that was built in 2005.

This thesis presents measurements of the tagging efficiency at various intensities at the new facility, showing that the tagging efficiency is independent of intensity and that there is no systematic error in measuring it at much lower intensities than under normal experimental conditions. The measurements at high intensities were done using lead absorbers that attenuated the photon beam. The experimental setup and the analysis of the data is presented. The tagging efficiency was found to be, within error bars, independent of the intensity over three orders of magnitude, ranging up to approximately 4% of full intensity.

Contents

1 Introduction **7**
- 1.1 Background . . . 7
- 1.2 Purpose and Method . . . 7
- 1.3 Structure of this Report . . . 8
- 1.4 Previous Measurements . . . 8

2 Experimental System for Nuclear Physics **9**
- 2.1 An Overview of MAX-lab . . . 9
- 2.2 Photonuclear Experiments at MAX-lab . . . 9
- 2.3 The Accelerator System . . . 11
- 2.4 MAX I used as a Stretcher Ring . . . 11
- 2.5 The Electron Beam and the Tagging Spectrometer . . . 13
- 2.6 The Photon Beam . . . 18
- 2.7 Photon Tagging . . . 19
- 2.8 Tagging Efficiency . . . 21
- 2.9 Ordinary Tagging Efficiency Measurements . . . 22

3 Experimental Setup **26**
- 3.1 Tagging Efficiency Measurements at High Intensities . . . 26
- 3.2 Lead Absorbers and Attenuation . . . 27
- 3.3 Choice of In-Beam Detector . . . 29
  - 3.3.1 Lead glass . . . 29
  - 3.3.2 HPGe detector surrounded by a NaI(Tl) detector . . . 30
  - 3.3.3 HPGe 2 . . . 31
  - 3.3.4 10"× 10" NaI(Tl) . . . 34
- 3.4 Electronics . . . 37
  - 3.4.1 Processing of signals from the detectors . . . 37
  - 3.4.2 Trigger system . . . 40
- 3.5 Performing the Experiment . . . 41
  - 3.5.1 Preparation of experiment . . . 41
  - 3.5.2 First set of measurements . . . 42
  - 3.5.3 Second set of measurements . . . 44

4 Data Analysis **46**
- 4.1 Raw Data . . . 46
  - 4.1.1 Energy spectra from the in-beam detector . . . 47

4.1.2 Timing information . . . 47
4.1.3 Number of events in the focal plane channels . . . 51
4.2 Extraction of the number of photons, N_γ . . . 53
4.2.1 Selection of prompt events . . . 53
4.2.2 Subtraction of random coincidences . . . 57
4.2.3 Choosing the energy interval . . . 62
4.2.4 Compensation for the attenuation . . . 65
4.2.5 Alternative method to find the number of photons . . . 68
4.3 Extraction of the Number of Counts in the Focal Plane Scalers, N_{fp} . . . 69
4.4 Calculation of Tagging Efficiencies . . . 73
4.5 Error Estimation . . . 73
4.6 Calculating the Average Tagging Efficiency . . . 74
4.7 Correction for Ghost Events . . . 76
4.8 Analysis of the Pb-glass Tagging Efficiency Measurements . . . 78

5 Results **82**

6 Summary and Conclusions **87**

A Attenuation Coefficients **91**

B Different Choices of Energy Region **93**

List of Abbreviations

HPGe	High Purity Germanium
NaI(Tl)	Sodium Iodide doped with Thallium
Pb-glass	Lead glass
FP,fp	Focal Plane
PMT	PhotoMultiplier Tube
TDC	Time-to-Digital Converter
QDC	Charge-to-Digital Converter
ADC	Analogue-to-Digital Converter
LINAC	LINear ACcelerator
SLED	Stanford Linear Accelerator Center Energy Doubler
NIM	Nuclear Instrument Module
VME	A computer hardware bus standard

Populärvetenskaplig sammanfattning

MAX-lab är ett svenskt nationellt laboratorium i Lund där forskning inom ett stort antal områden sker. Anläggningen består dels av två linjära accelerator som kan accelerera elektroner till nästan ljusets fart, dels av tre stora ringar som dessa elekroner kan fås att cirkulera i. Ett av användningsområdena för dessa elektroner är för produktion av högenergetiska fotoner, det vill säga ljus med väldigt kort våglängd, mycket kortare än ultraviolett ljus och alltså inte synligt för det mänskliga ögat.

De högenergetiska fotonerna har precis rätt våglångd för att kunna användas för att studera atomkärnors egenskaper. När en foton träffar en atomkärna påverkas kärnan, och genom att undersöka resultatet av kollisionen kan slutsatser dras om vad atomkärnan består av, vilka krafter som verkar mellan de ingående delarna och vilka egenskaper dessa krafter och partiklar har. Dessa experiment görs av kärnfotogruppen vid MAX-lab i samarbete med ett stort antal universitet runt om i världen.

För att kunna utföra denna forskning krävs inte bara tillgång till fotoner, utan också ett omfattande experimentellt system som är uppbyggt kring produktionen. Bland annat måste fotonerna kollimeras till en väldefinierad stråle. Detta görs genom att placera en cylinder av metall med ett hål i mitten framför produktionsstället. De fotoner som går igenom hålet kommer till experimentområdet och resten, som hade fel riktning, kommer att träffa kollimatorn och absorberas. Resultatet är en väldefinierad stråle av fotoner.

En viktig aspekt av experimentuppställningen är kunskapen om hur många fotoner som når experimentområdet. Detta är nödvändigt för att kunna beräkna tvärsnitten för de reaktioner som studeras, det vill säga sannolikheten för att de ska ske. För att kunna beräkna hur många fotoner som haft möjlighet att interagera med atomkärnorna, görs regelbundet mätningar av den så kallade "taggingeffektiviteten" hos systemet. Mätningen av denna faktor kan dock normalt inte göras vid så höga intensiteter på fotonstrålen som används vid experimenten. Detta beror på att en detektor måste placeras direkt i fotonstrålen, vilket skulle förstöra detektorn om intensiteten är hög. Istället mätes faktorn vid mycket låga intensiteter och antas vara densamma vid höga intensiteter.

I denna uppsats beskrivs hur detta antagandets riktighet har testats genom att dels utföra standardmätningar av taggingeffektiviteten och dels mätningar av densamma vid höga intensiteter. Mätningarna vid höga intensiteter gjordes med hjälp av att använda blyplattor som dämpade strålintensiteten innan fotonerna nådde experimentområdet.

Analys av mätningarna visar på att intensiteten inte påverkar taggingeffektiviteten. Inom de felmarginaler som finns är taggingeffektiviteten densamma över ett spann av strålintensiteter på mellan ungefär 0,001% och 4% av full intensitet. Slutsatsen är att

mätningar av taggingeffektiviteten kan göras vid låga intensiteter utan att introducera något stort systematiskt fel i experimenten som utförs vid kärnfysikanläggningen på MAX-lab.

Acknowledgments

First and foremost I would like to thank my supervisor Lennart for introducing me to the very interesting research in nuclear physics conducted at MAX-lab, for helping me out with everything and for being very patient. I would also like to express my gratitude to the rest of the nuclear physics group - Bent, Kurt, Kevin, Magnus and Jason - for always answering my questions and making me feel very welcome. Also the machine operators who provided me with beam for the experiments deserve lots of my gratitude, especially Anders Hansson who also helped me with the experimental setup during some long but very interesting evening and night shifts. I am also very grateful to Daniel Karlsson for his support and for his help with programming and proof-reading. Last but not least I would like to thank Luke Myers, whom I made the second set of measurements together with and who has helped me a lot throughout the analysis of the data.

Chapter 1

Introduction

1.1 Background

MAX-lab is a Swedish national laboratory situated in Lund. It is operated jointly by the Swedish Research Council and Lund University, and is shared by research groups from many different scientific areas. One of those is nuclear physics.

The main constituents of MAX-lab are three electron storage rings and an accelerator system. MAX I, the first ring that was built, can also be used as a stretcher ring. In this mode, it is used for generation of a continuous beam of highly energetic electrons. This electron beam is directed towards a metallic foil, which causes production of bremsstrahlung photons. Those photons are used for probing the structure of nuclei in various photonuclear experiments.

The bremsstrahlung comes out from the foil in the shape of a cone and only some fraction of it passes through a collimator placed after the foil. This fraction is related to the so called tagging efficiency which is important when, for example, absolute cross sections for nuclear reactions are to be determined.

The tagging efficiency can not, however, be determined once and for all. It changes with the setup and may also change from time to time during an experiment due to e.g. different steering of the beam or drifts in the power supplies. Therefore, the tagging efficiency is usually measured every day during the course of an experiment.

To determine the tagging efficiency, a straightforward method is used. A detector for ionizing radiation is placed directly in the photon beam that comes out of the collimator and counts the number of photons. The problem is that if the intensity of the beam would be as high as during an ordinary experimental run, the detector would be ruined. Therefore the tagging efficiency is measured at very low intensities, and is then assumed to be the same at higher intensities. Some investigations ([2, 4]) indicate that this should be the case, but it has never before been verified for the upgraded accelerator system that was installed at MAX-lab in 2005.

1.2 Purpose and Method

To make sure there is no methodological error connected with measuring the tagging efficiency at low intensities, the assumption about the independence of the tagging efficiency on the intensity needs to be tested properly.

This thesis presents the performance and analysis of measurements of the tagging efficiency at high intensities, and comparisons with measurements at low intensities, made in order to test the validity of the assumption.

The setup is basically the same as for ordinary tagging efficiency measurements. The difference is that lead disks are inserted before the detector but in a position where they should not be able to affect the tagging efficiency in any way. These lead "absorbers" will attenuate the beam by absorbing a known fraction of the photons. This will allow for a higher intensity to be used, still keeping the count rate in the detector at a reasonable level.

The measurement of the tagging efficiency at high intensities was performed twice. The first time was in the first week of the run period in May/June 2007. Due to some problems with the beam, it was not possible to make any reliable conclusions from the first measurement. Hence, a second measurement was done in September 2007.

1.3 Structure of this Report

In chapter 2, the experimental system that is used for research in nuclear physics at MAX-lab is described. Chapter 3 covers the experimental setup that was used to determine the tagging efficiency at high intensities - the basic idea, detectors, electronics and data acquisition system. Chapter 4 describes the data analysis. The results are presented in Chapter 5 together with the conclusions.

1.4 Previous Measurements

In the early 90s, before the upgraded accelerator system was installed at MAX-lab and the injector still consisted of a racetrack microtron instead of the current two linear accelerators, the dependence of the tagging efficiency on various factors was investigated by B.-E. Andersson [2]. Four different photon detectors were tested for measuring the tagging efficiency. Using a lead glass detector, the tagging efficiency was determined to be the same, within error bars, when the intensity was reduced by a factor of about 1000 from full intensity. To be able to approach full intensity, lead plates and a NaI(Tl) detector was used. The count rate in the NaI(Tl) detector was kept constant when up to three lead absorbers were inserted, and the tagging efficiency was determined for intensities of about 0.01, 0.1 and 1% of full intensity. No significant deviation in the tagging efficiency was found when the intensity was varied over these three orders of magnitude. The effect of different radiator foils on the tagging efficiency was also investigated.

Another investigation of the effect of the intensity on the tagging efficiency of the old system was done in 1995 by D. Häger [4]. Two different detectors were used for determination of the tagging efficiency - a lead glass and a NaI(Tl) detector. Lead absorbers were placed before the NaI(Tl) detector which made it possible to determine the tagging efficiency at several different intensities. The measurements showed good agreement and the systematic uncertainty introduced into the measured cross sections due to the tagging efficiency was determined to be less than 3%.

Chapter 2

Experimental System for Nuclear Physics at MAX-lab

2.1 An Overview of MAX-lab

The accelerator system at MAX-lab consists of two LINAC:s (linear accelerators) that can provide a pulsed beam of electrons with energies up to 500 MeV to the MAX II and MAX III rings and energies up to 250 MeV to MAX I. A schematic picture of the laboratory is shown in Figure 2.1.

MAX II is the largest ring and is used for production of synchrotron radiation. After injecting electrons into the orbit of the ring, the energy is ramped up to 1500 MeV using the synchrotron capabilities of the ring. The electrons are then stored for several hours. When the electrons are being bent through the ring, and also in special insertion devices with the purpose of making the electrons change directions rapidly, the electrons radiate a small fraction of their energy as synchrotron radiation. The radiation that is produced be MAX II ranges from infrared light ($\sim$0.1mm) to hard X-rays($\sim$0.01nm) [1]. This energy loss is compensated for by using accelerating cavities. MAX III is also designed for synchrotron radiation research and has been taken into use during 2009. The electron energy in this ring is 700 MeV.

MAX I can be operated as a synchrotron/storage ring just like the other two rings, but with an electron energy of 550 MeV. It can also be operated as a pulse stretcher. In this mode, the electrons from the LINAC:s that enter the MAX I ring in short bunches are captured in the ring and slowly extracted. This creates an almost continuous electron beam that is used for production of highly energetic bremsstrahlung (braking radiation), which is used for photonuclear experiments. Approximately 18 weeks of beamtime per year is devoted to nuclear physics.

2.2 Photonuclear Experiments at MAX-lab

In photonuclear experiments, photons are used for probing the structure of nuclei and nucleons. The basic idea is that photons that are incident on a material cause nuclear reactions to happen, and the particles that result from the reaction are observed. From this, conclusions about the properties of the nuclei can be drawn. Since the wavelength

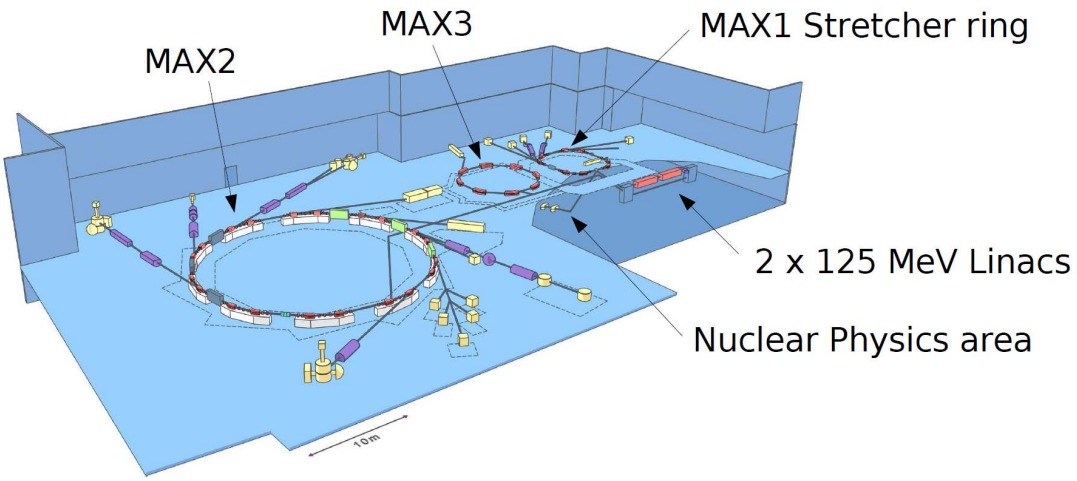

Figure 2.1: *An overview of MAX-lab showing the LINAC:s, the rings and the position of the nuclear physics area in the basement. Figure from [8].*

of the photon must be of the same order of magnitude as the structure that is being observed in order to cause a reaction, the energy of the photons has to be very high. Nuclear structures are on the order of 10^{-14} m which implies that the photon energies must be approximately $E = h \cdot f = \frac{hc}{\lambda} \approx 100$ MeV. Photons of these energies belong to the part of the electromagnetic spectrum referred to as gamma rays.

The synchrotron radiation produced by bending the electrons in storage rings, such as the MAX-rings, is not energetic enough to be used for photonuclear experiments and another approach must be used. When electrons are decelerated and possibly stopped, they can send out a much larger fraction of their energy through the bremsstrahlung process than is possible by bending them through the storage rings in order to get synchrotron radiation. This makes the bremsstrahlung process very suitable for photonuclear experiments.

A second requirement on the photon beam is the necessity of a continuous beam rather than the pulsed beam which is produced in the LINAC:s. The stretching of these pulses will improve the statistics of an experiment with several orders of magnitude [13], and therefore the electron bunches are stretched in MAX I to the desired continuous beam. The beam from MAX I is not entirely continuous, but has a duty factor of around 50%. Other important features of the experimental system for nuclear physics is the tagging technique which allows for a determination of the energy of the individual photons, and the collimation of the beam.

The available tagged photon energies currently range from about 15 MeV up to 190 MeV, with a possible future increase to over 200 MeV. Photons in this region can be used for studying many interesting phenomena. Examples are nuclear Compton scattering which can be used to deduce the polarizability of nucleons (see for example [12]) and pion production at threshold (see for example [3]), both of which can be used to test models for quantum chromodynamics.

The nuclear physics facility at MAX-lab will be described more thoroughly in the following sections.

2.3 The Accelerator System

The electrons are provided by a thermionic RF electron gun. The electrons are extracted from a glowing piece of BaO at 900℃ using an alternating high voltage that oscillates with a frequency of 2.998 GHz. This causes the electrons to come out in bunches with a period of $\sim\frac{1}{3\text{GHz}} = 0.33$ ns. The electric field in the gun also accelerates the electrons to approximately 1.8 MeV. At this energy, the electrons already have a speed that is close to the speed of light [6].

The electrons are transported in a pipe which is surrounded by strong electromagnets that steer the electrons that are of the right energy through the beamline. There are two 60° bending magnets that serve as an energy filter which removes the low energy "tail" of the electron bunches. There are also several quadrupoles and other magnets that are used to focus and steer the beam. By tuning the current in the magnets, the beam current can be optimised, but it can also be made to decrease, thus regulating the beam intensity when low intensity is wanted. The most common way of steering the beam away so that a fraction of it hits the wall of the beamline instead of passing through it, is to use the two 60° dipole magnets that constitute the energy filter. However, there are several other possibilities to lower the intensity.

To further increase the energy of the electrons after the gun, the electrons are accelerated in two LINAC:s that are powered by klystrons via SLED cavities, which make the klystron pulses shorter but more powerful [6]. In the LINAC:s, the power is used to create electric fields that oscillate with a frequency of 2.998 GHz (same as the for the gun). This causes the fields to vary in such a way that the electrons are accelerated in each cavity inside the LINAC:s. Due to the fact that the electrons do not increase their speed noticeably after the gun, the cavities which contain the accelerating electric fields are equidistant. Each LINAC is 5.2 meters and can increase the energy of the electrons with up to 125 MeV, so the upper limit is 250 MeV. For injections into MAXII and MAXIII, the electrons are recirculated through the LINAC:s, but this is not possible for injection into MAXI due to space limitations [5].

When MAXI is used as a pulse stretcher, the energy that is given by the LINAC:s determines the energy of the beam delivered to the nuclear physics area as no further energy increase takes place afterwards. The LINAC:s can be set to give beams of different energies, depending on the requirements of the experiment. Currently, the maximum energy that has been used during a nuclear physics experiment is slightly above 200 MeV.

The accelerator system, as well as the beamlines for the electrons, the rings and all other areas that the electrons pass are kept at a very low pressure, in order to minimise the loss of electrons due to particle collisions.

2.4 MAX I used as a Stretcher Ring

The pulses from the LINAC:s are about 100 ns long and one such pulse is injected into MAXI every 100 ms when it is used as a pulse stretcher. The circumference of the ring is 32.4 m, which corresponds to 108 ns orbit time for a particle that travels with the speed of light. The pulse fills the ring partly, and the fraction which is filled depends on a variety of factors. The current in the ring can be as high as about 30 mA in the ring.

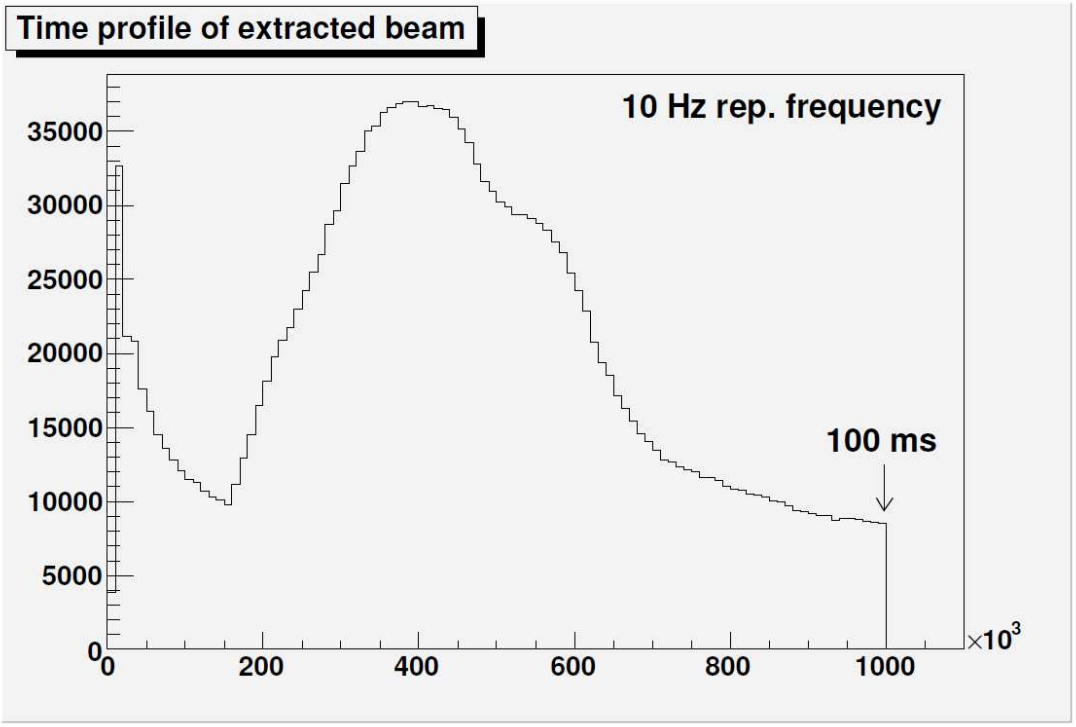

Figure 2.2: *The time profile of the extracted beam from MAXI. This is only the large-scale structure - there is also a micro-structure that is not seen on this scale. Also note that the first millisecond is inhibited. Figure from [8].*

The properties of the electrons that are captured in the ring do not depend on how they were directed or treated before the MAX I ring.

Pulses are injected into the beam via a septum magnet. An injection kicker, placed half a turn after the position for injection, gives the electrons a kick so that they end up in the right position in the ring and are captured in the orbit. There is also an accelerating cavity that bunches the electron beam and compensates for the energy losses by synchrotron radiation [11].

All the electrons in the ring follow slightly different paths, and by disturbing the electrons using a kicker magnet (also referred to as the "shaker"), the electrons will be driven toward the so called third betatron resonance. When the electrons reach this resonance, they will quickly divert from the ideal orbit. Special magnets will steer these electrons towards the extraction device, which presents both a magnetic and an electric field to those electrons that have left the closed orbit. These fields bends the diverting electrons into the beamline that leads to the nuclear physics area. The extraction is made continuous by slowly increasing the field in the shaker magnet over the 0.1s until the next pulse is injected. Those electrons that initially had relatively large deviations from the ideal orbit will reach the resonance early in the cycle, but others will need a stronger kick before they can be extracted [11].

The "large scale" time structure over one period (the time from when an electron bunch enters the ring until the next one does, 0.1s), is shown in Figure 2.2. The so called

duty factor is the fraction of time when there is beam, weighted with the instantaneous beam intensity. As will be explained later, the experimental setup requires a continuous beam rather than a pulsed one, and hence a high duty factor is of great importance. At MAX-lab, the duty factor of the stretched beam has been found to be somewhere around 40%. This is a very large improvement compared to the initial duty factor - $\frac{100[\text{ns}]}{100[\text{ms}]} = 10^{-6}\%$ - of the pulse from the injector.

What is not seen in Figure 2.2 is the very fine structure that arises from the ring not being completely filled with electrons. This results in a structure with electrons being extracted during the fraction of the circling time that the ring is filled, and then, during the pause where the ring is empty, basically no electrons are extracted.

What else is not seen is the sharp spike in the beginning of the cycle that consists of electrons that are not captured in the orbit of the ring but are extracted directly. This direct and unstretched electron beam is usually partly removed using an abort kicker. This is simply an electromagnet that gives a kick to the electrons that come out of the ring during the very first part of each cycle. This kick makes them hit the wall of the beamline and remove them from the beam that is delivered to the nuclear physics experimental area.

To avoid the background that is produced when the electrons hit the beamline, the data acquisition is inhibited for the first millisecond so that all events that occur during this period are ignored. It may seem like the inhibit makes the abort kicker unnecessary, but the direct beam would hit the target and cause a momentarily high count rate if the kicker had not been employed. This sudden, high intensity may cause problems such as baseline distortions in the detectors.

There is also a 2 ns time-structure in the beam that arises from the bunching of the injected pulse and a superimposed structure from the extraction shaker [8].

2.5 The Electron Beam and the Tagging Spectrometer

The stretched beam is transported in a beamline to the nuclear physics area in the basement of MAX-lab. The beam is bent into the horisontal plane by a 30° dipole bending magnet, and into the correct angle in this plane by a 50° dipole bending magnet. The bending through the 30° magnet, in which the magnetic field is accurately known, is used to assure that the energy is correct [10].

The electron beam is directed towards a radiator, which is a thin metal foil. Several radiators of different materials and thicknesses are available. Commonly, aluminum foils with thicknesses on the order of 100 μm are used. Some of the electrons that are incident on the foil, are slowed down and deflected by electromagnetic interactions, mainly with the nuclei in the target, and send out bremsstrahlung. The electrons are not slowed down equally, and most of them do not even interact at all if the foil is thin. This results in a continuous distribution of bremsstrahlung photon energies, ranging from zero (no photon) up to the energy of the incoming electrons. A bremsstrahlung spectrum is seen in Figure 2.3.

The energy of the photon is the energy of the incoming electron minus the energy of the decelerated electron;

$$E_{\text{electron, incoming}} = E_{\text{electron, outgoing}} + E_{photon} \tag{2.1}$$

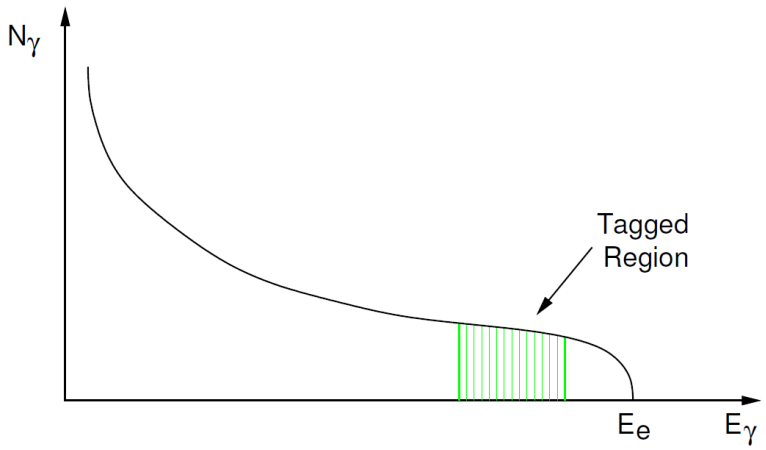

Figure 2.3: *Bremsstrahlung spectrum; the number of photons as a function of their energy. E_e denotes the energy of the incoming electrons, which is the highest energy the photons can have. An example of a "tagged" region, i.e. a region of the photons corresponding to electrons that are analysed in the spectrometer, is indicated in the figure. Picture from [8].*

The energy of the recoiling nucleus can be safely neglected for those electron energies that are of relevance for experiments at MAX-lab. For the very thin radiators that are used at the facility, it is also possible neglect the energy losses that the electrons suffer in the elastic scatterings that they undergo as they pass through the electromagnetic fields of the nuclei in the radiator [8].

Since the energy of the incoming electrons is well known, the photon energy can be determined by measuring the energy of the electron that emitted the gamma ray. This measurement is done in a tagging spectrometer, which is a large magnet that is placed after the radiator. The magnetic field is mainly of dipole character. The photons travel through this magnet unaffected, but the electrically charged electrons experience a force which makes them follow a curved path. There are two different tagger spectrometers available, and each has its own set of radiators. The Endpoint Tagger is used to analyse electrons that have very low energies (corresponding to photons that are close to the bremsstrahlung endpoint) and the Main Tagger is used for tagging photons that are further away from the bremsstrahlung endpoint. The Main Tagger allows for a larger span of electron energies to be analysed. The two tagger magnets are shown in Figure 2.4, and the Main Tagger is shown in Figure 2.5. The beam that does not interact with the radiator is bent into a shielded beamdump by the field in the Main Tagger and collected by a Faraday cup.

The energy of the electrons determines the radius of the path in a dipole field; $r = \frac{\gamma m v}{qB}$. Electrons that have lost much of their energy follow a path with a smaller radius than more energetic electrons. However, the electrons come out of the radiator in a cone, which means that even electrons with the same energy come out in different directions. Therefore, the magnetic field in the spectrometer magnet is constructed in such a way that it focuses all electrons with the same energy towards a horisontal line outside the magnet. This line is what is called the focal plane.

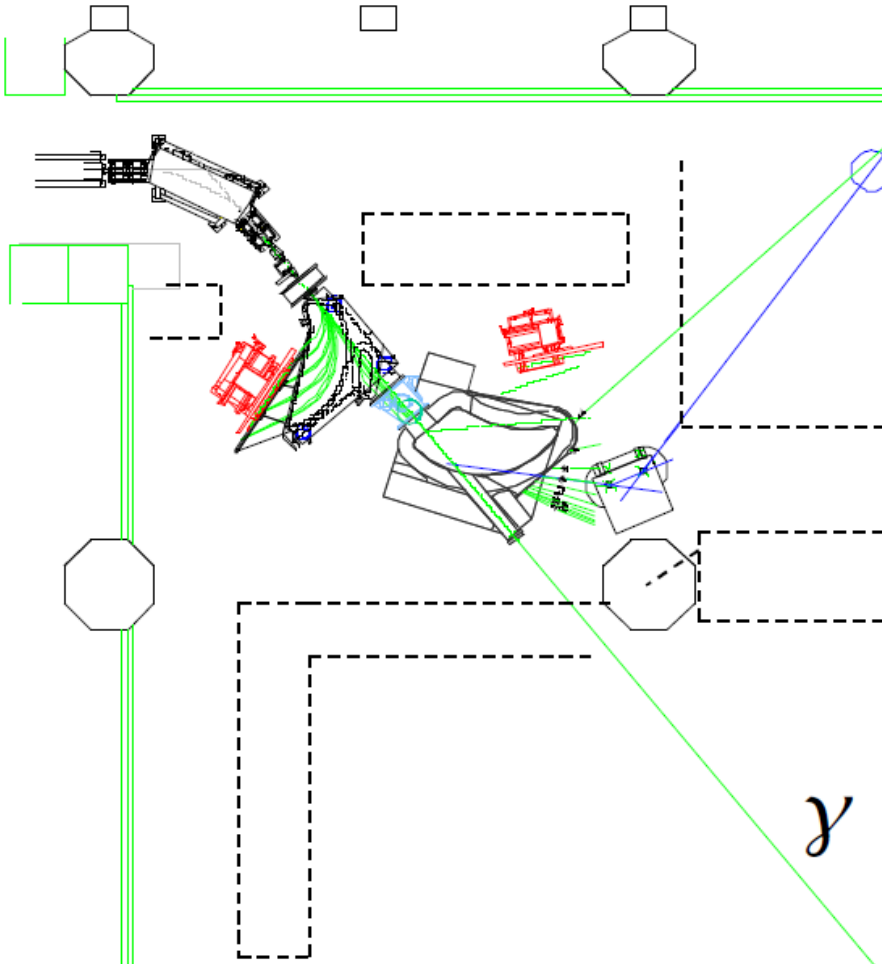

Figure 2.4: *The experimental area for nuclear physics. The beam comes in from the upper left corner of the figure, through the 50° bending magnet. If a radiator foil is placed before the Endpoint tagger, electrons that radiated a photon will be bent to the right in the Endpoint Tagger. The paths of the electrons are drawn in green, and the focal plane hodoscope is drawn in red. If the Main Tagger is used instead, there is no field in the Endpoint Tagger and the radiator foil is placed after it. The electrons are bent to the left through the Main tagger. The focal plane hodoscope is then moved to the position indicated in the figure. To safely dispose of the electrons that do not interact at all, they are directed towards a shielded beamdump that is common for both both tagger magnets. When the Endpoint Tagger is used, the Main Tagger still has a field which bends the electrons that did not interact with the radiator into this dump. The photons that are created continue ahead through the tagger magnets and reach the experimental area, in which the target and detectors are placed. The photons that do not cause any reactions in the target are dumped in a shielded photon beam dump. Picture from [8].*

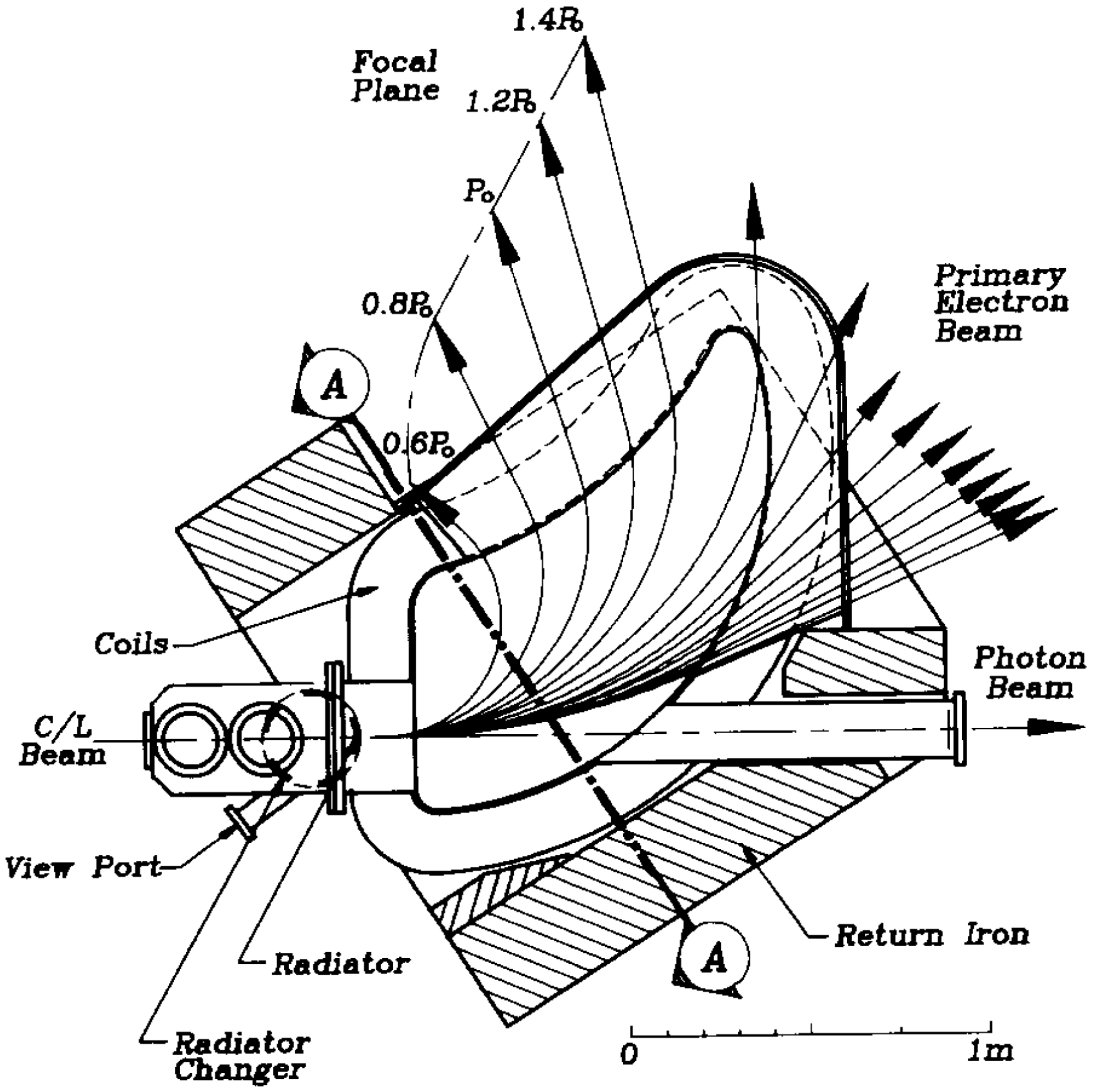

Figure 2.5: *Top view of the Main Tagger magnet. The electron beam comes in from the left and hits the radiator foil. The electrons that emit radiation are bent in the tagger magnet towards the focal plane. The field in the magnet is designed in a way that enables focusing on the focal plane. Figure from [20].*

Figure 2.6: *Photo showing the SAL hodoscope. The black sticks seen in the figure are the wrapped scintillators and light guides, and the metallic tubes contain the PMT:s. The exit of the tagger magnet is seen in the left part of the photo.*

To determine the path of the electrons through the tagger and hence their energy, a hodoscope is placed outside the tagger magnet along the focal plane. This is a detector array that is used to detect the position of the electrons coming from the tagger magnet. The hodoscope that is currently used at MAX-lab is the so called SAL hodoscope. It consists of two overlapping rows of scintillating sticks; 31 in one row and 32 in the other. Each scintillator is 25 mm wide, 50 mm long and 3.2 mm thick, and made of NE 110. The scintillators are connected via light guides to photomultiplier tubes (PMT:s) [20]. A picture of the hodoscope is shown in Figure 2.6 and a schematic view of the overlapping rows of detectors is shown in Figure 2.7. The two rows of detectors can be moved with respect to each other, and different overlaps can be chosen. A hit in two overlapping scintillators produces a signal that indicates the presence of an electron in the energy region defined by the overlap. The background is suppressed significantly by requiring a signal in two detectors.

The hodoscope can be moved along the focal plane. The energy region that it covers defines the "tagged region", and a photon that corresponds to an electron whose energy has been determined in the spectrometer is referred to as a "tagged" photon. By moving the hodoscope along the focal plane of either spectrometer, different tagged regions can be chosen. When the Main Tagger is used, the electrons reach the focal plane at an angle

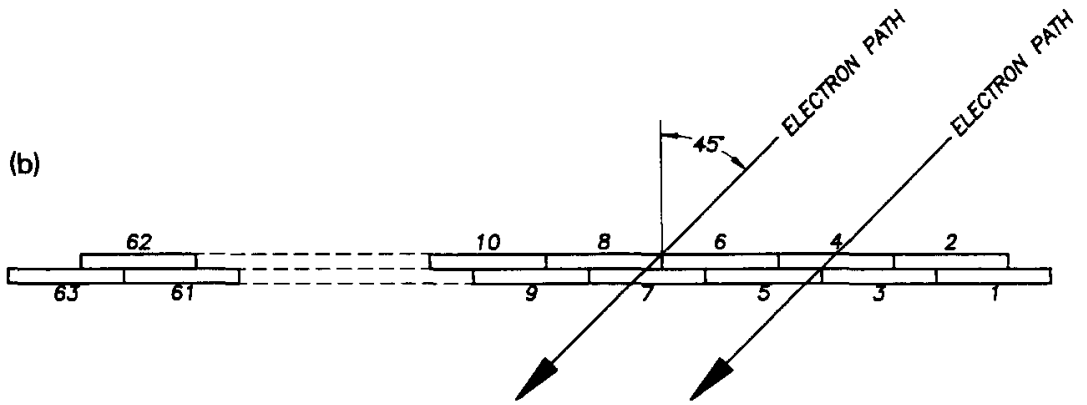

Figure 2.7: *Top view of the SAL hodoscope, which consists of two rows of overlapping scintillating sticks. When used together with the Main tagger, the electrons hit the focal plane at an angle of 45 °, and the overlap is set so that there are 62 channels of approximately the same widths. Figure from [20].*

of 45° and an overlap which gives channels that are approximately 0.5 MeV. However, all channels are not equally wide, as it is very difficult to get exactly the right overlap. Also, the same physical width of the overlap gives energy bins of different sizes depending on the energy. The channels that detect high-energy electrons cover a somewhat larger energy range than the channels that detect low-energy electrons. The magnitude of this effect depends on the tagger region and the tagger settings.

2.6 The Photon Beam

The bremsstrahlung photons are emitted by the decelerating electrons in a conical distribution in the forward direction. The opening angle of the cone depends on the energy of the incoming electrons. The angular distribution is also dependent on the radiator and the energy of the emitted photon and is described by a complicated formula given in, for example, reference [9]. The dependence of the photon energy is such that the higher the energy of the photon is, the more likely it is to be emitted at small angles, i.e. close to the beam axis [7]. An approximate formula for the opening angle of the cone is

$$\Theta_{\text{opening}} \approx \frac{1}{\gamma} = \frac{1}{\frac{E_e}{m_e c^2}} [\text{rad}] \tag{2.2}$$

where E_e is the energy of the incoming electron, m_e is the electron mass and γ is the gamma factor for the incoming electrons [3].

Other effects than the bremsstrahlung process that are relevant to take into account when describing the interaction of the electron beam with the radiator is the elastic multiple scattering and the production of Møller electrons, i.e. atomic electrons that are knocked out by the incoming electrons. However, according to [19], effects such as the energy loss of the electrons through elastic scatterings as well as absorption of photons in the radiator, are effects that can be safely neglected for those radiators thicknesses that

are commonly used. The effects of the multiple elastic scattering and Møller electrons on the experimental system will be discussed further in the next sections.

It is necessary to collimate the bremsstrahlung photons to a well-defined beam, as the target is positioned several meters from the radiator where the spread of the cone could otherwise be so large that some fraction of the photons in the beam would miss the target. Also, for some experiments where spatial resolution of the detection of the reaction products is of importance, the position of the collision must be well-defined. Assuming a beam energy of 150 MeV and a distance of 5 m from radiator to target, the diameter of the beam spot corresponding to the opening angle given by Eq. 2.2 would be approximately 3.4 cm.Therefore, a collimator is placed after the spectrometer magnet. The collimator insert can be changed, and during many experiments, collimators made of so called "heavimet" (a tungsten alloy), with hole diameters of 12 or 19 mm, are used. The collimators are approximately 15 cm long and are placed approximately 2 m from the radiator and are aligned with the beam axis. This means that only photons with a small angular distribution with respect to the beam axis will reach the experimental area, and the beam size will be limited.

Almost all photons that do not pass the hole but hit the collimator will interact with the material in some way. Many different particles are created in the electromagnetic showers that result from these processes, and to make sure that as few of these as possible hit the target, a strong magnet is placed downstream from the collimator. This magnet deflects the charged particles that are created in the collimator. Further downstream along the beam, a "scrubber" collimator is placed. This is a larger, fixed collimator that is aligned with the first one. The scrubber removes many of those particles that are created in the collimator.

What comes out of the scrubber is a well-defined beam of photons whose energies can be individually determined. The beam is then ready to be used for photonuclear experiments. A target is placed in the beam, and some fraction of the photons will interact with the nuclei in the material. The reaction products that are created in the various photonuclear reactions come out of the target and are detected by one or more detectors.

2.7 Photon Tagging

One very interesting property of the photons is, of course, their energy. They have an "energy tag" - the corresponding electron that has been analysed in the spectrometer - but the photon has to be associated to the correct electron. This is realised by using time coincidences. The time it takes for the electrons to travel through the spectrometer and to hit the focal plane detector is, for all practical purposes, the same for all electrons. The time it takes from the moment the photon is created to the detection of a reaction product is also the similar for events of the same type. This means that there is a correlation in time between the detection of the electron and the detection of an event caused by its corresponding photon, which can be used to correlate the photon to the right electron and hence determine the energy of the individual photons.

The tagging technique is presented schematically in Figure 2.8. When a reaction

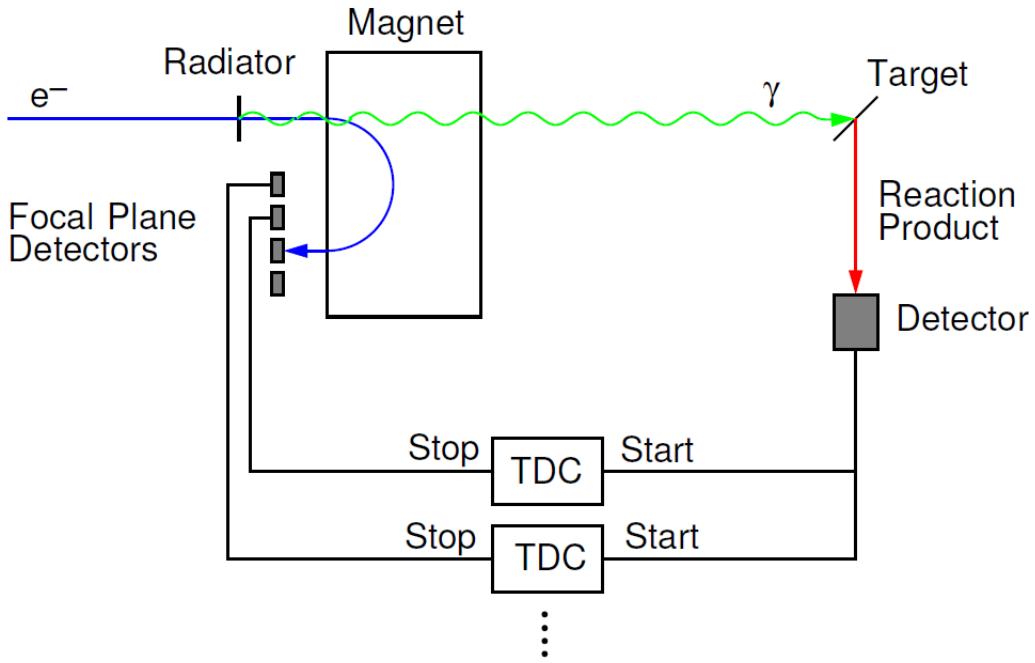

Figure 2.8: *The principle of tagging of bremsstrahlung photons. The photons are related to the correct electron using the timing. The TDC:s are started by the detection of a reaction product from a reaction induced by a photon. The TDC:s are stopped by the signals from the hodoscope. The electron that emitted the photon that caused a reaction in the target will arrive though the tagger magnet to the hodoscope within a certain time span, and hence, the correlation between the photon and the electron can be made. Figure from [8].*

product is detected, a start signal is sent to a set of TDC:s (time-to-digital converters; clocks). The TDC:s are stopped by signals from the detector channels in the hodoscope. The signals from the hodoscope are delayed using long cables in order to make them arrive after the start of the TDC:s. The reason for starting the TDC when a reaction product is detected and not whenever there is an electron in the hodoscope is, of course, that many photons do not react in, or even reach, the target. It would be unnecessary to start the system for photons that do not participate in the experiment, especially since it is not even possible to determine their energy unless they cause a reaction in the target.

Every detector in the focal plane hodoscope is connected to an individual TDC, but they are all started at the same time. If the TDC value from one of the focal plane channels (fp channels) is between certain limits (the so called prompt region) the start and stop signal can originate from a reacting photon and the electron that produced it, which enables a determination of the photon energy. However, there is a possibility that events that do not originate from an electron-photon pair happen to arrive within a time span that positions them in the prompt region. These events are referred to as random coincidences. This issue needs to be properly addressed in order to make it possible to use the tagging technique.

The need for a stretched beam instead of a pulsed one becomes apparent when these random coincidences are analysed. The number of events in the focal plane detectors is proportional to the instantaneous intensity of the beam, and the same holds for the number of events in the detectors in the experimental area. The chances for a random coincidence to happen is proportional to the product of the count rates of the reaction products and in the focal plane detector, respectively. Hence, the number of random coincidences increase as I^2 while the number of real, coincident events are directly related to the beam intensity, and go as I, where I is the instantaneous beam intensity. This means that the signal-to-noise ratio is proportional to $I/I^2 = 1/I$. A pulsed beam with a very high intensity in short intervals would yield very bad signal-to-noise ratios, and the intensity of the pulse would have to be small in order for the tagging technique to be applicable at all. This would give very little useful data, as no data is produced during the beam-off periods. A much better option is to use a stretched beam, which gives a continuous production of data, while still keeping the signal-to-noise ratio at a reasonable level.

2.8 Tagging Efficiency

Many photons do not even reach the experimental area since the beam is collimated. When total cross sections are to be measured, it is important to know how many photons that were incident on the target. This can be related to the number of particles that are detected in the hodoscope, which is an easily measurable quantity.

The tagging efficiency, ϵ_{tag}, is defined for each of the tagger channels as the fraction

$$\epsilon_{tag} = \frac{N_\gamma}{N_{fp}} \tag{2.3}$$

where N_{fp} is the number of events that are detected in the focal plane channel and N_γ is the number of photons of corresponding energies.

The tagging efficiency obviously depends on the diameter of the collimator and the spatial distribution of the photons. The general tendency of the dependence on energy is such that the tagging efficiency is higher for higher energies of the photons, since the opening angle of the cone is smaller for these photons which causes a larger fraction to pass though the collimator.

If the radiator had been infinitely thin and the electron beam would irradiate only a point of the radiator, the bremsstrahlung cone had been defined by Eq. 2.2 (approximately). However, the beam has a certain size which affects the tagging efficiency. Also, when the electrons traverse the foil, they will undergo elastic multiple scattering. This increases the angular spread of the electron beam itself, which affects the angular spread of the photons. The characteristic (root-mean-square) angle of the electrons after passing a radiator foil is described by the formula

$$\Theta_{\mathrm{rms}} = \frac{21}{E_e} \cdot \sqrt{\frac{t}{l_r}} [\mathrm{rad}] \tag{2.4}$$

where E_e is the energy of the incoming electron beam, t is the thickness of the radiator (in $\mathrm{g} \cdot \mathrm{cm}^{-2}$) and l_r is the radiation length of the radiator, given approximately by the formula

$$l_r = \frac{716A}{Z^2 \cdot ln(183Z^{-\frac{1}{3}})} [\mathrm{g} \cdot \mathrm{cm}^{-2}] \tag{2.5}$$

where Z is the atomic number of the material in the radiator [14]. A thick radiator will cause a larger spread of the electron beam, which means that the tagging efficiency will decrease with the thickness of the radiator.

Also Møller electrons, i.e. electrons that come out of the radiator as a result of atomic electrons being knocked out by the incoming electrons, affect the tagging efficiency since the process adds electrons that are counted in the hodoscope but do not produce any photons. The energy distribution of electrons that result from Møller scattering depends on the particular tagged region and and can also vary within it, which means that the magnitude of the effect of Møller scattering can differ over the focal plane channels. However, the process always lowers the tagging efficiency.

The probability for Møller scattering increases with the Z-value of the radiator (it basically follows the Bethe-Block formula), but the number of bremsstrahlung events increase as Z^2 [17], which means that for higher atomic numbers of the radiator, the relative importance of the Møller scattering is decreased.

2.9 Ordinary Tagging Efficiency Measurements

The tagging efficiency is usually measured once every day during the run periods. Normally, the measurements take approximately half an hour to perform. To determine the tagging efficiency one needs to measure the number of electrons that hit a certain channel in the focal plane detector array, and the total number of corresponding photons that come out of the collimator.

To count the number of tagged electrons, a scaler is connected to each hodoscope channel. A scaler is simply a counter that registers all signals from the detectors. To count the photons that pass through the collimator, a detector is placed directly after

it. The active area of the detector should cover the full area of the collimated beam. If the volume of the detector is large enough, virtually all photons will be absorbed.

The flux of photons is very high during the experiments, and to put a detector in the beam under these condition would not be possible, both due to pile-up problems and because the detector would be destroyed. The large deposit of energy could cause radiation damage to the detector material and the large current within any photomultiplier tube connected to such a detector would also cause damage. Hence, the intensity is reduced during the tagging efficiency measurements. The assumption usually made is that the measured tagging efficiency is the same as the tagging efficiency at high intensities, if a correction for the background in the room is made according to the following argument.

The particles that are detected in the focal plane channels can be separated into three parts:

1. Electrons that are associated with the production of a bremsstrahlung photon (N_{brems}). The rate at which these electrons are detected is proportional to the instantaneous beam intensity - $\dot{N}_{brems} = \alpha_{brems} \cdot I$

2. Other particles that are created by the beam ($N_{bcg,beam}$) such as Møller electrons that are created in the radiator, but also particles that are produced if the beam scrapes the walls of the beamline. The rate of this part is assumed to be proportional to the beam intensity. However, there is a possibility that an increased beam intensity could cause the beam to hit new places in the tagger etc., which could cause the number of beam-induced background events to be non-linear with the beam intensity. For this argument, however, it is assumed to be proportional to the beam intensity - $\dot{N}_{bcg,beam} = \alpha_{bcg,beam} \cdot I$

3. Background in the room which is not related to the beam intensity: $\dot{N}_{bcg,room} = \alpha_{bcg,room}$. This part consists of decays from the naturally occurring radioactive nuclei in the surrounding concrete and in the air, but also from the radioactivity that is induced by the irradiation. The very short-lived induced radioactivity will rather fit in the group of particles that has a detection rate which is proportional to the beam, but the nuclei that have long decay times should be associated with the constant background in the room. Those nuclei which, in this context, have intermediately long live-times, i.e. on the order of minutes, should also be considered being part of the background. The count rate that results from those events depends on the intensity, but is not proportional to it. Since the count rate varies with time after a change in the intensity has been done, it should preferably be measured both before and after any measurement that is done in conjunction with a change in intensity and that needs to be corrected for the background.

The number of bremsstrahlung photons is proportional to the beam intensity: $\dot{N}_\gamma = \alpha_{photons} \cdot I$. The in-beam detector also sees some background, but these events are not coincident with events in the focal plane. Therefore, they will not interfere with the measurement, as will be explained later.

The tagging efficiency as a function of the average intensity $\bar{I}$ is

$$\epsilon_{tag}(\bar{I}) = \frac{N_\gamma}{N_{fp}} = \frac{N_\gamma}{N_{brems} + N_{bcg,beam} + N_{bcg,room}} = \\ = \frac{\alpha_{photons} \cdot \int I dt}{(\alpha_{brems} + \alpha_{bcg,beam}) \int I dt + \alpha_{bcg,room} \int dt} = \\ = \frac{\alpha_{photons}}{\alpha_{brems} + \alpha_{bcg,beam} + \alpha_{bcg,room} \frac{\int dt}{\int I dt}} = \\ = \frac{\alpha_{photons}}{\alpha_{brems} + \alpha_{bcg,beam} + \frac{\alpha_{bcg,room}}{\bar{I}}} \tag{2.6}$$

At high intensities, the background in the room becomes negligible and the tagging efficiency is essentially

$$\epsilon_{tag} = \frac{\alpha_{photon}}{\alpha_{brems} + \alpha_{bcg,beam}}. \tag{2.7}$$

However, when measuring the fraction at low intensities, the background plays a larger role and needs to be taken into account and corrected for in order to get a value that corresponds to the actual tagging efficiency at high intensities.

To trigger the system during a tagging efficiency run, three different settings can be used. The option that is often chosen is to use the focal plane as the trigger. Then the spectra from the detector in the beam will contain a "pedestal" with events with zero energy, corresponding to those times when there is an electron hitting the focal plane, which produces a trigger which leads to the read-out of the modules, but no corresponding photon. The tagging efficiency can be then be calculated as the number of times when there is a photon detected in the in-beam detector divided by the total number of times the detector is read out. Another option is to use the in-beam detector as the trigger, or require a coincidence between the in-beam detectors and the focal plane.

There is no need to correct for the background counts in the in-beam detector, since they are not coincident with events in the focal plane. The in-beam events that are considered in the analysis of the data are always only those that are coincident with an event in the focal plane, and therefore the effect of the background is strongly suppressed. Some background events in the in-beam detector will be randomly correlated with events in the focal plane detectors, but the rates at which this happens is very small when the intensity is low. At higher intensities, the effect is larger and the background can start to be of importance, but this will be compensated for by a general subtraction of random events. Hence, the issue of background in the in-beam detector does not need to be addressed separately. The numbers of events that are recorded in the focal plane scalers, however, need to be corrected for the background because the scalers are counting continuously and independently of the triggers.

The deadtime of the system is another important thing that needs to be taken into account. During the time it takes for the system to read out the events from the detector in the beam, the scalers must be inhibited since there is no chance for a photon that originates from any of those electrons to initiate a reaction.

It has already been concluded that if the high-intensity beam should produce a background that is not linear with the intensity, the tagging efficiency would be different

at different intensities in a way the cannot be easily corrected for by subtracting the background. Another possibility is that the spread of the beam could be affected by the intensity which could affect the spread of the photon beam.

By performing tagging efficiency measurements at high intensities, the effect of any of the possible problems can be found; either problems with the background subtraction, the possible spread of the beam or issues with the induced background or some other problem not thought about yet.

Chapter 3

Experimental Setup

The basic idea behind the tagging efficiency measurements at high intensities is the same as for the standard measurements carried out at low intensities, with the only difference that lead absorbers are inserted in order to attenuate the photon beam. This poses some further requirements on the detector that is placed in the beam. Different detectors will have different advantages, and several setups were tested. The following section is devoted to the experimental setup, such as choice of detector, electronics schemes and general considerations that were taken into account.

3.1 Tagging Efficiency Measurements at High Intensities

The limitation of the intensity during ordinary tagging efficiency measurements is due to the capacity of the detector in the photon beam. To be able to do measurements at higher intensities of the electron beam, disks of lead can be placed in the photon beam. This will allow for an increased intensity of the electron beam since the photon beam that hits the detector will be attenuated.

The lead absorbers are placed after the radiator and the tagger magnet but before the photon beam collimator. Since they are placed after the position where the electrons and photons take different paths and where they can not affect the electron beam in any way, it should not affect the possible discrepancies in the tagging efficiency but merely produce a scaling of the number of photons that hit the detector. The idea is find the number of photons that were completely unaffected by the absorbers and then re-scale this number at the end of the analysis. However, the absorbers will cause production of a large low-energy background which has to be dealt with in the analysis.

It was decided to use a coincidence trigger for the experiment, so that only those events that contained a hit in both the in-beam detector and the focal plane were read out. This increases the live-time of the system as no unnecessary events are recorded, and makes the spectra cleaner with respect to the background.

For the first set of measurements the plan was to use a small HPGe (High Purity Germanium) detector as the in-beam detector. Since this detector is small, the probability to capture the entire electromagnetic shower is small. The probability for doing so also decreases with the photon energy, the hence the tagged region was chosen to be very low (from about 12 MeV) in order to get a reasonable probability for capturing the whole energy. The Main Tagger was used, as it is suitable for tagging the lower energy

part of the bremsstrahlung spectrum.

For the second set of measurements, that was performed since problems that occurred during the first attempt caused the first data set to be unreliable, the energy was higher on both the electron beam and the tagged region, but the Main Tagger was used also this time. However, the radiator position that was used for the second set of measurements was 33.05 cm upstream of the ordinary radiator position, since the measurements were done in conjunction with tests of the so called goniometer.

3.2 Lead Absorbers and Attenuation

The lead absorbers that were used in the experiment were about 2.4 cm thick. The ability of a material to attenuate electromagnetic radiation depends on both the material and the energy of the photons. Photons undergo Compton scattering, photoelectric effect and pair production when traversing a material. The electrons that are produced in those processes produce bremsstrahlung, and knock out more electrons. These processes continue as long as there is energy enough, and in this way the original photons creates a "shower" of particles and photons. Lead is particularly good at attenuating photons due to the high Z-value (Z=82). While traversing 2.4 cm of lead, approximately 10% of the photons will pass through the disk completely unaffected. The photons that interact with the lead absorbers will be "removed" from the beam if a collimator is placed downstream of the lead plates, since most of the secondary radiation in the electromagnetic showers is not parallel to the beam axis. Some of the lead absorbers used in the experiment are shown in Figure 3.1.

The cross sections for the various possible interactions are complex expressions, but the total probability per unit length, μ, for the interaction of a photon with lead has been determined and can be found in tables. This property is known as the attenuation coefficient of the material. On the web page of The National Institute of Standards and Technology [16], accurate coefficients for the different photon energies of interest can be found. The attenuation coefficient used for each of the focal plane channels is the one that corresponds to the central energy of the channel.

The fractional loss of the intensity I for a photon beam that travels through a piece of material of thickness dx is

$$\frac{dI}{I} = -\mu \cdot dx, \tag{3.1}$$

giving that the intensity after attenuation is

$$I = I_0 \cdot e^{-\mu \cdot dx} \tag{3.2}$$

where I_0 is the incident intensity.

The lead absorbers were placed just before the ordinary photon beam collimator. The position is shown in Figure 3.2. In this way the collimator is used doubly - not only does it collimate the ordinary beam, but it also excludes those photons that are affected by the absorbers. The scrubber magnets that are placed downstream are also used doubly, since they deflect particles that are created both in the collimator and in the lead disks.

Figure 3.1: *The lead absorbers. The circular disks are approximately 2.4 cm thick and have a diameter of about 5 cm.*

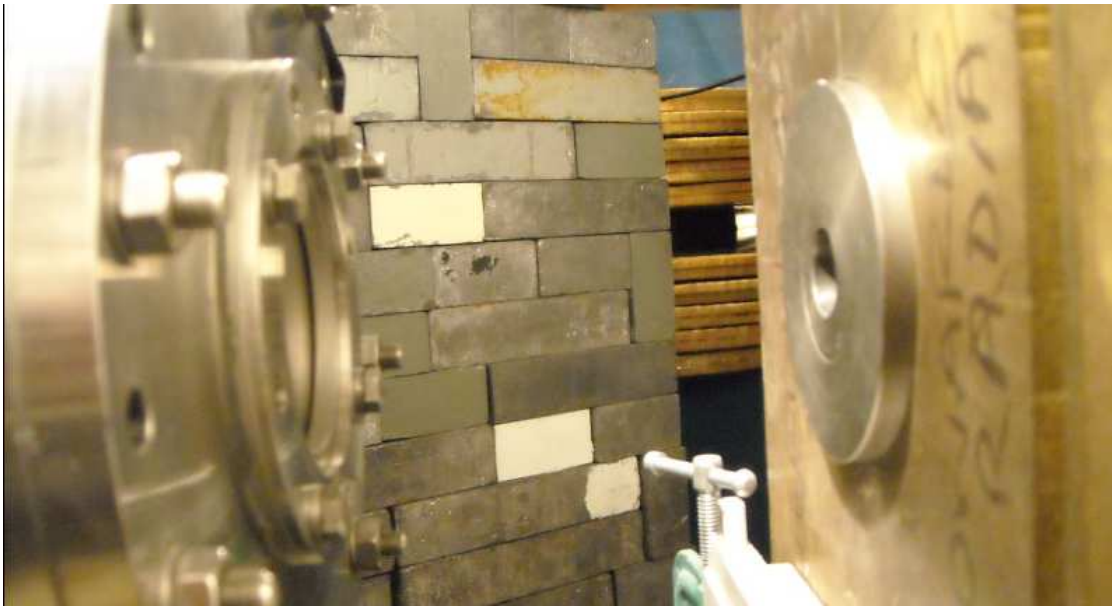

Figure 3.2: *The position where the absorbers were inserted. To the left, the exit of the tagger magnet is seen, and to the right, the collimator (circular) in its holder. In order to make room for the absorbers, the collimator was pushed into the holder. The absorbers were put either inside the collimator holder or, due to space limitations, in the space between the tagger exit and the collimator holder. Photo from [5].*

All of the secondary radiation can not, however, be stopped from hitting the detector. They will show up as a shower of particles with lower energy than the photon that produced them. Most often, only a fraction of the electromagnetic shower reaches the detector and the summed energy of the secondary particles is substantially lower than the energy of the tagged photons that pass through the absorbers unaffected. With a good resolution and a suitable size of the detector, the unaffected photons can be separated from the background in an energy spectrum. Certain events can be difficult to separate, e.g. when a large fraction of the shower reaches the detector or when a photon is being deflected just slightly by Compton scattering.

3.3 Choice of In-Beam Detector

The method of the measurement sets certain requirements on the detector that is placed in the beam. A fast response time is a great advantage because a higher beam intensity can be used without causing pile-up problems. A good resolution means that the energy deposited by a particle inside the detector is accurately measured. Another important issue is that the detector should be large enough to capture a large fraction of the electromagnetic shower that develops inside it when being irradiated. A combination of good resolution and a suitable size makes the peak from the unaffected photons easier to separate from the background that arises when the absorbers are put into the beam. The different detectors that were tried — a Pb-glass detector, two NaI(Tl):s and two HPGe:s — will be described in the following sections.

3.3.1 Lead glass

A lead glass detector is normally used for tagging efficiency measurements at MAX-lab. Lead glass detectors use the phenomenon of Cerenkov light. Lead glass has a very high refractive index, allowing particles to travel faster than light; $v = \frac{c}{n}, n \geq 1$. When a particle travels through an insulator faster than the speed of light in the medium, a light flash is emitted. This light is transformed into an electrical signal in a photomultiplier tube (PMT).

In order for a photon to produce at least one secondary particle that travel faster than light, and hence produce a signal in the detector, the energy of the incoming photon must be larger than approximately 300keV [2]. This gives an inherent discriminating level which removes some of the background. The detector also has a very short response time, allowing rather high count rates to be used without causing any pile-up problems.

The lead glass detector was planned to be used for reference measurements on the tagging efficiency, so that a direct comparison with the everyday measurements could be made. However, during the first set of measurements, the energy of the electron beam was set to be very low for reasons mentioned above, and the resolution of the detector is very poor at those energies. Therefore, it was not even possible to distinguish a peak in the energy spectra. The distribution of the events continued down to the very lowest part of the energy spectrum that was recorded, where it ended abruptly due to the threshold that was set in the electronics. This means that some of the events are lost below the threshold. A further reduction of the threshold would probably allow for noise to pass though the discriminator, and therefore this detector was deemed inappropriate for this

measurement. For the second set of measurements, the tagged energy range was higher and reference measurements with the Pb-glass detector were carried out.

The poor resolution of the Pb-glass detector was the reason for not even considering to use it as the in-beam detector for the measurements at higher intensities, where the photon peak must be distinguishable from the low-energy background.

3.3.2 HPGe detector surrounded by a NaI(Tl) detector

The detector setup that was first planned for the high intensity measurements consisted of a HPGe detector and a cylindrical NaI(Tl) detector with a hole in the middle that was just large enough for the HPGe to fit inside.

HPGe

A HPGe detector is a semiconductor detector, in which electron-hole pairs are created when charged particles travel though the so called depletion region where there are no free charges. The strong electric field applied over the depletion region collects the electron and holes and an electric signal is produced. The pulses are very small and can not be transported very far without being distorted, but have to be amplified close to the detector itself. Therefore, this detector had a built-in preamplifier. The active area of the detector was circular with a diameter of around 6 cm. The active crystal was placed behind a thin window, which protected the detector from the outside environment.

HPGe detectors have very good resolution, since very many information carriers can be created when the incoming particle excites the electrons in the material over the very small band gap (a few eV). The downside of this is the noise that appears due to thermal excitations already at room temperature. To reduce the noise to a tolerable level, the crystal is cooled by liquid nitrogen ($\sim$-196 ℃) that is filled into a dewar that is mounted on the detector and thermally connected to the active area.

The plan was to place this detector in the beam and surround it by the NaI(Tl) detector described in the next section. This would provide a very suitable detector system, since the Compton scattered photons that do not leave all their energy in the HPGe would end up in the surrounding detector and could be suppressed in the analysis afterwards. The excellent resolution of the full-energy peak would then allow for an easy separation of the full-energy peak from the low-energy background that is produced in the absorbers. Since the measurement aims at a comparison of the tagging efficiencies at different intensities, and is not an absolute measurement, the fraction of photons that end up in the full-energy peak of the detector does not need to be accurately known for the various energies.

However, the detector that was considered for this setup turned out to be impossible to use since the built-in preamplifier was customised for detection of particles of lower energies and could not handle the large signals from the bremsstrahlung photons. This was not noted until the actual experiment started, as the radioactive sources used for the testing naturally had energies that were lower than the lowest possible tagged region. The maximum particle energy that could be processed by the pre-amplifier before the linearity was lost was around 20 MeV. Above this energy, all output signals were equally large due to saturation of the pre-amplifier. Only about ten focal plane channels, corresponding to the lowest photon energies, could be detected properly. This can be seen in Figure

3.3. In this figure, every event is shown as a dot. Every slot on the y-axis corresponds to photons that were related to a hit in a certain focal plane detector (0-61), and the energy of the detected photon is on the x-axis. The energy spectrum is not calibrated, so the numbers on the x-axis are the ADC channels. All energy spectra that follow are also un-calibrated.

The black diagonal "stripe" seen in the figure across the topmost channels corresponds to the full-energy peak and should tend to higher energies as the number of the focal plane channel is decreased. However, below channel $\sim$50 the full-energy peaks end up in the same position, which is explained by the pre-amplifier reaching its maximal output.

Cylindrical NaI(Tl)

The cylindrical NaI(Tl) detector with a central hole that was used in this setup was last used some years ago, and had to be prepared and tested before use. NaI(Tl) (sodium iodide with impurities of thallium) is a scintillating material which means that when it is struck by radiation, the material is excited and de-excites via the emission of photons. The photons are collected and transformed into electrical pulses by 6 PMT:s. The outer diameter of the detector is approximately 30 cm and the inner diameter is around 9 cm. The length is approximately 30 cm. The detector is shown in Figure 3.4.

The resolution of NaI(Tl) detectors is poor compared to that of semiconductor detectors since the average energy needed to produce an information carrier is much larger. The energy needed to produce one scintillation is on the order of tens of eV:s [17], which means that the average energy needed to produce one photoelectron in the PM-tube cathode is on the order of tens to hundreds of eV. The energy required to produce an electron-hole pair in a semiconductor is on the order of eV:s. However, using NaI(Tl) for detection of those events that only deliver some fraction of their energy in the HPGe and then escape into the surrounding detector does not require very good resolution. It is basically enough that there is a signal in the NaI(Tl) in order to exclude the event and thereby suppress the Compton background in the HPGe spectrum. The drawback of NaI(Tl) is the long response time, which limits the tolerable count rate in the detector.

3.3.3 HPGe 2

A second cylindrical HPGe detector, which was designed for detection of particles of higher energies than the one that was originally considered for the experiment, was also tested. This detector was, unfortunately ,somewhat larger than the other HPGe, which made it unable to fit inside the cylindrical NaI(Tl), so no Compton suppression could be made. The detector was tested in measurements with 0 and 2 absorbers. The size of the detector crystal was large enough to have a reasonable probability for capturing a large fraction of the electromagnetic shower that develops in the detector, for a little less than half of the focal plane channels, as can be seen in Figure 3.5. The slots in the spectra that correspond to high photon energies (low focal plane channels) have no real full-energy peak due to the fact that a large fraction of the shower escapes from the detector. Generally, the low probability for capturing all of the shower that is created by the incoming photons at these energies gave wide peaks that could not, without the Compton suppression, be immediately distinguished from the low-energy background

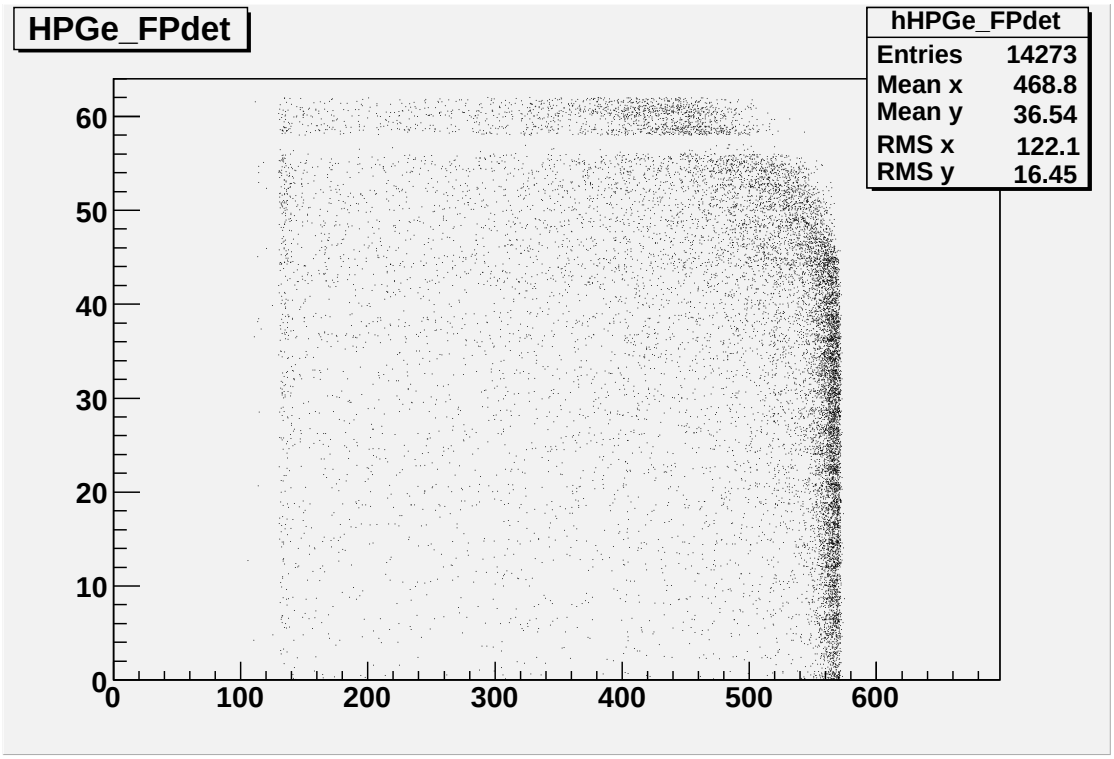

Figure 3.3: *Spectrum showing the events in the HPGe placed in the beam, separated according to which focal plane channel there was a simultaneous hit in. The slots on the y-axis represent the different focal plane channels, numbered from 1 to 62. Since photons that correspond to electrons in a certain focal plane channel have a certain energy, the response of the detector for each energy is seen along the x-axis, which represents the energy that is measured by the detector. For the high channel numbers, this is seen - the full energy peak is seen as the darker, diagonal stripe that tends to higher energies as the channel number decreases. This is the correct behaviour since lower channel numbers correspond to higher photon energies. However, for numbers below approximately 50, the full-energy peak loses its shape and the position does not correspond to the higher energies that it should represent. This is due to a built-in pre-amplifier that is constructed to work for lower energies. In this figure, it is also clearly seen that focal plane channels 56 and 57 are not working. A side remark: The time span during which events in the in-beam detector and the focal plane channels are considered being "simultaneous" is rather large in the raw data presented here, which means that one event may contain a hit in more than one focal plane channel, and hence contribute with more than one dot in the spectrum. However, it does not make any difference for this argument.*

Figure 3.4: *The NaI(Tl) detector. The central hole is where the active part of the HPGe detector should be (partly) inserted. The cylindrical NaI(Tl) crystal is connected to six PM tubes, which are seen in the figure.*

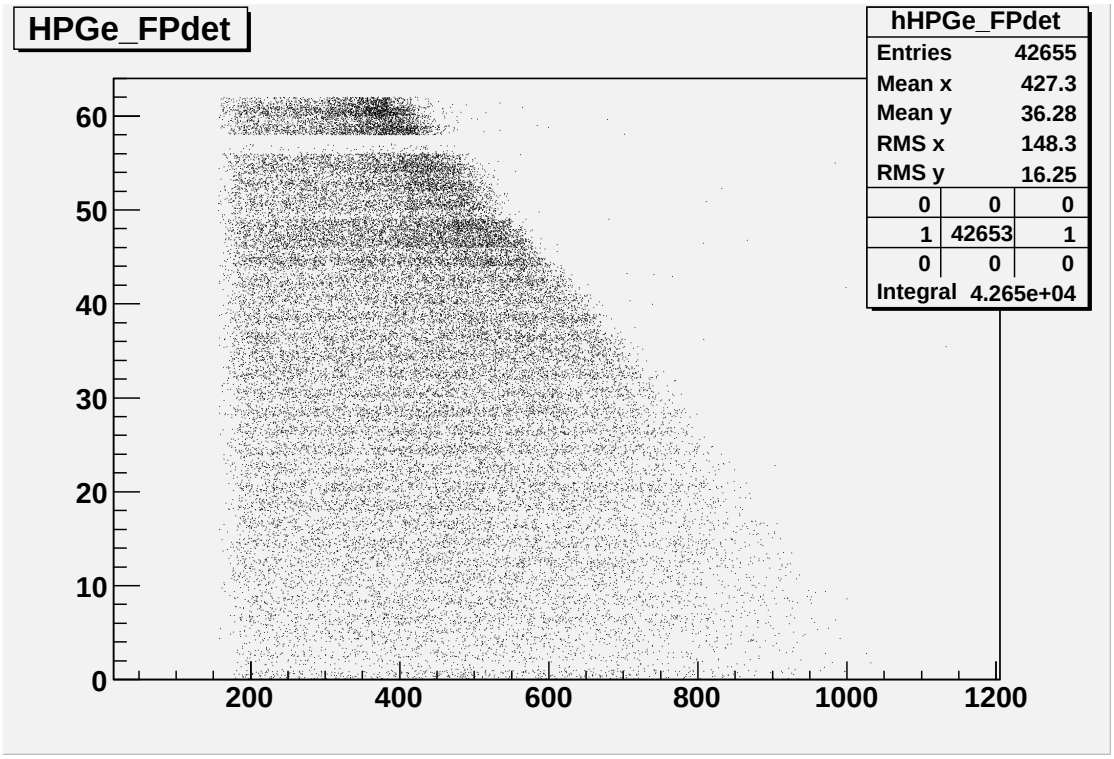

Figure 3.5: *Energy spectrum showing the events in the second HPGe separated according to which focal plane channel there was a simultaneous hit in, just like in Figure 3.3. This detector does not lose its linearity for high energies, but the detector is small and very few photons are full absorbed within the active area. Hence there is no full-energy peak for the high energy photons (= low energy residual electrons and low focal plane numbers). The spectrum was recorded for the measurement with 0 absorbers and very low intensity.*

even for as few as 2 absorbers. This is clearly seen in Figure 3.6, which is a 1D spectrum corresponding to the second uppermost slot in Figure 3.5. The un-calibrated energy is shown on the x-axis and the number of counts in each energy channel is displayed on the y-axis. The problems related to the escape of particles from the detectors and the lack of Compton suppression, together with the fact that less than half the channels could be analysed properly, caused this detector to be considered inappropriate for this measurement.

3.3.4 10"× 10" NaI(Tl)

A cylindrical NaI(Tl) detector with diameter and length of 10 inches ($\sim$ 25cm $\cdot$ 25cm) turned out to be the best option for the measurements. The detector is informally known at MAX-lab as the "Göttingen detector".

This NaI(Tl) detector gives a full-energy peak with a larger intrinsic width compared to the HPGe detectors. However, the large size of the detector allows for the capture of a larger fraction of the shower. This is seen in Figure 3.7, which shows the energy spectrum of the photons that are coincident with focal plane channel number 60, corresponding

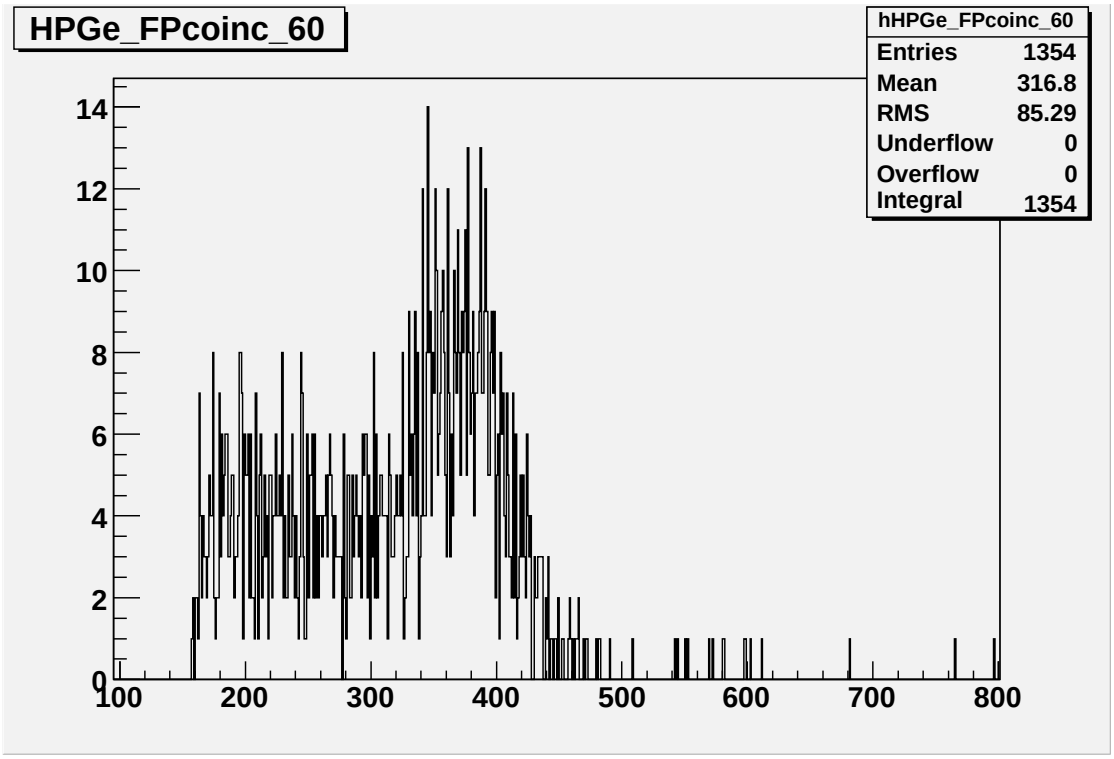

Figure 3.6: *Energy spectrum from the second HPGe, showing only the photons corresponding to hits in focal plane channel number 60, i.e. one of the upper slots in Figure 3.5. The spectrum is from the measurement using two absorbers and an intensity that it approximately 100 times higher than in the previous figure. The "full-energy" peak is not clearly separable from the low-energy background that starts to show up due to the secondary particles created in the absorbers. If this detector could have been placed inside the cylindrical NaI(Tl), a suppression of those photons that are not fully absorbed in the HPGe could have been made. Then the peak would probably be much more narrow, with a width corresponding to the inherent resolution of the detector.*

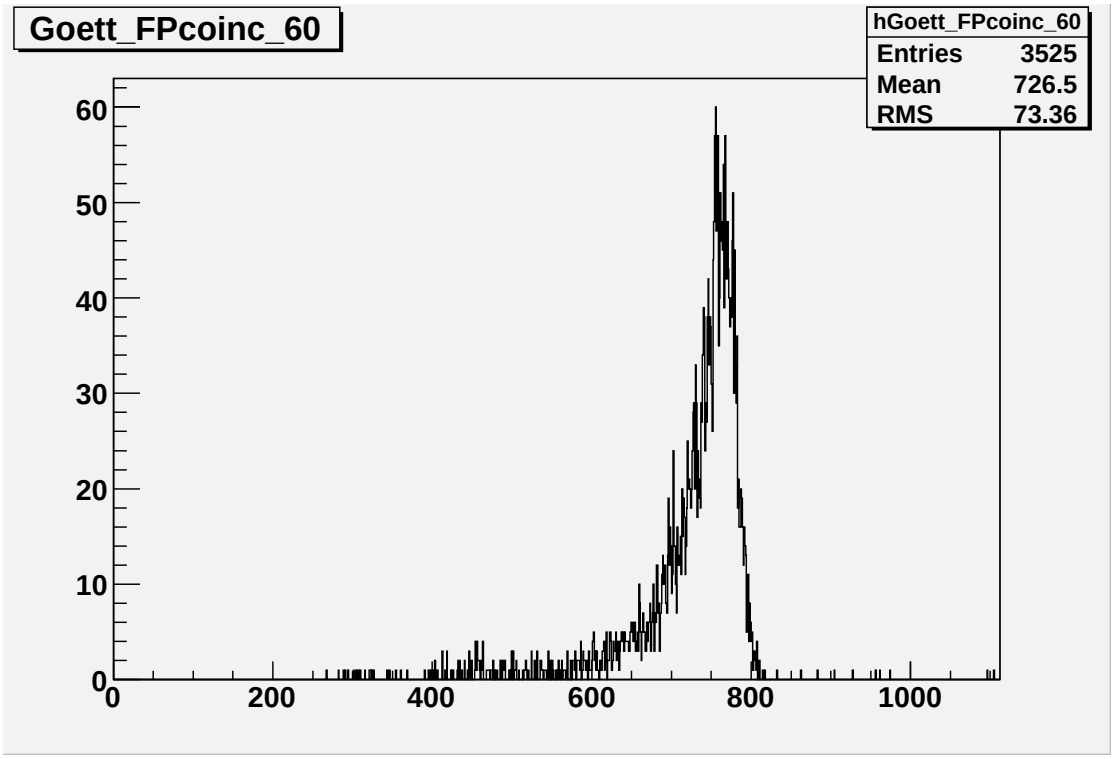

Figure 3.7: *Energy spectrum from the NaI detector for those events that contained a hit in focal plane detector number 60. Hence, the photons that are shown in this figure are almost mono-energetic with an energy of 14 MeV. The shape of the peak is a result of both intrinsic resolution and the probability for capturing the shower. The large probability for capturing the shower compensates for the poor resolution compared to semiconductor detectors, and makes it more suitable for this experiment.*

to a photon energy of 14 MeV. The data is from a measurement with no absorbers and very low intensity, meaning that there are almost no random coincidences and almost all photons that are seen in the spectrum are of a certain energy. There is a clear peak in the spectrum which does not extend all the way down to the threshold, which means that the photons that hit the detector were efficiently absorbed.

The large size of this NaI detector made it possible to capture a large fraction of the electromagnetic shower, which in turn made it possible to separate the photons from the low-energy background in spite of the less good resolution. This made the NaI detector more suitable for the measurements than the HPGe.

The drawback of the NaI(Tl) detector is the long response time, which is approximately 100 times as long as the response time of Pb-glass, meaning that the count rate must be kept about 100 times lower than for ordinary tagging efficiency measurements [2]. However, by inserting the absorbers, it is still possible to go to much higher beam intensities than during ordinary measurements.

3.4 Electronics

To collect the relevant data from the detectors and to store it properly, a system of electronic modules are needed. The arrangement of the detectors and the electronics used in this measurement are shown in the schematics in Figures 3.8 - 3.10.

3.4.1 Processing of signals from the detectors

The data needed for the determination of the tagging efficiency consists of the energy information for each event in the detector in the beam, the time between an event in the detector and all adjacent events in the focal plane detectors and the number of events in the focal plane channels.

In-Beam detector

A schematic of the basic electronics setup for the in-beam detector is shown in Figure 3.8, for the case when there is only one output from the in-beam detector, such as in the case of Pb-glass. The signal from the detector goes through a linear fan-in/fan-out, the purpose of which is to split the pulse in two. One signal goes to a QDC (charge-to-digital-converter), or, as in the first experiment, to a ADC (analogue-to-digital converter). ADC:s generally digitise the height of the pulse, and QDC:s digitise the integral of the total charge in the electric pulse. In any case, these modules provide a measure of the energy of the particle. The modules process the pulses reaching them only whenever there is a *gate*. The gate is generated and sent to the ADC/QDC from the trigger system which will be described later. Since QDC:s were used for the second experiment, which was the one that was fully analysed, the modules that digitise the pulses will hereafter be referred to as QDC:s.

The amplification and shaping that was applied to the signal before it was sent to the QDC is not shown in the figure, nor are the exact delay times that were used. The actual modules used are the ones stated in the figures or equivalent. This applies to all the electronics schematics.

The second signal from the fan-out goes to a discriminator. The discriminator is set to produce a logic output if the incoming pulse is larger than a pre-set limit. This threshold is set so that only those pulses that are considered being real signals and not only noise are accepted. The output of the discriminator, which is a NIM-standard logic pulse, is used as a trigger that tells the system that an event that could be of interest has occurred and that the QDC gate should be opened and the TDC:s started.

When the HPGe detectors were used, the electronics setup was slightly different. The output signal from the pre-amplifier that is mounted directly in connection with the detector, is already split in two branches. One output is optimised to represent the energy of the pulse, and the other is processed in such a way that the timing of the pulse should be as accurate as possible. The energy-signal goes to the QDC and the timing signal goes to the discriminator.

Focal plane detectors

The electronics for the 63 focal plane detectors is shown in Figure 3.9. The upper part of the picture shows how signals from two adjacent detectors are joined in an AND-gate. In

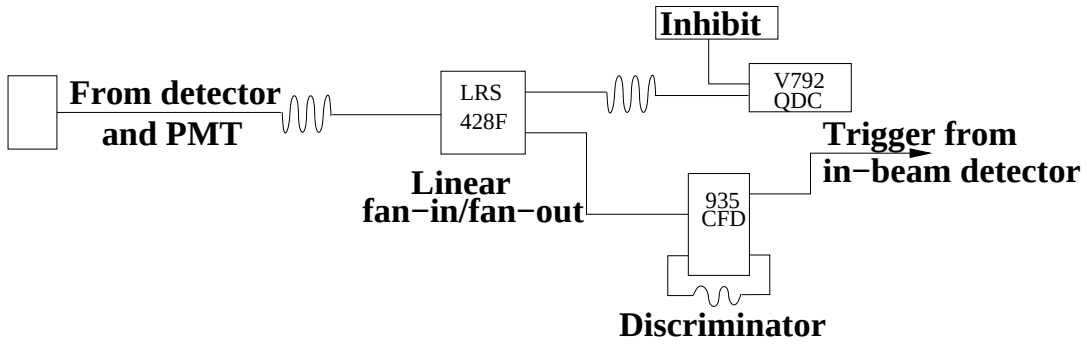

Figure 3.8: *Schematic picture of the electronics needed to extract the information from the detector placed in the beam. The pulse is split in a fan-in/fan-out. In the upper part of the diagram, the signals go to a QDC which integrates the charge in the pulse. In the lower part, the signal goes to a discriminator which gives a logic output when the signal is larger than the pre-set threshold. This signal serves as the trigger for the system. The reason for the delay of the pulse in the upper part is to make sure that the pulse to be integrated reaches the QDC after the trigger has caused the gate for the QDC to open. The figure is a modified version of an original from [15].*

order for it to be a proper event in a certain channel, both detectors must have a signal within a pre-set time span. In the case of an overlap, the signal is counted by the scaler. The total number of events in each focal plane channel is a quantity that is measured both during tagging efficiency measurements, and during ordinary experiments where it is related to the number of photons that hit the target via the tagging efficiency. The focal plane scalers do not, however, count all the time. Besides being inhibited during the first millisecond of the beam cycle, when the beam is not suitable for experiment, the counting is also inhibited during the dead-time of the system that occurs during the processing of the signals. This is done because none of the photons that are produced by the electrons that hit the focal plane during the dead-time have any chance of producing a signal that is seen by the data acquisition. The inhibit signal is produced in the trigger electronics. Note that the signal from every detector goes into two of those overlap modules, as every detector (except the ones on the edges of the hodoscope) is part of two channels.

The other output from the overlap module goes to a TDC, where it causes the TDC that was started by the trigger to stop. The signal from the focal plane is delayed in order for it to arrive after the start. The information from this TDC is used to determine which photon belongs to which electron, since there should be a fixed time between the start and stop for pairs of correlated photons and electrons.

The lower part of the figure shows how the "FP OR". This is a signal that indicates that there is a signal in one or more of the focal plane channels and it can be included in the triggering. Each of the four OR modules take signals from 16 of the channels (not detectors) as input and if there is a signal in any of those, there is an output which is transformed by the Level Translator into a pulse of suitable shape. The pulses from all four modules go into a fan-in/fan-out, which just outputs the sum of all the signals and hence acts as an OR module.

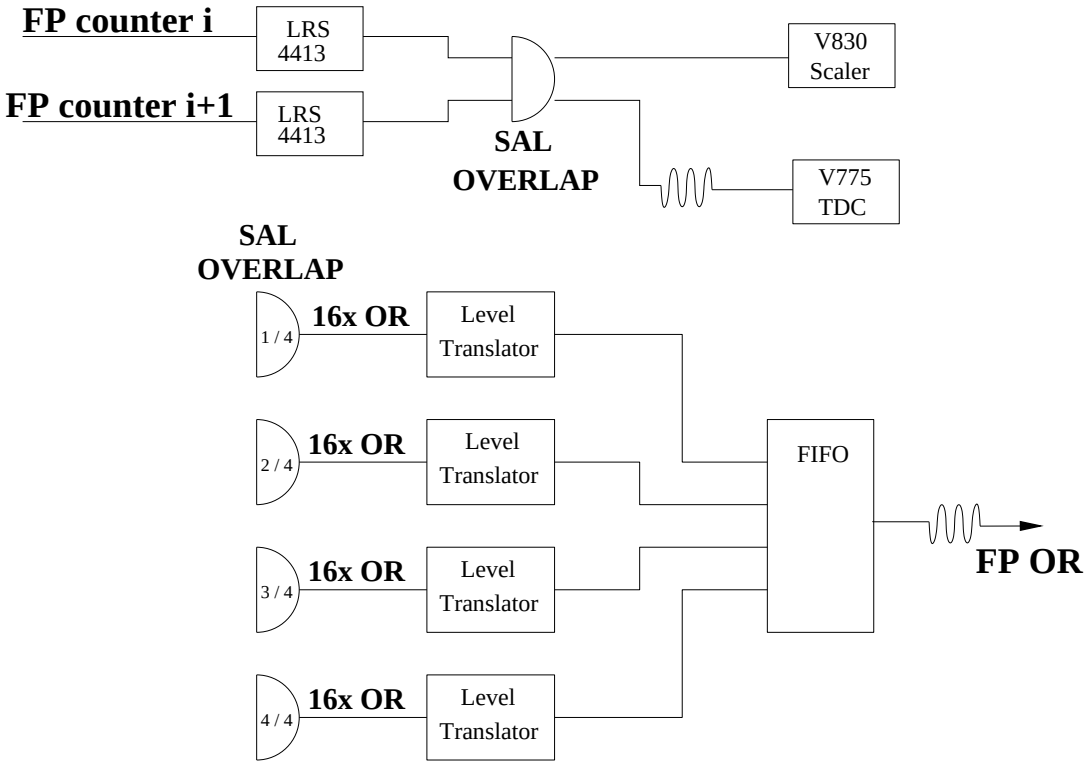

Figure 3.9: *The focal plane electronics. The upper part shows the electronics for each of the 62 channels in the focal plane. In case of an overlap, a signal is sent to a scaler that counts the event unless it is inhibited. The signal also stops the TDC connected to the certain channel. The lower part shows how the "Focal Plane OR" (FP OR), used in the trigger electronics, is constructed as a simple OR signals from all the channels. The figure is a modified version of an original from [15].*

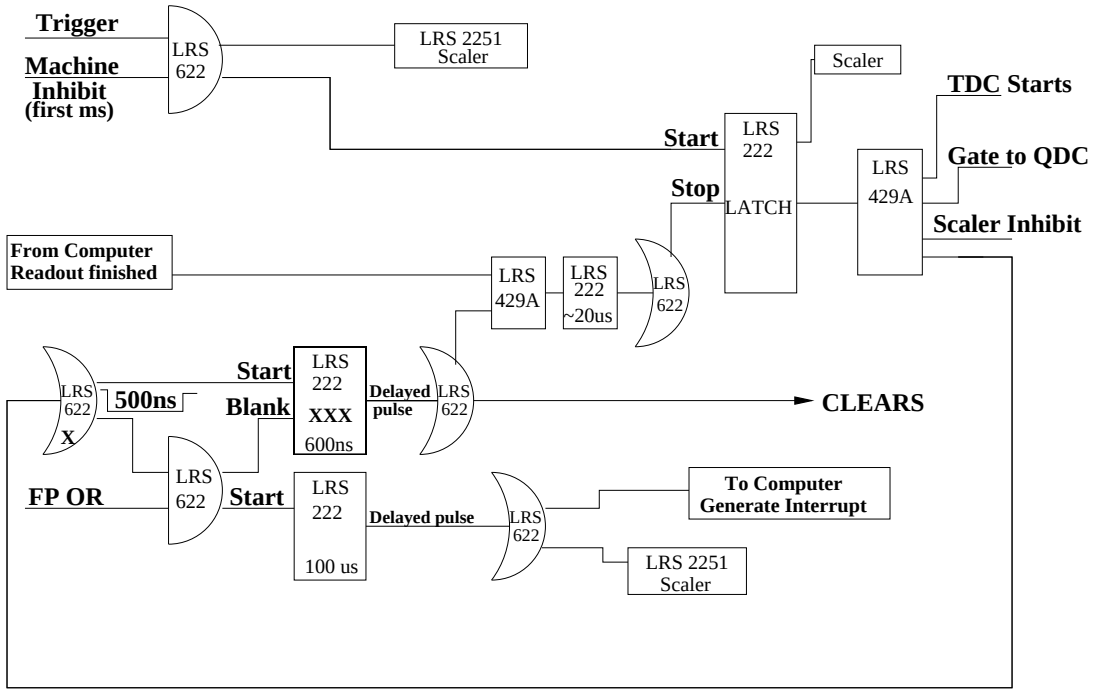

Figure 3.10: *The trigger system. The trigger pulse from the detector in the beam enters the system through the AND-gate in the upper left corner of the figure. The half-circles are AND-gates and the moon-shaped figures are OR-gates. When there is only one input into the OR-gates, they act as fan-outs. The logic modules that can be set to AND or OR mode are of type LRS (LeCroy Research System) 622 or equivalent. The other type of modules are LRS 222, which can be used as a latch or a delay, and LRS 429A, which is a fan-in/fan-out. The figure is a modified version of an original from [15].*

3.4.2 Trigger system

Not everything that happens in the detectors is of interest. The trigger system is constructed to handle the decision about when to read what is in the detectors and store it. There is also a possibility that several events happen very close to each other in time, and since the processing of an event takes a certain time, the later event has to be thrown away. This must also be handled by the trigger system.

For these measurements, it was decided to read out only those events that had both a signal from the in-beam detector and from a focal plane detector. The trigger setup that was used is shown in Figure 3.10. Starting from the upper left corner, the "Trigger"-signal, in this case the discriminated signal from the in-beam detector, goes to an AND-gate together with a signal that is off only during the first millisecond of each beam cycle.

The signal continues to the so called *latch*, which accepts the signal if is it open and ignores the signal if it is closed. Whenever a signal is accepted, the latch closes and is not re-opened until the event has been processed in a suitable way. The output of the latch is split in a fan-out and sent to several modules; it starts the TDC:s, opens the gates for the QDC and inhibits the scalers.

The fourth output from the latch via the fan-out goes to the module seen in the lower

left corner in Figure 3.10 (marked with an X). This module produces two output signals that are 500 ns long. One of these go to an AND gate together with the “FP OR”. If there is an event in the focal plane, the FP OR will be non-zero at some point, and the AND-gate will output a signal. This signal is delayed and then used for generating an "Interrupt", telling the computer to read out and store the information in the QDC and TDC:s. The delay of about 100 μs is because the modules need this amount of time to digitise the signals after the gates have been closed and the TDC:s stopped. The TDC range itself is 1μs.

If there is no signal from the focal plane during the 500ns, the event is uninteresting and it is unnecessary to read out the event. No interrupt is sent to the computer because the AND condition is not fulfilled. Instead, all the modules are cleared. This is done by the upper delay box (marked with XXX in the figure) which delays the 500 ns long signal for 600ns. If there is an event in the focal plane, the signal will be blanked during the time it is delayed within the module, but if there is no signal from the “FP OR”, this signal will be used to generate a “Fast Clear” signal that is sent to all ADC:s and TDC:s. It is also used to re-open the latch so that new triggers can enter the system.

Those events that are read out by the computer take around 1 millisecond to process. When the process is finished, the computer sends out a pulse, called "Readout Finished" in the figure, that re-opens the latch so that the next event that comes in can be processed.

The data is stored by the computer in a file, but in order to see the data as it comes in during a measurement, there is also an on-line data analysis code that sorts the events as they are read out and plots them in histograms.

3.5 Performing the Experiment

The actual work that was done consists of several parts that will be briefly described in this section. The first measurement was prepared and performed in May-June 2007 and the second experiment was done in September 2007.

3.5.1 Preparation of experiment

For the first set of measurements, the plan was to use the HPGe detector described in a previous section surrounded by the cylindrical NaI(Tl). The preparations consisted of testing of the detectors. No data sheet or any specification was found for the cylindrical NaI(Tl), besides that it was known to be made of NaI(Tl). To make the detector work, some connectors on the PMT:s had to be exchanged because they did not fit with the available cables and the high voltage settings were optimised. The characteristics of the detector was investigated. Also the properties of the HPGe was checked. The electronics setup for the tagging efficiency measurements was connected, and delays, gates etc. were adjusted, as well as the shaping and amplification of the pulses from the detectors. The "ordinary" trigger electronics, that is part of the electronics that is not changed much between experiments, was used.

3.5.2 First set of measurements

For the measurement in June 2007, the beam energy was chosen to be 114 MeV, and the tagged region between ∼13 and ∼51 MeV. The radiator foil was 151μm thick and consisted of aluminum. The collimator was 12 mm wide. The collimator was moved from its ordinary position to approximately 10 cm further downstream, in order to make the absorbers fit between the exit of the tagger magnet and the collimator.

When the beam-time started and the HPGe detector was subject to photons of higher energies than those from the radioactive samples used for the testing, it was realised that it was not possible to use this detector because of the built-in pre-amplifier. It was also noted that the resolution of the Pb-glass detector was too poor to do any reference measurements with. Next, the second HPGe was tested as well as the 10"$\times$ 10" NaI(Tl) detector. The NaI(Tl) detector was considered being the best one, and measurements with up to 5 absorbers were made. The countrate in the detector was kept approximately constant. Even if each of the absorbers attenuated the photon beam by a factor of 10, it was not possible to increase the beam intensity by a factor of 10 every time a new absorber was inserted due to the increasing low-energy background.

This first set of measurements was strongly affected by problems with a magnet; the abort-kicker magnet, which usually gives a kick to electrons in the first millisecond of the beam pulse so that they hit the wall of the beamline instead of going to the experimental area, was broken. The first millisecond contains those electrons that were not captured in the MAXI ring, and the intensity of this short beam pulse is too high to be useful. If it is let through to the experimental area, it causes pile-up problems since many events happen at almost the same time. This problem was seen in the measurements; the detector in the beam was "blinded" by the high intensity photon flux during the first millisecond. The pulses from the detector were investigated using an oscilloscope, and the baseline was not restored properly after the detector being hit by the direct beam. Those signals that arrived before the baseline was restored may be wrongly interpreted by the modules that treat those pulses, which can cause the spectra to not be truly representative. Part of the problems with the second HPGe could be due to this problem. In order to improve the measurements, the first 10 ms of each pulse were inhibited in the sense that the read-out of the detector was blocked. This inhibit did not change the fact that the detector was seeing the very high intensity from the first part of each pulse, but it allowed for the baseline to recover before the collection of data was started, and it made sure that the system was not swamped by triggers from the unstretched beam. Normally, an inhibit of 1 ms is used in order to avoid the background that can be induced by the electron beam hitting the wall of the beamline.

Due to the malfunctioning abort kicker, the data from this set of measurements can not be considered being reliable. A preliminary analysis of the data was carried out and the results are shown in Figure 3.11. The plot shows two reference measurements without absorbers and measurements with one, three and five absorbers. Note that the analysis is not complete; some corrections to it could cause changes in the tagging efficiencies given here. This analysis does not show any systematic decrease or increase of the tagging efficiency as a function of intensity, but the values did not show the desired consistency. However, this is possibly due to the problems with the beam, and it was decided to perform another set of measurements to get reliable results.

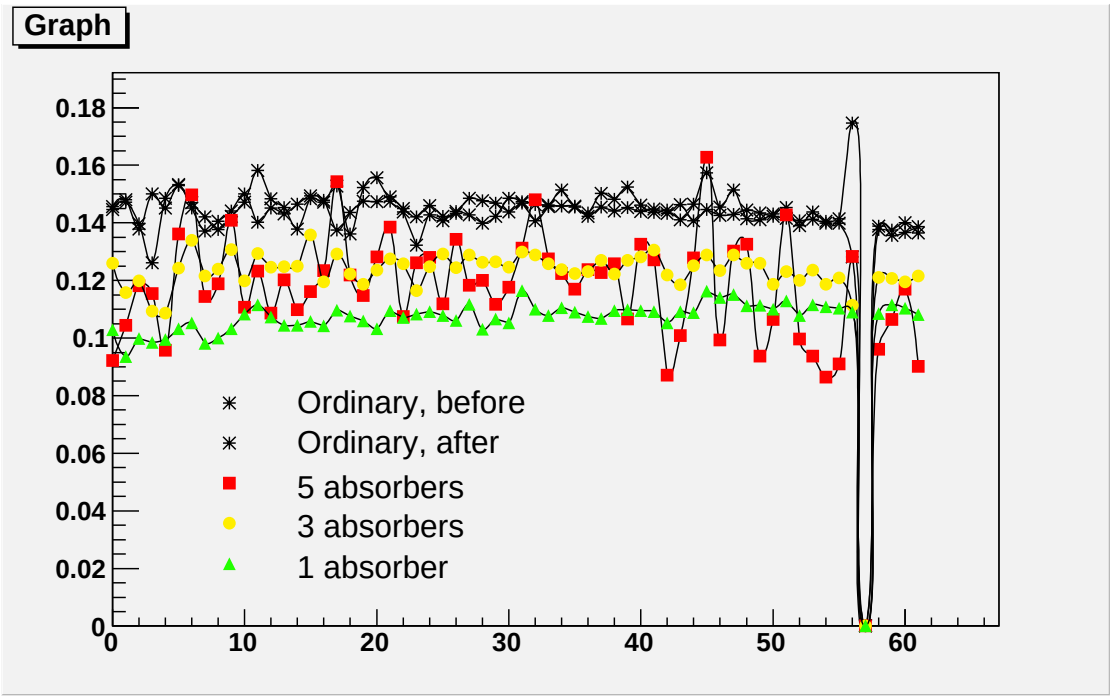

Figure 3.11: *Tagging efficiencies for each focal plane channel (0-61) resulting from a preliminary analysis of the data from the measurement in June 2007. Note that further corrections could change the values given here. The black stars show the reference measurement that was made at ordinary tagging efficiency intensity. The lowest, green line is the measurement with one absorber. The yellow and red, that are in the middle, are measured with 3 and 5 absorbers. Note that the tagging efficiencies are shown here without statistical errors. The statistical uncertainty is quite large; in the case of five absorbers, which had the worst statistics, it is clearly indicated by the large spread of the values. The most worrying feature is the discrepancy between zero and one absorbers, but if this had been due to a systematic dependence on the intensity, the run with three absorbers would end up below the one with one absorber.*

3.5.3 Second set of measurements

During a few experimental shifts in September 2007, the measurement was repeated. The 10"× 10" NaI(Tl) detector was used also this time. The energies used during this set of measurements were higher than for the previous; the beam energy was 144 MeV and the tagged region was between ∼51 MeV and ∼82 MeV. The reason for using this region was simply because those energies were of interest for other experiments and tests that were done in conjunction with the tagging efficiency tests. Since the 10"× 10" NaI(Tl) detector was used instead of the small HPGe:s, there was no need for keeping the tagged energy region as low as for the previous set of measurements. The collimator diameter was 19 mm and the radiator foil used was made of 50 μm Al.

First, some measurements with the lead glass detector, commonly used for the every-day tagging efficiency measurements, were made. Two different intensities were tested - ordinary tagging efficiency intensity and then an even more reduced intensity. Then the NaI(Tl) was placed in the beam, and measurements with 0, 1, 3 and 5 absorbers were made. Two different intensities were tested while using one absorber. Measurements without the radiator and without beam were also performed in order to make it possible to make corrections for the background. The data set is shown in Table 3.1.

The "FP countrate" refers to the average count rate in one of the focal plane scalers during each measurement, and gives a measure of the relative intensity of the beam. When the intensity was high, the scalers were read out every other second. To find the average number of counts for those runs, the total, un-inhibited number of counts in one of the focal plane scalers was divided by twice the number of scaler read-outs. In the cases of very low intensity, the scalers are read out either every other second or every fifth second, and the average number of counts were instead found by dividing the total number of counts in the scaler with the approximate time for the run, taken from the logbook. The countrates during the measurements range from about 10 Hz to 38 kHz. The highest intensity that has been used during an experimental run is approximately 1 MHz. Hence, the tagging efficiency was measured at intensities that range over three orders of magnitude; from about 0.001 ‰to 4% of full intensity.

The reason for not increasing the beam intensity by a factor of ten for each absorber that is inserted, is that the countrate in the in-beam detector must be kept at about the same level in order to avoid pile-up problems. It would seem like the the count rate in the detector would scale with the attenuation, but this is not true because of the background that is created in the absorbers. This makes it necessary to have longer runtimes for the measurements with many absorbers in order to get enough full-energy photons. The intensity for each run was chosen so that the number of triggers was kept constant.

Run nr	FP countrate (Hz)	Sort of measurement	In-beam detector
3665	200	TaggEff, 0 abs.	Pb-glass
3666	4	No radiator	Pb-glass
3667	3	No beam	Pb-glass
3668	20	TaggEff, 0 abs.	Pb-glass
3670	10	TaggEff, 0 abs.	NaI(Tl)
3671	2	No radiator	NaI(Tl)
3672	2	No beam	NaI(Tl)
3674	38 000	TaggEff, 5 abs.	NaI(Tl)
3675	38 000	TaggEff, 5 abs.	NaI(Tl)
3676	20	TaggEff, 0 abs.	NaI(Tl)
3677	20	TaggEff, 1 abs.	NaI(Tl)
3678	70	TaggEff, 1 abs.	NaI(Tl)
3679	$\sim$5	No radiator	NaI(Tl)
3680	3	No beam	NaI(Tl)
3681	1 800	TaggEff, 3 abs.	NaI(Tl)
3682	320	No radiator	NaI(Tl)
3683	10	TaggEff, 0 abs.	NaI(Tl)
3684	150 000	High int., rad. in	No detector
3685	7 000	High int., rad. out	No detector

Table 3.1: *The data set from the second measurement - run numbers, number of absorbers that were used, beam intensity, sort of measurement and choice of in-beam detector are shown. The first four measurements were done with the Pb-glass detector in order to have a direct comparison to the standard tagging efficiency measurements, and then the in-beam detector was exchanged and the absorbers added to the setup. All the tagging efficiency measurements done with the NaI(Tl) detector except run number 3677 were made at a trigger rate of 1000-1500. The measurements without beam were used to compensate for the background in the room. The "background" measurements done with beam on but without radiator turned out to be unnecessary for the analysis, except in that they give a rough estimate of the beam-induced background. Three reference measurements at ordinary tagging efficiencies intensities and without absorbers were made; first, in the middle of the run and last. The first reference measurement turned out to deviate from the other measurements in certain aspects (position of TDC-peak and energy peak) and therefore the second measurement was used as the standard reference. The last two measurements were made in order to check the beam-induced background.*

Chapter 4

Data Analysis

The data analysis was made using the C++-based program ROOT (see [18]), which is commonly used for analysis of data from nuclear physics experiments. The basis for the program used to perform the tagging efficiency analysis was a standard code that is used in the nuclear physics group at MAX-lab, which interprets and transforms the data from the electronic modules into a form which can be easily accessed. The code was developed by the author to be able to perform the certain tasks needed for the analysis of the tagging efficiency. The spectra and diagrams shown in this section are also produced within the ROOT framework.

4.1 Raw Data

The raw data acquired during the experiment consists of all the individual events recorded whenever a trigger signal was accepted, and the total number of signals detected in the focal plane detectors during the time the system was open for recording an event.

The only events that were read out were those containing signals from both the in-beam detector and from one or more of the focal plane channels. For every such event, there is information about the energy deposited in the in-beam detector (from the QDC) and information about the time difference between the stop and start of the TDC.

Energy and timing information will be used to extract the number of photons that passed through the absorbers unaffected. This number will be re-scaled to find the total number of photons, which is the numerator in the fraction that is the tagging efficiency;

$$\epsilon_{tag} = \frac{N_\gamma}{N_{fp}}. \tag{4.1}$$

The number of events in the focal plane, which constitutes the denominator, will be extracted from the focal plane scalers.

No data presented here contains any information from the first millisecond of each beam cycle, since the data acquisition was inhibited during this period in order to avoid the unstretched beam.

4.1.1 Energy spectra from the in-beam detector

In Figures 4.1 and 4.2, the total energy spectra from the NaI(Tl) from measurements with zero and five absorbers, respectively, are shown. In the first figure, showing the measurement at low intensity and no absorber, part of the bremsstrahlung spectrum is seen. The detector sees the entire bremsstrahlung spectrum, but the events are only accepted if there is also a signal in the focal plane within the pre-set time span. At this low intensity, virtually all accepted events come from truly correlated photons and electrons. Hence, only photons whose electron was detected in the hodoscope is seen. This part of the bremsstrahlung spectrum is referred to as the "tagged" part of the spectrum.

The energy spectrum from the measurement with 5 absorbers looks very different - the peak from the tagged photons is hardly visible, and the dominant feature of the spectrum is the background. The full distribution of events that the detector sees comes from both the entire bremsstrahlung spectrum but also from the showers of particles created when photons interact with the absorbers. When the count rate is high, there is a large chance for having random coincidences between events in the in-beam detector and the focal plane detectors, which means that the recorded energy spectrum will contain not just the truly coincident tagged photons. A further altering of the spectrum will take place because the showers of particles that originate from photons in the tagged region will show up in the spectra as true coincidences.

Two single spectra that show the energy distribution of those photons that correspond to a hit in the first and last focal plane channel, respectively, are shown in Figure 4.3 for two measurements at different intensities. Since there are almost no random coincidences in the measurement at low intensity, these spectra show the different responses of almost mono-energetic photons (within an energy span of about 0.5 MeV, which is the width of the focal plane channels) entering the detector.

The photons that correspond to low focal plane channel numbers (low electron energies) have higher energies than those corresponding to high numbers, which is clearly seen in the two sets of pictures. The spacing between the two full-energy peaks shown in the figure corresponds to a span of about 30 MeV, as this is the energy difference between the lowest and highest focal plane channel.

The reason for having much fewer events in channel number zero than number 61 is that the odd and even channels are not equally wide, as explained in Section 2.5. The different shapes of the peaks are due to fact that photons with high energy produce a larger shower of particles and the chances for capturing all of it decreases. This causes high-energy photons to produce a wider distribution with a less high peak. This explains the features of the total energy spectrum shown in Figure 4.1; the low-energy tail consists of those photons that are not fully absorbed and the slope in the upper part of the distribution is due to the decreasing height of the peaks.

4.1.2 Timing information

Figure 4.4 shows the sum of all the raw individual focal plane TDC spectra for zero absorbers. Each of the individual spectra contains a narrow peak that corresponds to the time between the start and stop of the TDC when the event consists of a photon and its corresponding electron. This peak is referred to as the "prompt" peak. The

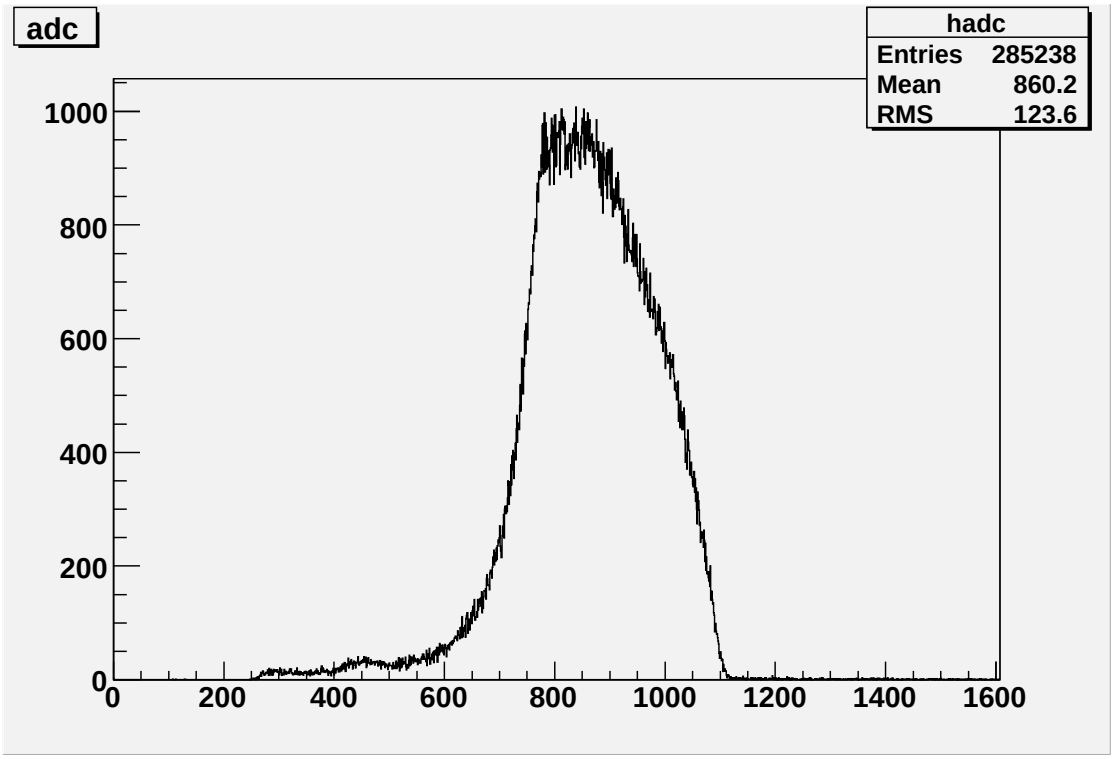

Figure 4.1: *Energy spectrum from the measurement with zero absorbers and low intensity. Since only those photons that are coincident with events in the focal plane channels are recorded, only the "tagged" region of the bremsstrahlung spectrum is seen. The unsharp edges are a consequence of the resolution of the detector and the fact that part of the shower of particles created in the detector by the photon can escape without leaving all its energy.*

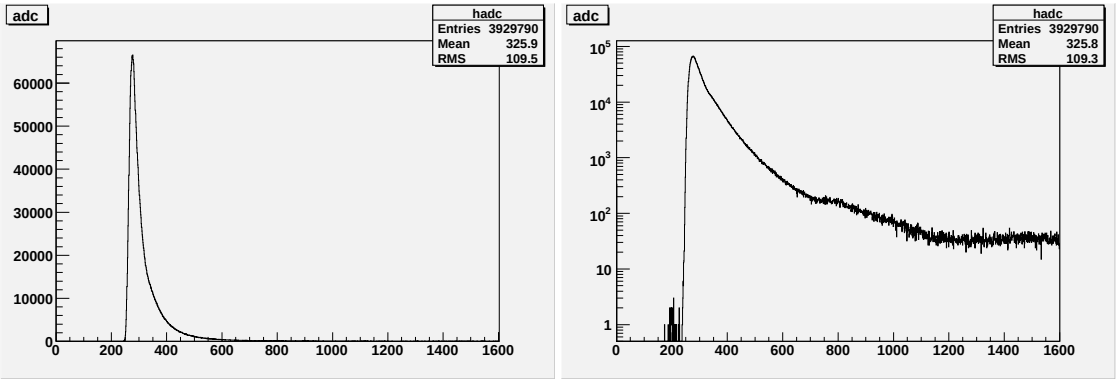

Figure 4.2: *Energy spectrum for five absorbers and an intensity that is about three orders of magnitude higher than for the measurement without absorbers. The background from non-tagged bremsstrahlung and showers of particles created in the absorbers dominates the spectrum. The peak from the tagged photons, which reaches from about channel 750 to 1100, can almost be seen when log-scale is used.*

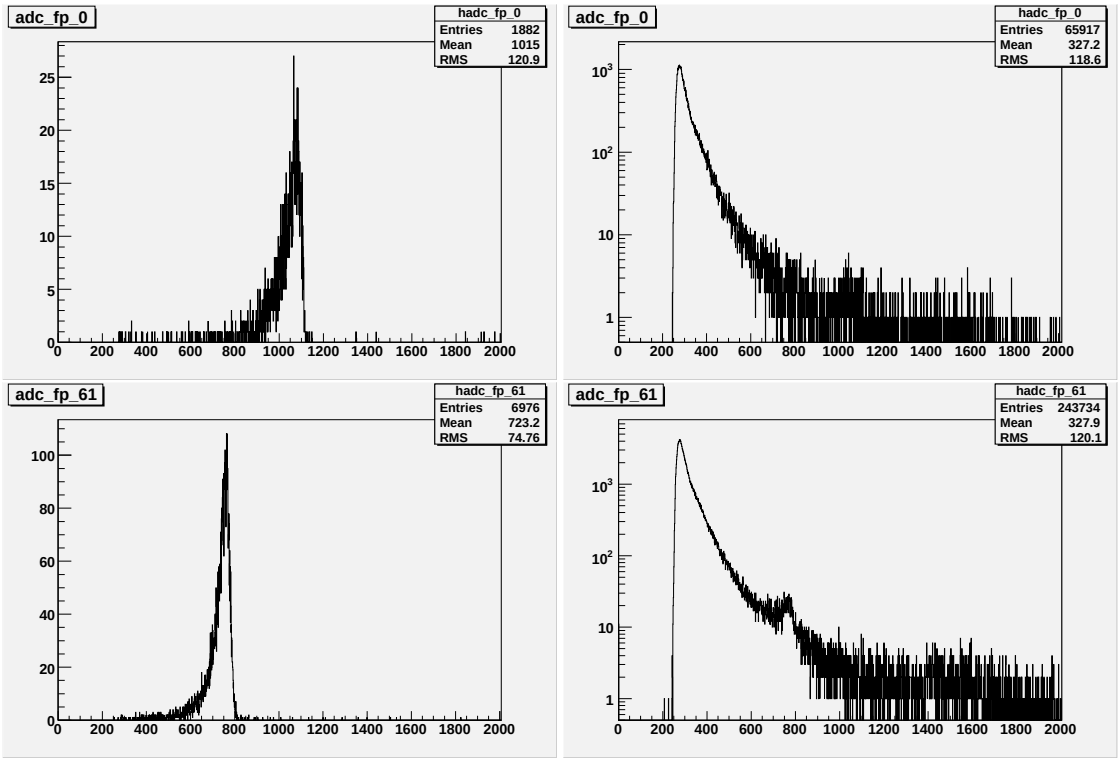

Figure 4.3: *Raw energy spectra from the measurement with zero absorbers (left) and five absorbers (right). In the two upper figures, only those events that correspond to a hit in focal plane channel number zero are displayed. In the lower part, the events that correspond to a hit in channel 61 is shown. The spectra to the right contains mostly randomly correlated events and the peak from the tagged photons is hardly visible. In the spectra to the left, where there are almost no random coincidences, the spectra show the response of the detector to almost mono-energetic photons. The difference in energy between photons that correspond to channel 0 and channel 61 channel is approximately 30 MeV.*

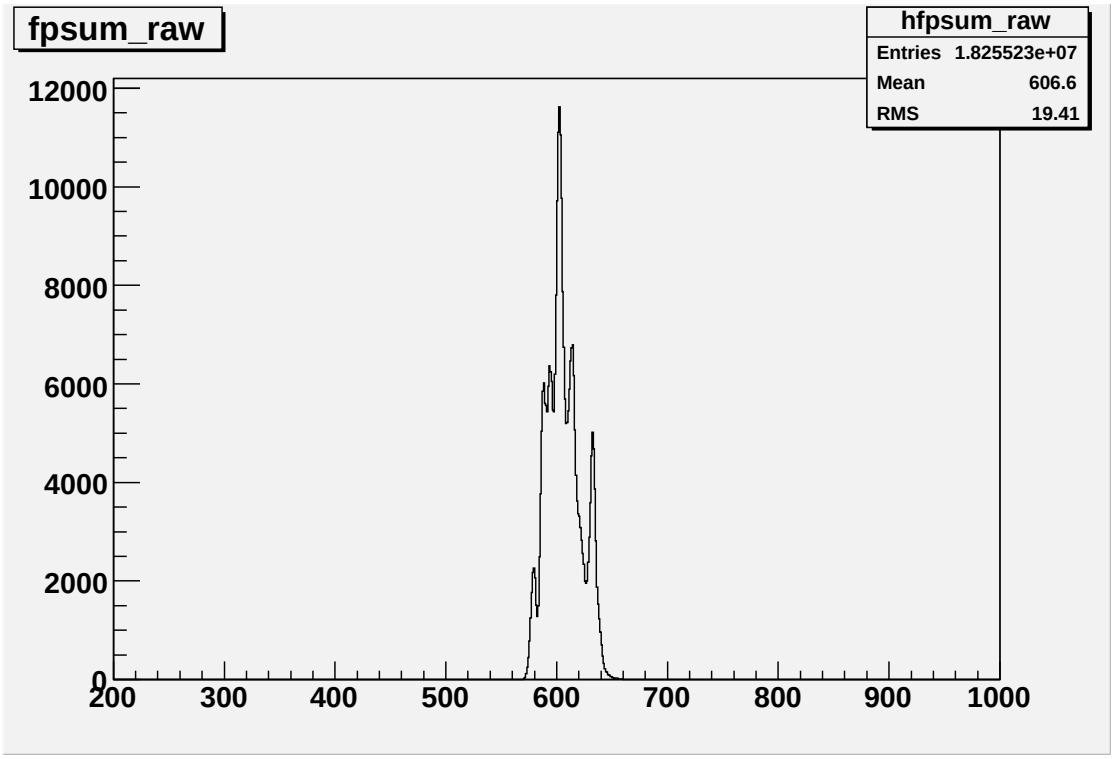

Figure 4.4: *Sum of all spectra from the individual focal plane TDC:s for a low-intensity measurement. The full spectrum, which stretches up to channel 4096, covers to a time span of* $\simeq$ *1000ns. Each of the individual TDC spectra contains a well-defined prompt peak, but they are not in the same position for all channels. The reason for this is that the electronics and delays are somewhat different for the different channels.*

time between the photons reaching the in-beam detector and the electron hitting the hodoscope is the same for all events. The reason for the different positions of the TDC peaks is not physical - it merely corresponds to the fact that the delays for the different channels are not exactly the same. Since only relative times are of importance, an alignment of the different TDC-spectra can be made in the software treatment of the data.

The individual prompt peaks have a FWHM of about 2 ns. The trigger system is set to accept events that have a corresponding hit in either focal plane channel within a time span of 500 ns. The photons that are of interest for the tagging efficiency calculation are those that are truly coincident and, hence, show up in the prompt region. Therefore, the energy spectra can be cleaned up considerably by applying a stricter condition on the allowed TDC-values in the analysis.

The sum of all raw TDC spectra from a measurement at high intensity is shown in Figure 4.5. The prompt peaks are now accompanied by all the randomly correlated events. The prompt peaks are positioned on the background of random events, which means that the prompt region will contain not only truly correlated events but also random coincidences that just happen to have a time difference between in-beam detector and hodoscope that is the same as for the prompt events. The structure of the

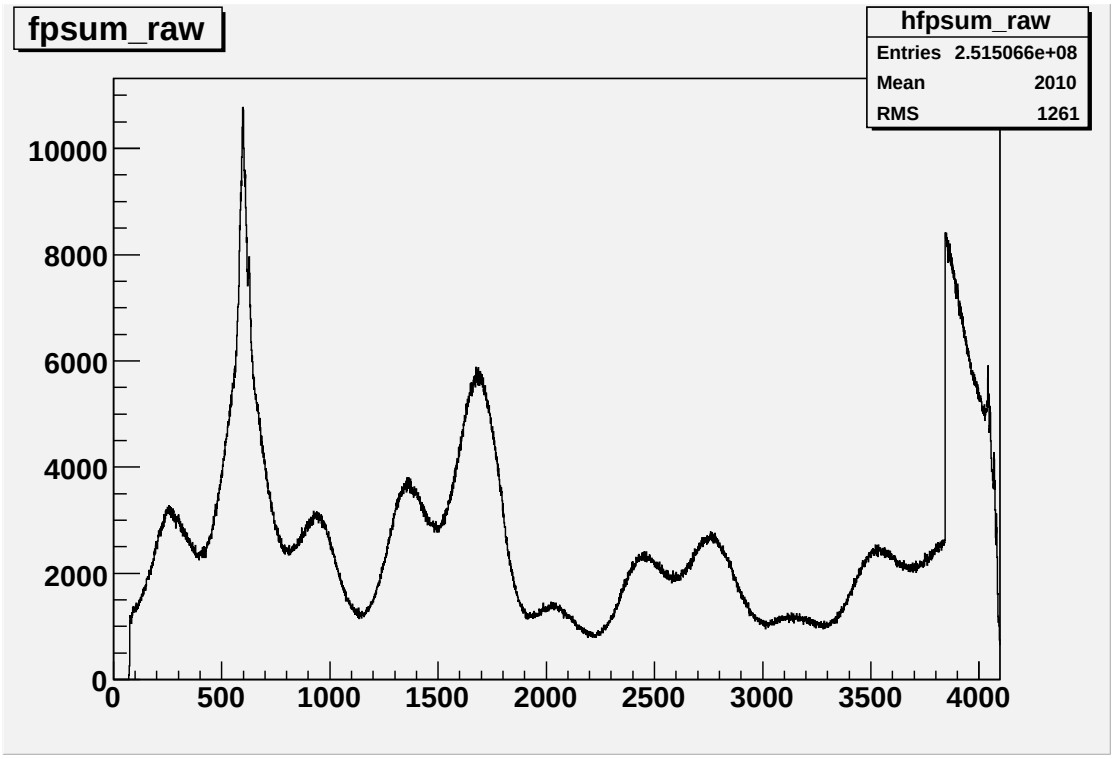

Figure 4.5: *Summed TDC spectrum containing all the individual TDC spectra from the measurement at high intensity and with five absorbers. The peak which contains the truly correlated photons and electrons is positioned on top of a substantial background of randomly correlated events.*

background reflects the time structure of the electron beam itself.

4.1.3 Number of events in the focal plane channels

The last piece of information comes from the scalers that count the number of signals in each of the channels in the focal plane. The scalers count all signals that arrive to the module during the time the module is "open" and not inhibited. Inhibit-signals are sent to the scalers when the latch in the trigger system is closed and no events from the in-beam detector can be accepted, and also during the first millisecond of the beam.

The number of counts in each of the 62 focal plane channels are shown in the histogram in Figure 4.6. In this histogram, the effect of the different widths of the odd and even channels, respectively, is seen very clearly. The difference in overlap between two scintillating sticks, as seen by the electrons that come from the tagger magnet, differs by approximately a factor of 2 between odd and even channels. When calculating the tagging efficiency, the differences between odd and even channels should cancel, as there are more photons related to electrons that hit the wider channels and vice versa.

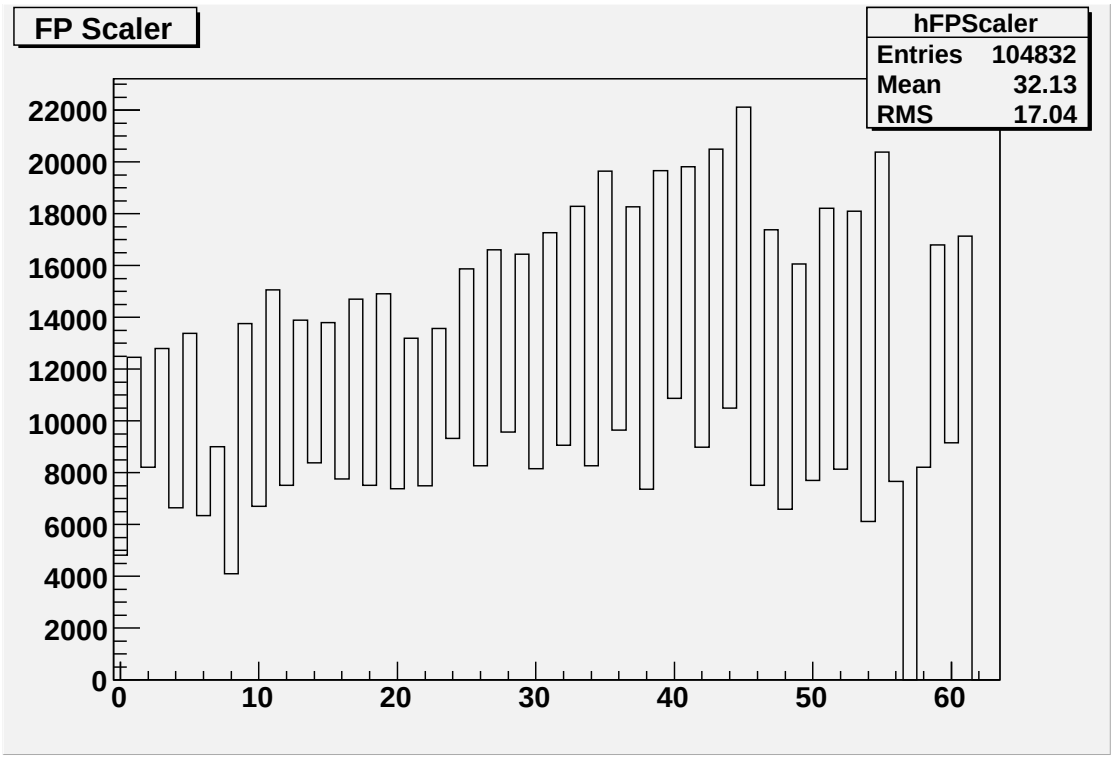

Figure 4.6: *Histogram showing the number of events in each of the focal plane channels. The "odd-even" effect, with different numbers of events in channels with odd or even number, is due to the different sizes of the channels. Channel 57 is empty due to malfunctioning electronics.*

4.2 Extraction of the number of photons, N_γ

The number of photons that pass unaffected through the absorbers needs to be extracted from the data, as this corresponds to the numerator of the tagging efficiency, scaled with the attenuation. This extraction is made by applying a stricter condition on timing between the in-beam detector and the hodoscope, and by requiring that the energy detected in the in-beam detector corresponds to that of a full-energy photon. A subtraction of random coincidences will also be made. The steps in the analysis will be described in this section.

4.2.1 Selection of prompt events

Alignment of TDC:s

The first step of the analysis was to align all the TDC-spectra. As seen in Fig. 4.4 (the sum of all the individual TDC-spectra) the prompt peaks are not in the same position for all focal plane channels. The alignment was achieved by fitting Gaussian peaks to all the spectra from the measurement with zero absorbers and recording the centroid TDC channel. An "offset" - the distance between the centroid TDC channel and an arbitrarily chosen point (same for all TDC channels) - was calculated for each focal plane channel and this number was added to the TDC value for all the events. Using this process, the raw TDC spectrum shown in Figure 4.5 was transformed into the spectrum shown in 4.7. The summed prompt peak is much more distinct in this figure, since all the individual peaks are in the same position.

The prompt peaks should, ideally, be in the same position for all the different measurements. However, inspection of the data showed that this was not the case. Individual TDC-spectra for all the different tagging efficiency measurements, for focal plane channel 0 and 61, are shown in Figure 4.8. The runs are sorted after the time so that the upper one (black) is the very first measurement that was made and the one furthest down in the list (brown) was the last one that was made approximately 15 hours later. An inspection of the spectra shows that the prompt TDC-peaks from the very first measurement are positioned slightly to the right of all the other measurements. The discrepancy is approximately 5 channels, which corresponds to a little more than 1 ns. This deviation seems to be the same for all the individual focal plane channels, and not only for channel number 0 and 61 that are shown in the figure. Apparently, something happened between (or during) the first two measurements which shifted the position of all the peaks — possibly some module in the trigger system, which starts all the TDC:s, did not reach thermal equilibrium until a few hours into the measurement. The cause for the change is still unknown, but the deviations can be corrected for in the analysis by choosing different prompt regions for the different runs.

Another issue is the stability in the timing information from different sorts of events, for example events with different energies. This was tested by separating the TDC spectrum into two parts; one that contained events that had deposited a large amount of energy in the in-beam detector and one that contained the low-energy events. The limit was set so that the tagged energy region was above the limit and most of the background was below it. A split TDC-spectrum from a high-intensity measurement is shown in Figure 4.9, and the distributions look somewhat different. A possible explanation for

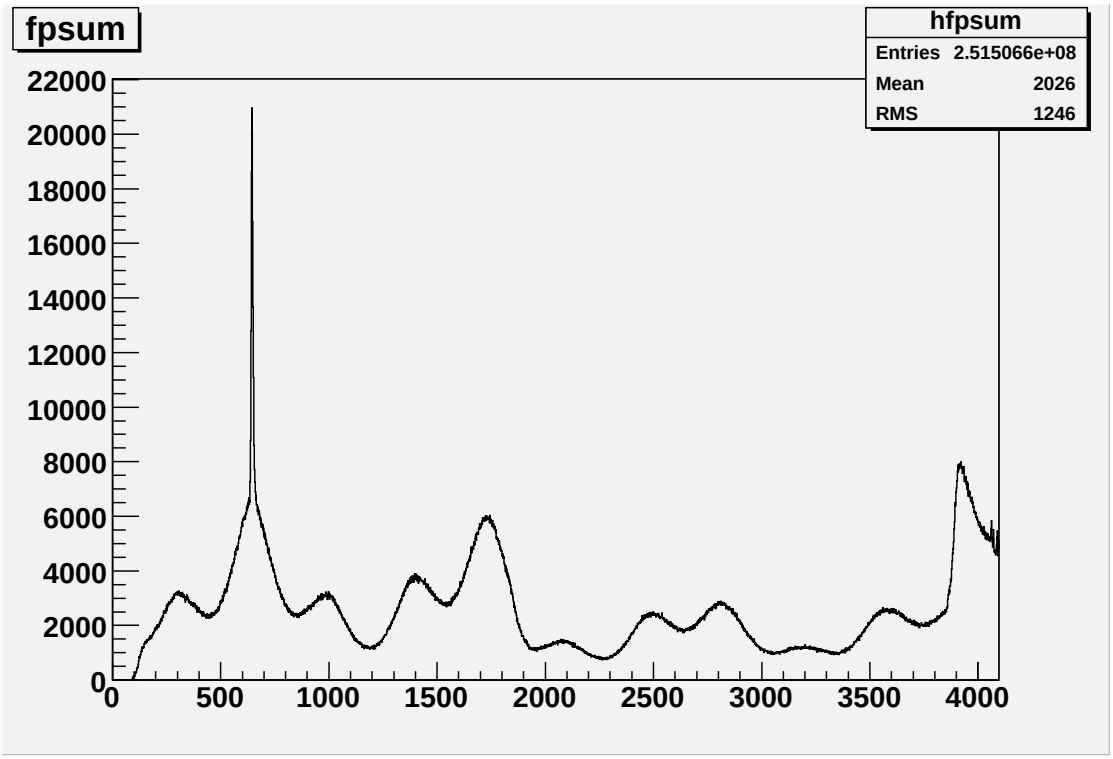

Figure 4.7: *TDC spectrum from the measurement with high intensity and five absorbers after shifting all the TDC values so that the prompt peaks are at the same position.*

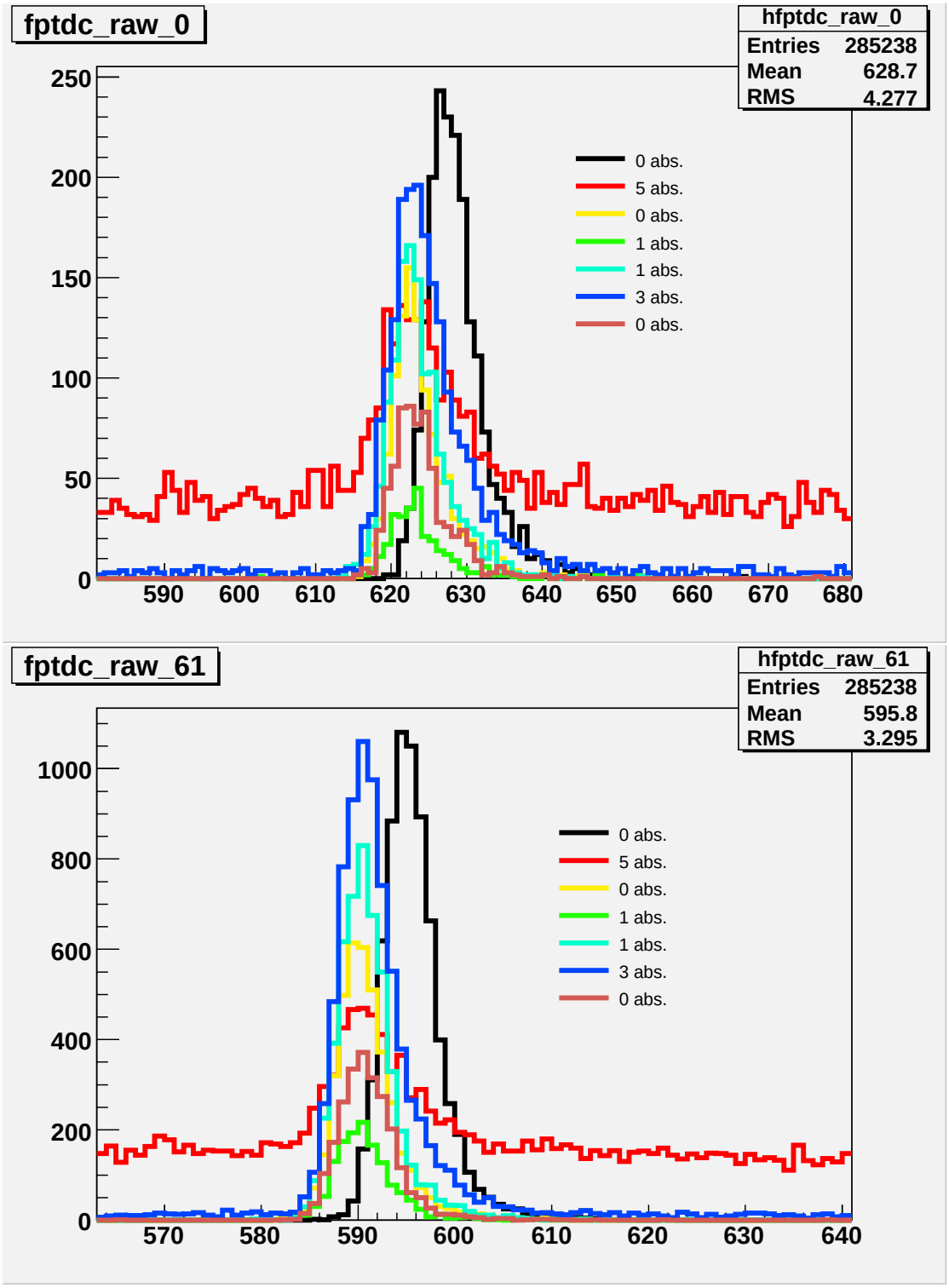

Figure 4.8: *Raw TDC spectra from focal plane channel 0 (left) and from channel 61 (right) for all the measurements. They are ordered according to the order in which they were done, with the first measurement first in the list. The peak from the first measurement is clearly positioned a little to the right of the rest of the peaks.*

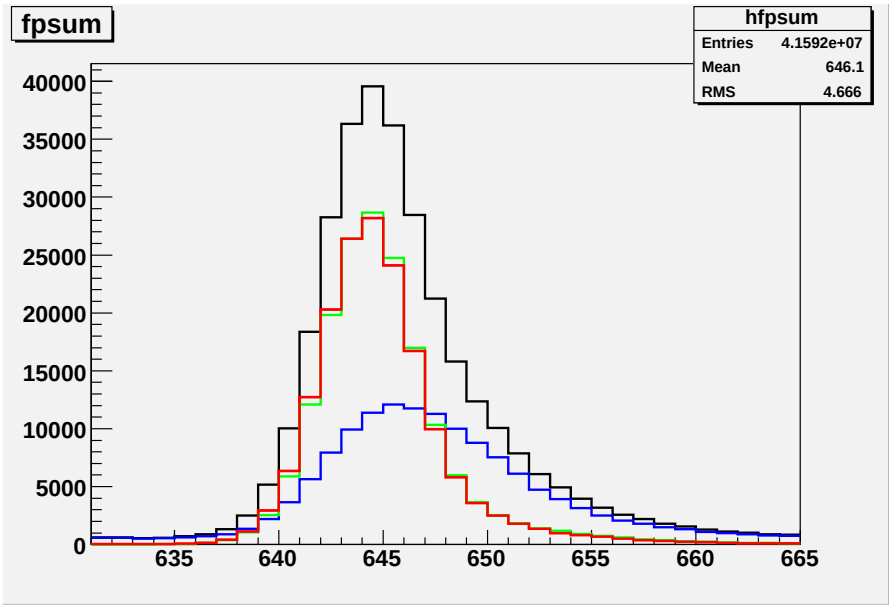

Figure 4.9: *TDC spectrum for the measurements with 3 and 0 absorbers. The black curve shows the full TDC-spectrum from the measurement with 3 absorbers, the red curve shows the events with high energy (above channel 580 in the energy-spectrum) that are most likely from tagged photons, and the blue curve shows the low-energy events that are most likely from showers of particles. The green curve is the full TDC-spectrum from the reference measurement at low intensity, where almost all the events originate from tagged photons, regardless of the energy that they deposit in the detector.*

this is that the high-energy events are from single photons hitting the center of the detector whereas the low-energy events arise from showers of particles that are created in the absorbers and are spread out over the active area of the detector. The time it takes to collect the light is, possibly, a little shorter for those events that are caused by a shower of particles.

Some support for this is given by the fact that if the TDC spectrum from a focal plane channel from a reference measurement is split into two equal parts, one with high energy and one with low energy, the TDC peaks seem to have the same shape. Therefore, it does not not seem like there is any systematic change as a function of energy, i.e. there is no visible timing walk. The reference measurement, split into two parts, is shown in Figure 4.10.

Selection of prompt area

The prompt area, which is the region in the TDC spectra where all truly correlated events will end up, was determined by visual inspection of the spectra from the reference measurement, where virtually all events correspond to true coincidences.

It was noted that the width and shape of the prompt peaks in the individual TDC spectra from different channels varied. Some spectra had a wider peak than others, which may depend on e.g. variations between the leading edge discriminators that are connected

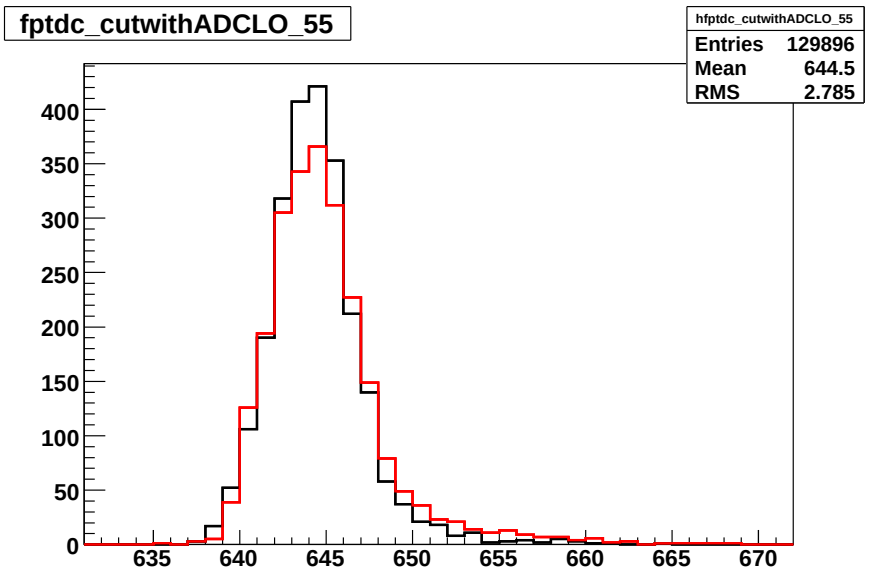

Figure 4.10: *TDC spectrum for focal plane channel 55 from a low intensity measurement, separated into high energy (black) and low energy (red). The similarity of the shapes indicates that there is no systematic dependence of the timing on the energy.*

to the focal plane detectors and on the different conversion gains (time/channel) of the different TDC:s. It was decided to set the limits for the prompt region individually for each channel. Figures 4.11 and 4.12 show two examples of chosen prompt regions.

It was decided that it is better to take somewhat larger regions rather than trying to choose them as narrow as possible, in order not to exclude any of the truly correlated events. Since a subtraction of the random coincidences inside the prompt region will be made anyway, it was not considered being crucial to minimise the width.

Since it was noted that the first measurement deviated from the others when it comes to the position of the prompt peak, the prompt region that was used for the first measurement was shifted 5 channels to the left compared to the limits set by looking at the reference measurement.

Energy spectra containing events from the prompt region only are shown in Figure 4.13. The figures are from the measurement with the highest intensity, and show channel 0 and 61. The spectra can be directly compared with those in Figure 4.3 which contain all events, regardless of the TDC value. The prompt energy spectra are cleaned up considerably by applying the condition on the TDC value, and they now contain much less background. The full-energy peak from the tagged photons can now be seen clearly.

4.2.2 Subtraction of random coincidences

As seen in the TDC spectra from the measurement at high intensity (see for example Figure 4.11), the prompt region contains many events that do not correspond to real coincidences between a photon and an electron, but are just randomly correlated events that happen to end up in the prompt region. There is no way of knowing which events

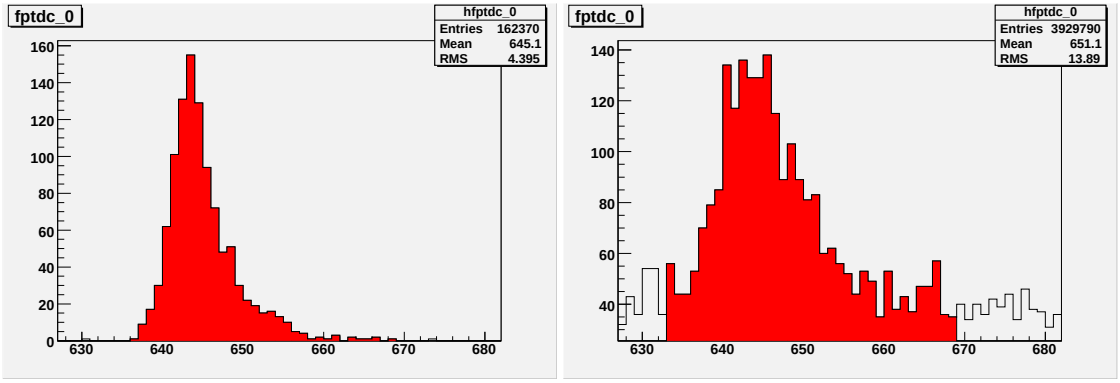

Figure 4.11: *The part of the TDC spectrum chosen as the prompt area for focal plane channel 0 is shown in red. The left spectrum is from the low-intensity reference measurement, which was used to determine what area to use. The right spectrum is from the measurement with the highest intensity.*

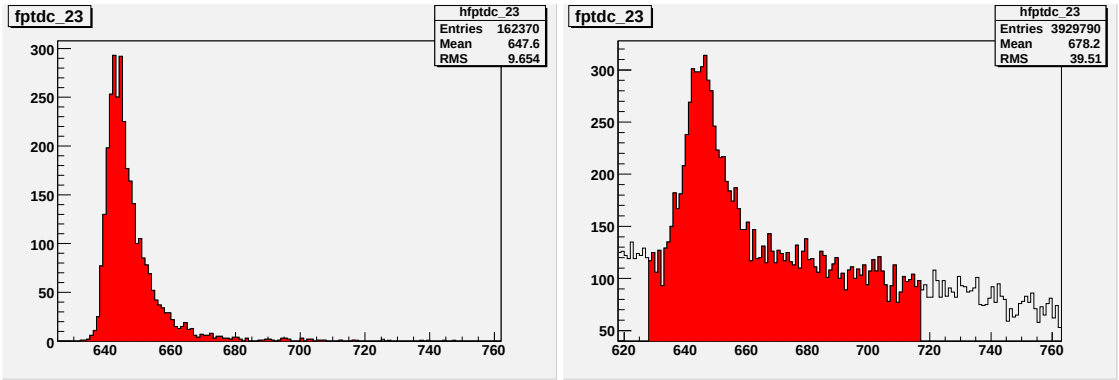

Figure 4.12: *The prompt region chosen for channel 23, shown for the reference measurement and for the one with the highest intensity. This channel 23 had an unusually wide TDC peak. This is most likely due to some problem with the electronics belonging to the detector that is part of both channel 23 and 22, as channel 22 is also a wider than most other channels.*

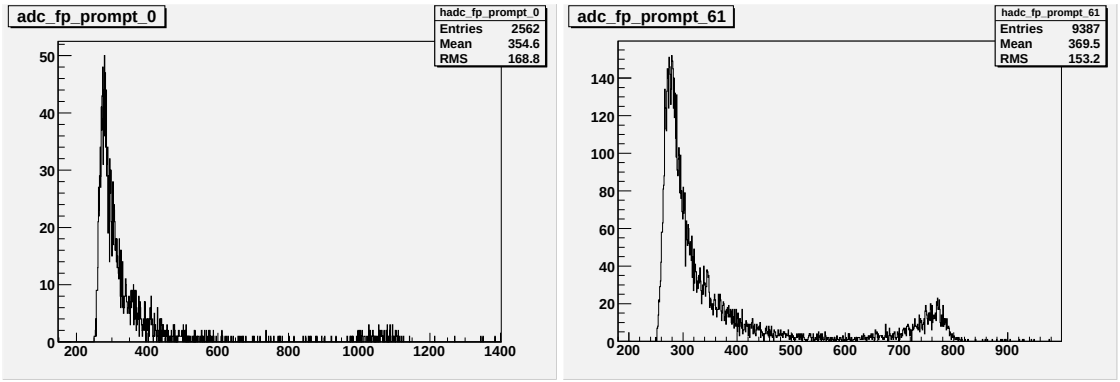

Figure 4.13: *Energy spectra from channel 0 and 61 from the measurement with 5 absorbers. The spectra contain only events whose TDC value are within the prompt region. The spectra contain much less of the background events that correspond to showers of particles from the absorbers and bremsstrahlung photons that are just randomly correlated to events in the focal plane. Therefore, the peaks from the tagged photons can be seen clearly.*

are real coincidences and which ones are not. However, it is possible to subtract the randomly correlated events in spectra of other quantities, for example the energy, of the events within the prompt region.

It is assumed that the energy distribution of the random events will be the same regardless of which part of the TDC spectrum they come from. Therefore, the part of the prompt energy spectrum that arises from randomly correlated events can be suppressed by subtracting off an energy spectrum that is constructed so that it contains random coincidences only.

An important issue is how to construct the random spectrum, so that the right amount of events are subtracted from the prompt spectrum. One method is to choose a region in the TDC spectrum that contains as many purely random events as there are inside the prompt peak. Another method is to use a large region of random events for the construction of the energy spectrum, and re-scale it in order to get the right amount of events. The latter method has the advantage of better statistics, giving a smoother and more representative energy distribution. For this analysis, the latter method was chosen. Figure 4.14 shows the chosen region of the TDC spectrum, and an energy spectrum showing the events from this region.

There are several methods to normalise the energy spectrum of random events so that it represents the same number of events as the randomly correlated events inside the prompt region. The first method tried was to use the fact that there are no truly correlated tagged photons above the full-energy peak. Therefore, all events above the peak in the prompt region must originate from random events, and the completely random spectrum was re-scaled so that the number of events above the full-energy peak were the same in both the prompt and the random spectrum. As there are very few events above the full-energy peak (see Figure 4.13), the statistics were considered too poor for using this method.

Instead, a curve was fitted to each of the TDC spectra around the prompt peak. The

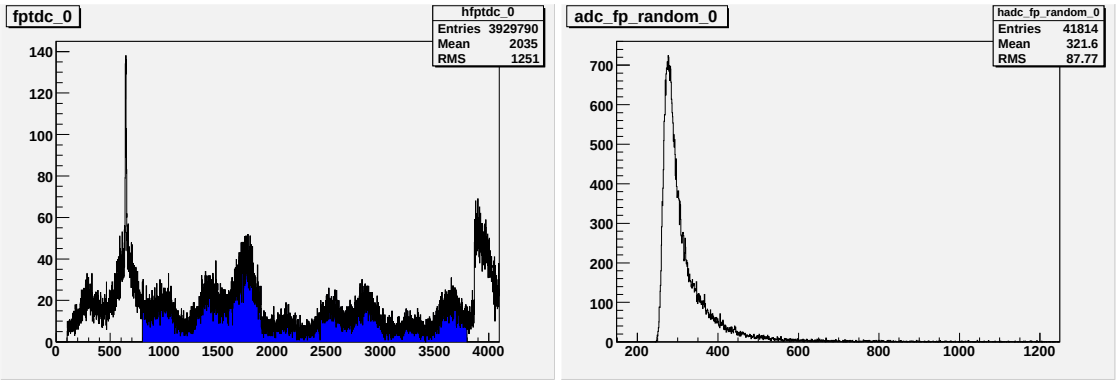

Figure 4.14: *Left: The chosen region in the TDC-spectrum for randomly correlated events, shown for channel 0 from the measurement at high intensity. The region is chosen to be the same for all channels. Right: "Random" energy spectrum from the measurement with 5 absorbers. Only those events that have a TDC value within the chosen random region are displayed. The events are from focal plane channel 0, but all the "random" energy spectra look the same regardless of the focal plane channel number.*

curve consisted of a Gaussian plus a second order polynomial. The Gaussian reproduced the prompt peak reasonably well, and by using the polynomial the background underneath could be fitted well in the region around the peak. There is nothing that explicitly shows that the background can be represented by a polynomial under the prompt peak just because it looks like it around the peak, but the assumption seems reasonable. The procedure of fitting a curve to the TDC spectrum is shown in Figure 4.15.

The fitted polynomials were integrated over the prompt region in order to find the number of random events below the prompt peaks. These numbers were used to normalise the completely random spectra before they were subtracted from the prompt spectra for each channel. This process should result in energy spectra that represent truly correlated events only. Examples of energy spectra after the subtraction of random events are shown in Figure 4.16. For comparison, the same channels as in Figure 4.13, which shows the energy spectra before the subtraction, are displayed. As seen in the figure, the low-energy part of the spectra is suppressed. What should, ideally, be left in the spectra are those photons that are in the energy region defined by the focal plane channel, and the showers of particles that are created in the absorbers by photons within this region.

In the measurements with zero and one absorber, the random coincidences are very few and it is not possible to make a reliable fit to the background of random coincidences. Therefore, it was decided not to do any subtraction of random events for those measurements. The error made by not making any correction for random coincidences was estimated using the summed TDC-spectrum from the measurement with one absorber with the highest intensity. The number of events in a region of random events that was similar to the region underneath the prompt peak was divided by the total number of counts in the prompt region. The summed spectrum was used in order to get somewhat better statistics. The prompt and random regions that were used are shown in Figure 4.17. The prompt region that was chosen is an "average" of the individually

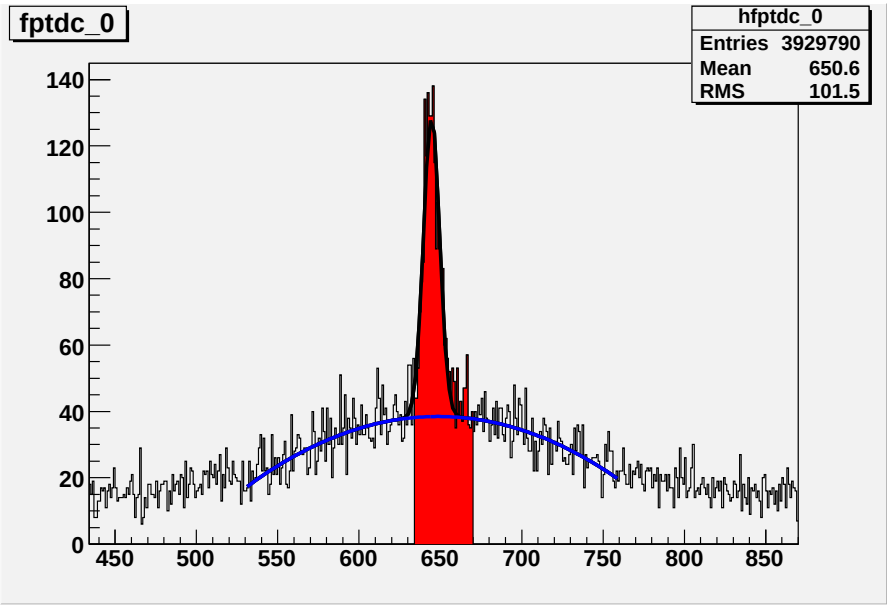

Figure 4.15: *The normalisation of the energy spectrum from purely random coincidences was made by fitting a curve to each of the individual TDC spectra. The figure shows a TDC spectrum from a high-intensity measurement, and the curve that was fitted to the area that contains the prompt peak. The chosen function that was fitted to the spectra was a Gaussian (for the peak) and a second order polynomial (for the background of random events). The region high-lighted in red is the prompt region for this certain channel, and the number of random events in the prompt peak was found by integrating the fitted polynomial function (blue) over this region. The random energy spectrum, of which an example is shown in Figure 4.14, was re-scaled so that it contained as many events as the integral under the polynomial.*

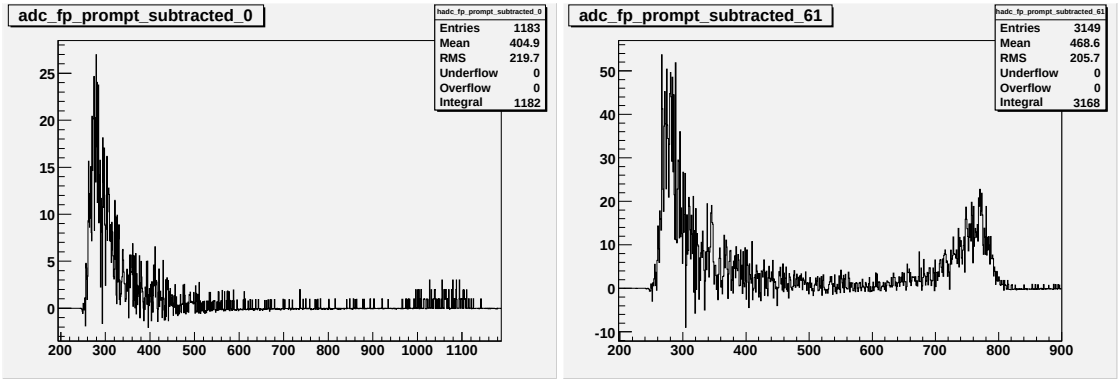

Figure 4.16: *Same energy spectra as in Figure 4.13, but now a subtraction of random events has been made. Some fraction of the low-energy background still remains, just like it should, because of the showers of particles created in the absorbers by tagged bremsstrahlung photons that are truly coincident with events in the hodoscope.*

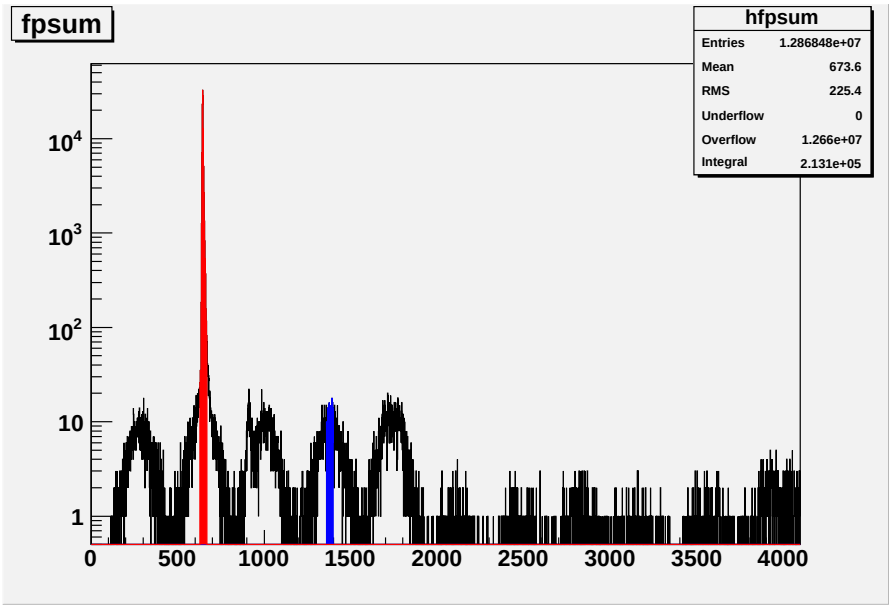

Figure 4.17: *The summed TDC spectrum from the measurement with the highest intensity that was made with one absorber. The random coincidences are very few - on a linear scale the random coincidences are not visible. The error that is made by not making any subtraction of random events inside the prompt peak, was estimated by calculating the fraction between the number of events in the random area (blue) and the number of events in the prompt area (red). As the spectrum is the sum of all the channels, an "average" of the prompt regions that have been set for each channel was used. The fraction was 0.2% which was considered being negligible. It should also be noted that it is only a fraction of the random events from the prompt region that are inside the full-energy region, meaning that the error in the tagging efficiency caused by not excluding random coincidences is even smaller than 0.2%.*

set regions for each of the channels.

The fraction between the number of events in the random region and the prompt region was determined to be approximately 0.2%, which was considered being a negligible correction. It should also be noted here, that this is an estimate of the number of random events in the entire prompt energy spectrum. Since only those events that are in the full-energy region will be counted, the correction will actually be smaller than 0.2%. For the other measurement with one absorber at lower intensity, and for the measurements without absorbers, the correction will be even less important.

4.2.3 Choosing the energy interval

As seen in the energy spectra in Figure 4.16, there are still many true coincidences that correspond to photons that have been affected by the absorbers. It is only the full-energy photons that should be counted and then re-scaled with the attenuation of the absorbers. Since the full-energy peak is not clearly separated from the low-energy background, especially not for the high focal plane numbers, it is not possible to include

the entire distribution of the full-energy events. Therefore, a region will be chosen for each of of the energy spectra, and only those events that are inside this area will be used in the analysis.

Detector stability

The response of the detector to radiation can vary a little over time due to fluctuations in, for example, the high-voltage that is applied to the PM-tubes. Therefore, the full-energy peak from the photons may move in time. The energy spectra for a certain channel, for all the measurements, are shown in Figure 4.18. It seems like the position is consistent for all measurements but the first one (shown in black). A function was fitted to the top of the peak, and it is positioned approximately 10 channels to the left of the top of the peak from the measurement with three absorbers. The trend seems to be the same throughout the focal plane.

The first measurement was made at low intensity and with good statistics in order to provide a reference, but since it deviates from the rest of the measurements when it comes to the position of both the TDC peak and the energy peak, it was decided to use the second low-intensity measurement for determining what limitation to impose on the energy spectra. The first measurement was analysed using an energy span shifted 10 channels to the left compared to the spans used for the other measurements, in order to cover the same part of the distribution. Possibly, the region should also have been chosen somewhat smaller, to compensate for an overall compression of the spectrum, but this effect was not taken into account.

Selection of full-energy region

Ideally, the resolution of the detector and the probability to capture a large fraction of the electromagnetic shower should be good enough to provide a distribution of the full-energy photons that is fully separated from the background of particles created in the absorbers. This is, however, not the case. The spectra in the upper part of Figure 4.19 show the full distributions of the unaffected, full-energy photons from the reference measurement, and the distributions is several hundreds of channels wide. As seen in the lower part of the picture, showing the high-intensity measurement, the full-energy distribution extends into the background of showers from particles created in the absorbers.

It is not possible to include the entire distribution for the measurements with absorbers because of this overlap. However, in order to make a comparison between the different measurements of the tagging efficiency, it is not necessary to count all the photons. It is enough to count the same fraction of the events for each of the measurements. Any part of the full-energy distribution can be chosen, as long as it does not extend into the low-energy background. It is preferable to choose the region so that the limits are not in areas where there are many counts, as a slight instability in the detector could then cause the number of counts, and thereby the fraction of the distribution that is counted, to vary unnecessarily much. It is also preferable to include as much as possible of the full-energy peak in order to minimise the statistical uncertainty in the number of counts.

The upper limit of the interval was set by hand for each of the focal plane channels, by looking at the reference measurement. The limit was set well above the full-energy

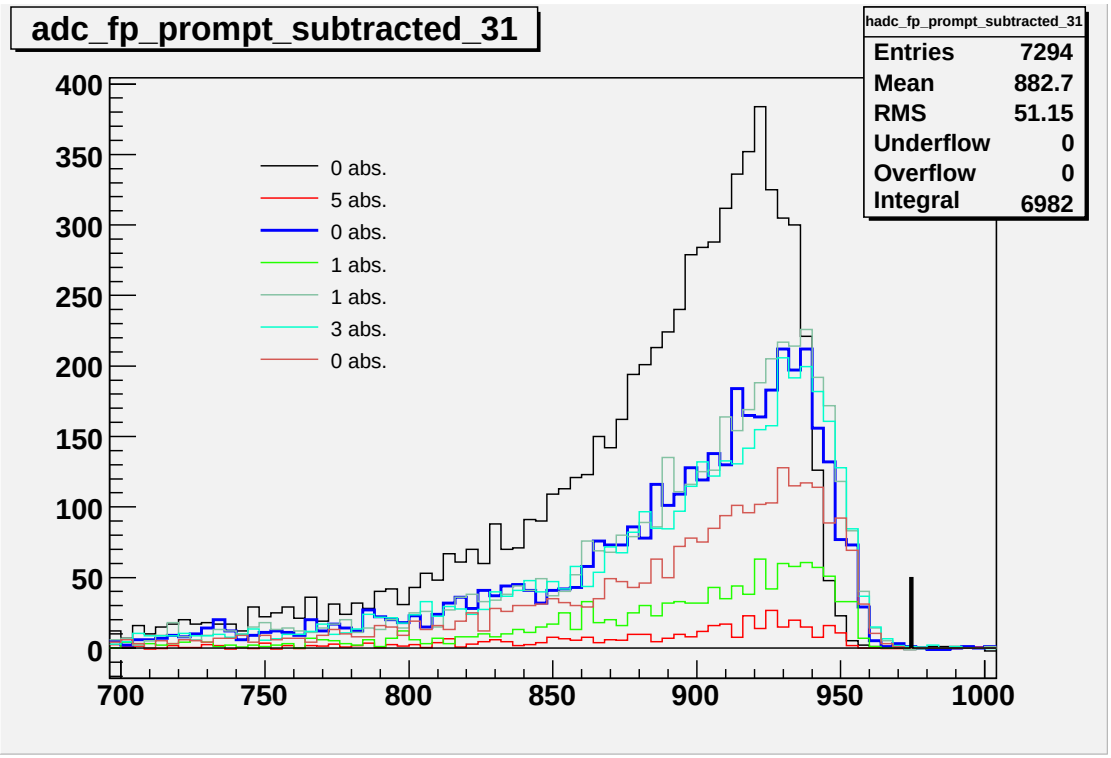

Figure 4.18: *Energy spectra from channel 32 from all the different runs. The order in which the measurements were done is the same as the order of the labels. The data from four adjacent channels in the histogram has been added (binned) together in order to make the picture clearer. All measurements but the first seem to be in the same position. The first measurement deviates from the others by approximately 10 channels - a curve was fitted to the top of the peak from the first measurement and the one with three absorbers, and the discrepancy was 10 channels. The third measurement (run number 3676, see Table 3.1), represented by the thick blue line, is the reference measurement that was used for setting the restrictions on TDC values, and also for determining what energy region to use. The black vertical line indicates the upper limit for the full-energy region that was chosen for this channel.*

peak. In Figure 4.18, the chosen upper limit for this certain focal plane channel is shown as a black vertical line. It was decided to set the lower limit for the interval at 250 ADC channels below the upper limit. The chosen intervals for the focal plane channels corresponding to the highest and the lowest energy, respectively, are shown in Figure 4.19. By using intervals constructed in this way, the lowest interval ends at channel 576. A visual inspection of the lower right part of the figure, showing the focal plane channel with the lowest energy for the measurement with the highest intensity, indicates that the full-energy region does not extend into the low-energy background, which is the most important requirement on the interval. At the same time, the interval covers most of the distribution. The exact fraction that is contained within the intervals depends on the energy that the focal plane channels correspond to, since resolution and how many of the photons whose energies are fully absorbed by the detector depends on the energy. The fraction of the total number of events contained within the chosen interval is calculated from the reference measurement. For focal plane channel number 0 the fraction is 92%, and the corresponding fraction for channel 61 is 96%.

For the very first measurement, which had a deviating full-energy peak position, the limits are moved 10 channels to the left, in order to cover the same part of the distribution.

Two other full-energy regions were also tried, one which was 50 channels wider and one that was 50 channels smaller. They all had the same upper limit. This was done in order to check if the limit has any impact on the relative tagging efficiencies. The final result from this analysis, using these two variations of the limits, shows that 250 channels is a good choice for the full-energy region. The procedure is described in Appendix B.

Background subtraction

Even though a subtraction of random events is made, and a limited full-energy interval is chosen, there may be some events originating from the background, that are inside the chosen area. Therefore, an attempt to subtract off the background was made by fitting a function to the background and then extending this function into the full-energy region. Among the simple functional forms, an exponential seemed to produce the best fit. The integral of the fitted function within the chosen full-energy region was subtracted from the number of counts in the region. The procedure is shown in Figure 4.20.

It turned out that this background subtraction does not make any large difference for the number of events in the full-energy region - the difference is much less than 1% for most of the channels. However, this does not mean that the background necessarily is much less than 1%, since it may happen that the true functional form is not an exponential. Nonetheless, it indicates that the correction is small. It does not seem possible to make a more reliable background subtraction than the one that was performed, and since it seems to be a small effect, it was decided to not do any background subtraction at all.

4.2.4 Compensation for the attenuation

The photons that have been extracted from the data as described above are, ideally, only those that passed though the absorbers completely unaffected. The number of incident photons can then be found by dividing by the attenuation factor:

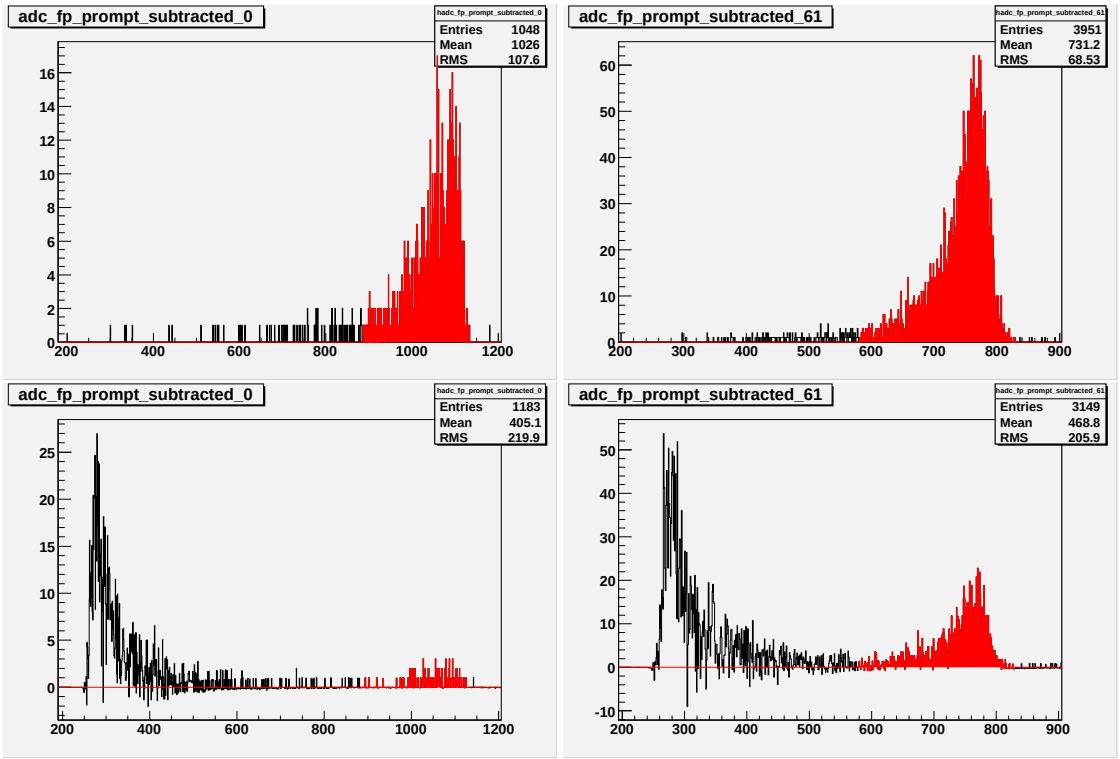

Figure 4.19: *Energy spectra with the chosen "full-energy" region in red. Upper left: Energy spectrum from channel 1, from the reference measurement at low intensity. Below: Same spectrum but for 5 absorbers. To the right, the same spectra but from channel 61 are shown. The red regions are the chosen energy intervals for those channels, and only those events that are inside these regions will be counted and used for the calculation of the tagging efficiency. The intervals cover large parts of the full-energy distributions, as seen in the upper part of the figure. Still, the intervals do not extend into the background. Channel number 61, shown in the lower right of the figure, is the channel with the lowest photon energy and hence the one where the chance for an overlap is the largest. The figure seems to indicate that only very little of the background is included in the chosen interval.*

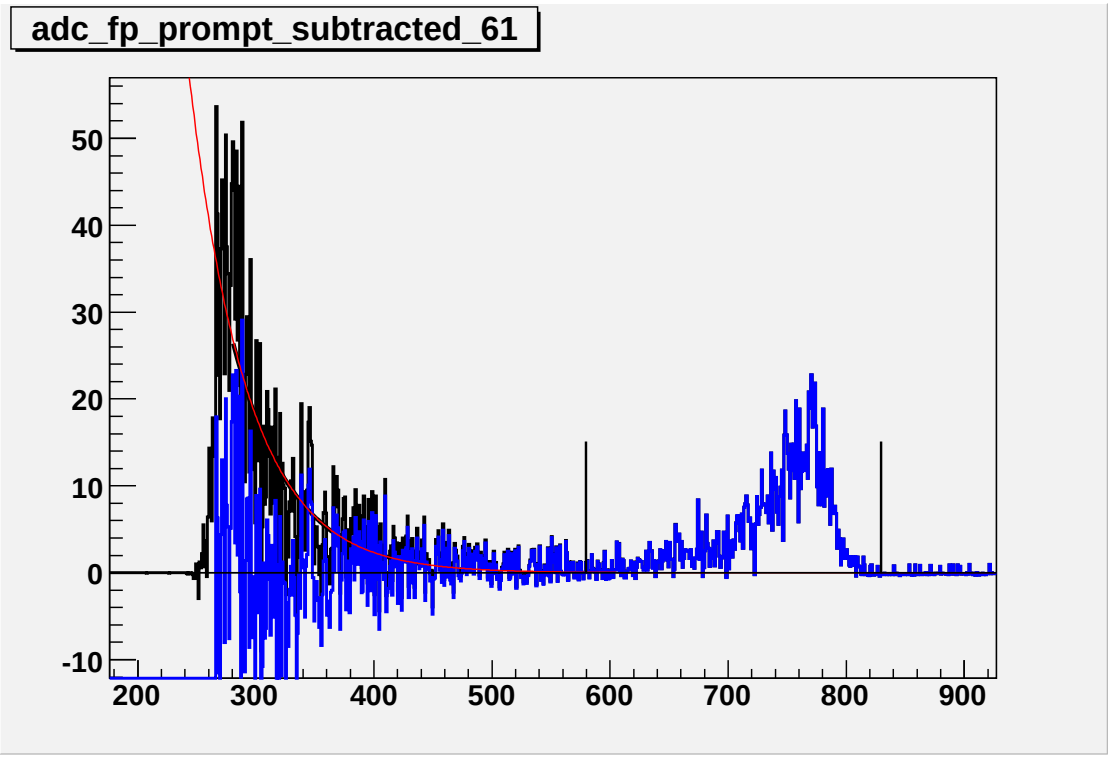

Figure 4.20: *A background subtraction was made by fitting an exponential function to the low-energy background. The black curve is the randoms-subtracted energy spectrum from channel 61. The red line shows the exponential curve that was fitted to the background between channel 280 and 440 in the energy spectrum. In the blue histogram, the fitted exponential has been subtracted from the original histogram. The difference between the two histograms within the chosen "full-energy" interval is negligible. However, it should be noted that the true functional form of any background within the full-energy region is not necessarily an exponential, just because such a function seems to fit in the low-energy region. Nonetheless, it indicates that the background within the chosen full-energy interval is small.*

Nr of absorbers	Total thickness (g/cm^2)	Estimated error (g/cm^2)
1	26.944	0.25
3	79.763	0.44
5	134.680	0.56

Table 4.1: *The thickness of the different combinations of absorbers and the estimated errors in the thicknesses. The uncertainty in thickness for an individual absorber was added in quadrature to get the uncertainties for the combinations of several absorbers.*

$$I_0 = \frac{I}{e^{-\mu \cdot dx}}. \tag{4.2}$$

The attenuation coefficient μ depends on the photon energy. For every focal plane channel, the coefficient that applies to the centroid energy of the channel is used. A list of all centroid energies and the attenuation coefficients is found in Appendix A.

The lead absorbers came with a specification of the thicknesses, measured by the National Bureau of Standards (now called NIST). Their weight and diameter were also measured using a scale and a caliper, and the thicknesses agree well with the specification. The thicknesses, given by the specification, are presented in Table 4.1. These were the numbers that were used for the analysis.

The re-scaled number of photons, N_γ, found by dividing the number of detected photons by the attenuation factor, is the numerator of the tagging efficiency; $\epsilon_{tag} = N_\gamma / N_{fp}$.

4.2.5 Alternative method to find the number of photons

An alternative method to extract the number of photons was also investigated. The two methods agree up to the selection of a prompt area, but take different paths after that. The new method does not directly include any subtraction of random events, but takes advantage of the fact that the energy distribution of full-energy photons is the result of the response of the detector to photons of different energies only.

The distribution of full-energy photons can be seen in the upper part of Figure 4.19, that shows the prompt events from two focal plane channels for the reference measurement, which contains almost exclusively tagged photons. A function can be fitted to each of the energy spectra, and these shapes define what the distributions of full-energy photons must look like also in the cases where random coincidences and low-energy background from the absorbers is present.

Corresponding energy spectra from the measurement at the highest intensity is shown in the lower part of Figure 4.19. If the high-energy part of the energy distributions for the different intensities are compared, the shapes are very similar in this region. This should be the case if the background in the high-energy region is very low. Considering the distribution of random events (shown in Figure 4.14), and the fact that most of the background produced by tagged photons that are affected by the absorbers have substantially lower energy than the unaffected photons, it is reasonable to expect that the high-energy part of the prompt energy distribution really represents full-energy photons only. Therefore, this part of the spectrum can be used to quantify the distribution of full-energy events.

The high-energy part of the true full-energy peak was found to be well represented by a Landau function. To quantify the characteristics, a Landau function was fitted to the spectra taken at low intensity (upper part of Figure 4.19). Two of the parameters in this function define the width of the function and the mean value of the distribution, respectively. The third parameter provides an overall scaling of the distribution. The first two parameters depend on the shape of the energy distribution, whereas the scaling only depends on the amount of photons.

Another Landau function is then fitted to the high-energy region of the energy spectrum from a high-intensity measurement, under the condition that the first two parameters are the same as those found when fitting the function to the low-intensity measurement. The fraction between the two scaling parameters gives the relation between the amount of full-energy photons that hit the detector in each of the measurements. Since virtually all events in the low-intensity measurement correspond to tagged photons, a rescaling of this number with the fraction between the two scaling factors will give the number of photons in the high-intensity measurement. In order to get results comparable to the ones from the previous method, it was decided to just count the events in the low-intensity measurement that are within the same "full-energy" region that was used for the previous method, and rescale this number. This gives numbers of photons that are directly comparable to the previous method, but found in a different way. Figure 4.21 shows the entire procedure.

The numbers of counts found by this method coincided well with the numbers found by the previous method for all measurements except the one with 5 absorbers. In this case, the un-weighted average number of counts over the entire focal plane was found to be $\sim 2\%$ larger than was found with the previous method. However, this method also suffers from the poor statistics of the high-intensity measurements. The uncertainties in the scaling factor found by fitting the function to the energy spectra from the 5 absorber measurement is approximately, in average, 7%. Since the number of photons is directly proportional to this factor, the uncertainty in the final number of photons is at least 7%. There is also an error in the fit to the reference measurement, and a statistical error in the number of counts in the reference measurement.

The difference between the two methods turned out to be small (only 2% for the measurement at the highest intensity), and this discrepancy is covered by the uncertainty from the fitting. It is not straightforward to determine which method is the optimal one to use, but the fact that they coincide well suggests that either method can be used. The consistency in the results is reassuring, as it shows that the number of photons found is the same, within error bars, when two different methods are used.

4.3 Extraction of the Number of Counts in the Focal Plane Scalers, N_{fp}

The number of events in each of the focal plane channels is counted by the scalers, as shown in the electronics scheme in Figure 3.9. As established in section 2.9, the number of events should not be corrected for the beam-induced background, but only for the background in the room. The background in the room was measured by turning off the beam but keeping everything else unchanged, including the trigger. Hence, a signal in the in-beam detector is still needed in order to get a trigger, and a coincidence between

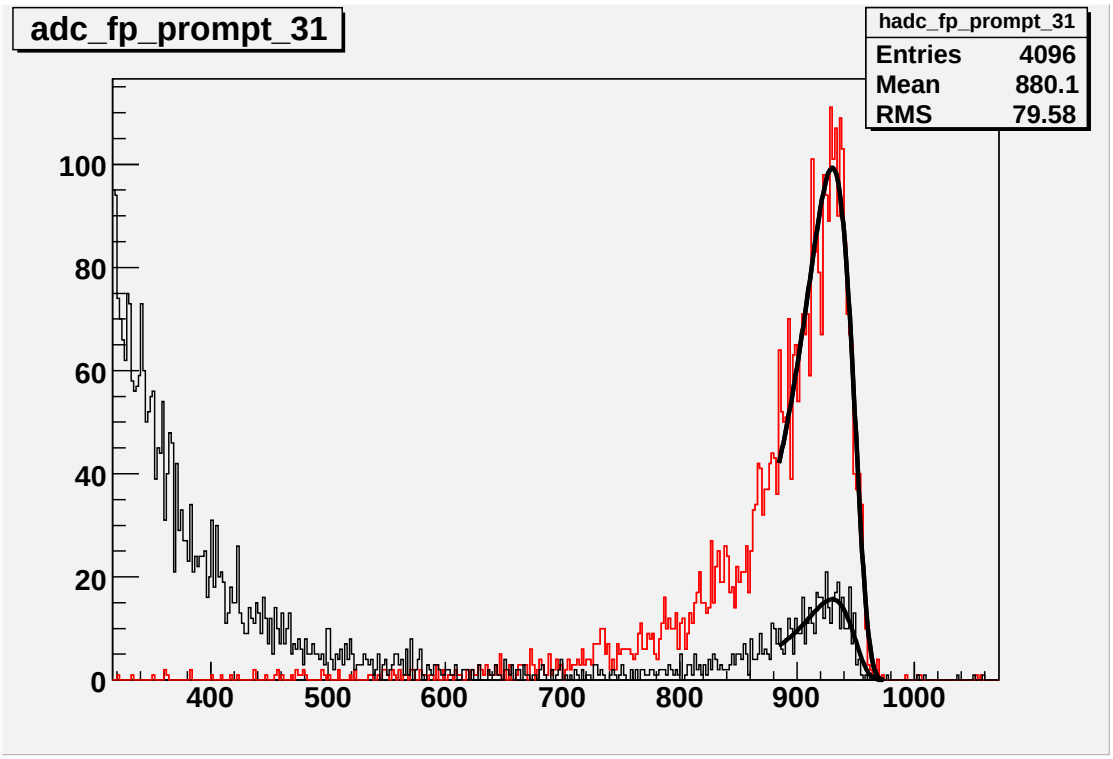

Figure 4.21: *The procedure of finding the number of photons by using the shape of the full-energy distribution. First, a Landau function is fitted to the high-energy part of the full-energy peak in the clean spectrum from the reference measurement (red). Then, a Landau function with the width and position fixed to the values found in the previous fit, is fitted to the spectrum for a measurement at higher intensity (black, here with 5 absorbers). The number of counts in the reference measurement is then rescaled with the fraction of the heights of the fitted functions. The region to which the functions are fitted vary for the different focal plane channels. The width of each of these regions was 90 channels, and they end at the channels that were determined to define the upper limit for the peak, as described in Section 4.2.3. The histograms are re-binned so that the number of counts in two adjacent bins are added. Still, there are not very many counts in each bin. It was noted that the fit was improved by setting the weights of all the bins to the same value, regardless of the number of counts in the bins. The error in the scaling factor for the high-intensity measurement was estimated by performing the same fit but without setting all weights to the same value, in order to get the entire error that results from both the uncertainty in the fit itself and from the statistical uncertainty in the data.*

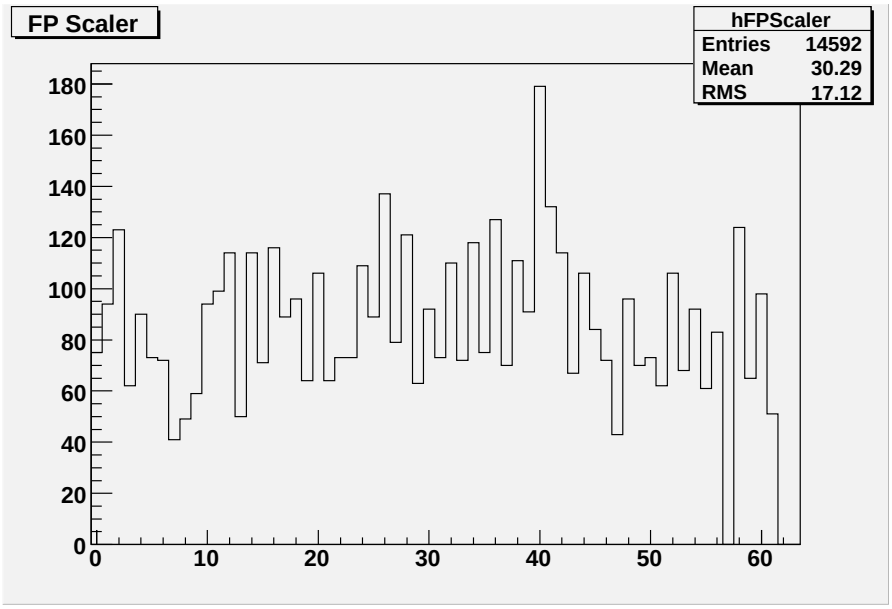

Figure 4.22: *The number of hits recorded in the scalers for each of the focal plane channels during the measurement of the background in the room. The scalers are recording signals from the focal plane channels as long as they are not inhibited. The inhibit signals shut down the scalers during the time the electronics is busy with processing events.*

the in-beam detector and the focal plane is required to get a read-out. Two background measurements were done during the course of the experiment. The characteristics of these two measurements seemed to be the same, and it was decided to use the first one to do the correction, as it was done for a longer period of time than the second.

Before the background can be subtracted from the tagging efficiency measurements, the background must be re-scaled so that it represents the same time as the actual time during which the scalers were open for recording signals during the measurements. The focal plane scalers are inhibited during the same time as the latch is closed. Hence, the time during which they are open is not the same as the actual clock time for the measurement.

In Figure 4.22, the number of counts in each focal plane channel during the long background measurement is shown. Since a coincidence between in-beam detector and focal plane is required in order to get a read-out, there are very few events that are read out. This means that the latch is closed only for a very small time, and the same applies to the scalers. Therefore, the live-time of the system can be approximated to be 100%, and the time the scalers were recording the background is the same as the actual clock time for the measurement.

For the tagging efficiency measurements, the scalers were inhibited for a much larger fraction of the time. Therefore, the actual live-time of the system, as opposed to the actual clock time, is needed. The total dead-time of the system can be calculated by summing the time it takes to process all the events. The events read out by the computer take approximately 1 ms to process, and in the case of a “fast clear”, when the event

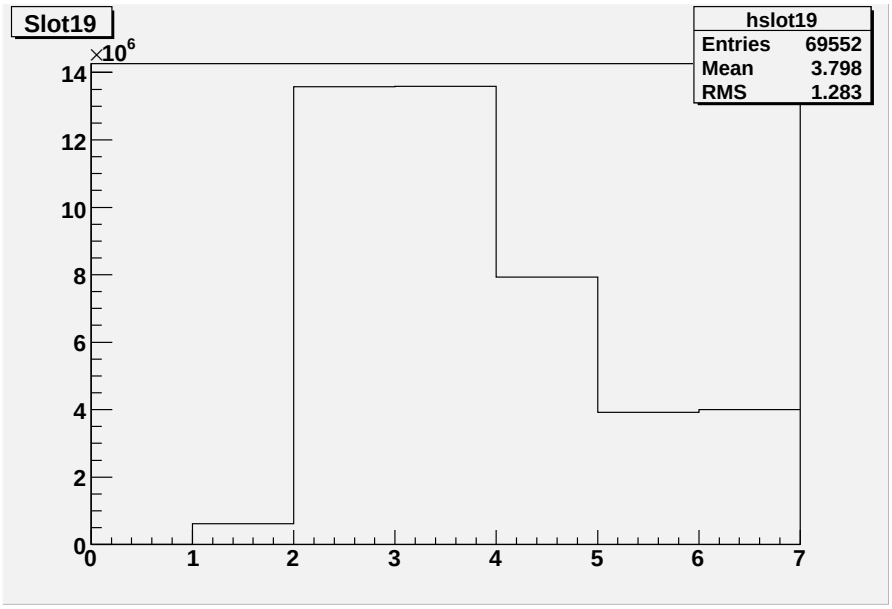

Figure 4.23: *The accumulated number counts in the scalers for the measurement with 5 absorbers. Bin number 3 contains the total number of triggers, bin 4 contains the number of signals that come out of the latch. Bin 5 is the number of interrupts sent to the computer and bin 6 is the number of fast clears. The number of interrupts and "fast clears" sum up to the number of signals from the latch. The number on the x-axis refers to the number of the bin to the right.*

is not read out, the scalers are inhibited for approximately 20 μs. The time it takes to complete a read-out of the data was calculated from a high-intensity run that was done earlier in the run period, using the same electronics but with a different trigger system which did not require a coincidence between a trigger and a focal plane hit. At the high intensity used for this measurement, the system was swamped by triggers and the dead-time was virtually 100%. Hence, the time for a read-out can be calculated directly from the number of interrupts per second. The number of interrupts (read-outs) were around 1250, which gives a read-out time of 0.8ms.

The number of read-outs and "fast clears" are counted by scalers. An example of a histogram containing the total number of events in the scalers is shown in Figure 4.23. The total dead-time was used to calculate the total time during which the scalers were counting during the measurements. This time was divided by the time for the background measurement (which was assumed to have 100% live-time), and this factor was used to re-scale the number of background counts in each of the focal plane channels. The re-scaled numbers of events in the scalers now represent the entire background that is accumulated during the measurement, and are subtracted channel by channel.

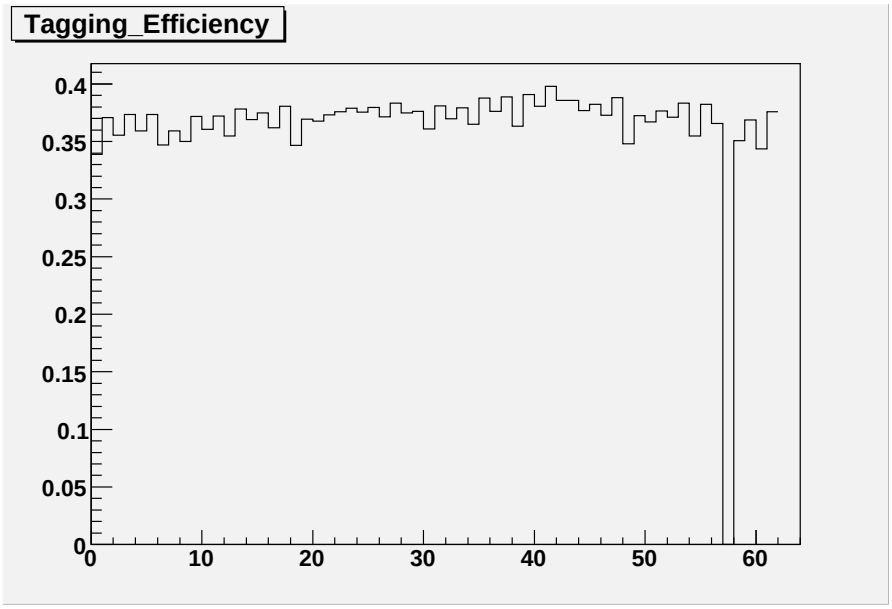

Figure 4.24: *Tagging efficiencies for each of the focal plane channels for the reference measurement. The electronics of channel 57 does not work properly and therefore the channel is empty.*

4.4 Calculation of Tagging Efficiencies

The tagging efficiency is now simply calculated by dividing the number of incident photons by the number of counts in the focal plane for every channel. The tagging efficiency for the reference measurement at low intensity is shown in Figure 4.24. The tagging efficiency varies between 35 and 40% for the different focal plane channels. It is approximately constant over the entire focal plane, except for in the upper part where there seems to be a slight dip. The tagging efficiency is a function of many variables, and one of them is the energy. Therefore, the tagging efficiency over the focal plane is not always constant. However, for these particular settings of electron energy, radiator thickness and material, tagged region etc., it turns out to be approximately constant.

4.5 Error Estimation

The complete function used to calculate the tagging efficiency, for each channel, is the following:

$$\epsilon_{tag} = \frac{N_{prompt,in\,peak} - \frac{N_{random,in\,prompt\,area}}{N_{events\,in\,random\,area}} * N_{random,in\,peak}}{N_{FP\,scalers} - \frac{Runtime*Livefactor}{Runtime,bcg} * N_{FP\,scalers,bcg}} * e^{Att.coeff*Abs.thick}, \quad (4.3)$$

where the different factors are explained in Table 4.2 together with the estimated errors in the each of the parameters. The errors are of both statistical and systematic origins. The number of counts in a given interval of the TDC spectra and energy spectra

were assigned uncertainties that are the square root of the number of counts. Also the number of counts in the focal plane scalers were assigned uncertainties equal to the square root of the number of events.

The time during which the background measurement was done could only be deduced from the logbook, where only the minute during which a run was started and stopped was written down. The error in the runtimes of the rest of the measurements, which were done at high enough intensities that the scalers were read out every other second, were estimated to 2 s. The variation of the attenuation coefficient over the energy range of a focal plane channel was used as an estimate of its uncertainty. The additional intrinsic uncertainty in the attenuation coefficients themselves was not considered.

The uncertainty in the attenuation coefficient was set so that the possible span of coefficients covers the energy range of the focal plane channel. The error in the "live-factor" originates mostly from the uncertainty in the time it takes for the computer to read out the contents of the modules. It was estimated that the total uncertainly in the livefactor is 10%.

The error in the thickness of the absorbers was estimated using the two different sets of values for the thicknesses - the ones given by the specification and the ones that were measured. The largest discrepancy between a pair of values was 0.25 g/cm^2, and this was used as the uncertainty in thickness for the individual absorbers. In order to get the total uncertainty for the measurements with several absorbers, the individual uncertainties were added in quadrature.

These parameters are assumed to be independent, and hence the following form of the Gauss error propagation formula is used for calculating the total uncertainty in the tagging efficiencies:

$$\sigma^2_{\epsilon_{tag}} = \sum_{x_i} \left(\frac{\delta \epsilon_{tag}}{\delta x_i} \right)^2 \cdot \sigma^2_{x_i}. \tag{4.4}$$

The uncertainties that turned out to be most important were those in the number of prompt counts and in the uncertainty of the absorber thicknesses. At low intensities, where the background subtraction in the focal plane scalers plays an important role, the uncertainties in the number of events in the focal plane during the background measurement also made a difference for the total error. The other uncertainties contribute only marginally to the total error.

4.6 Calculating the Average Tagging Efficiency

In order to get data points with smaller statistical uncertainties, the average tagging efficiency for the entire hodoscope region was calculated according to the following formula:

$$\bar{\epsilon}_{tag} = \frac{\sum_{i=0}^{61} \epsilon_{tag,i} \cdot N_{fp,i}}{\sum_{i=0}^{61} N_{fp,i}} = \frac{\sum_{i=0}^{61} \frac{N_{\gamma,i}}{N_{fp,i}} \cdot N_{fp,i}}{\sum_{i=0}^{61} N_{fp,i}} = \frac{\sum_{i=0}^{61} N_{\gamma,i}}{\sum_{i=0}^{61} N_{fp,i}} \tag{4.5}$$

where $\epsilon_{tag,i}$ is the tagging efficiency, $N_{fp,i}$ is the number of counts in the focal plane scaler, and $N_{\gamma,i}$ is the number of photons that are associated with focal plane channel i.

Variable	Description	Estimated error
$N_{prompt,in\ peak}$	Number of prompt counts inside the full-energy peak	$\sqrt{N_{prompt,in\ peak}}$
$N_{random,in\ peak}$	Number of counts inside the full-energy peak, from the random region in the TDC spectrum	$\sqrt{N_{random,in\ peak}}$
$N_{random,in\ prompt\ area}$	Number of random events within the prompt TDC area, found by fitting a function to the background	$\sqrt{N_{random,in\ prompt\ area}}$
$N_{events\ in\ random\ area}$	Total number of events within the chosen region of random events	$\sqrt{N_{events\ in\ random\ area}}$
$N_{FP\ scalers}$	Number of counts in the focal plane scaler	$\sqrt{N_{FP\ scalers}}$
Runtime	Time for the measurement	2 s
Livefactor	Livefactor for the measurement; calculated using the number of interrupts and fast clears, and the respective time for those	0.1*Livefactor
Runtime,bcg	Time during which the background was measured	60 s
$N_{FP\ scalers,bcg}$	Number of counts in the focal plane scaler	$\sqrt{N_{FP\ scalers,bcg}}$
Att.coeff	Attenuation coefficient that applies to the center of the channel	0.0001 cm^2/g
Abs.thick	Thickness of the absorbers in $g/cm2$	See Table 3.1

Table 4.2: *All the different quantities that are used for the calculation of the tagging efficiency, together with the estimated uncertainties.*

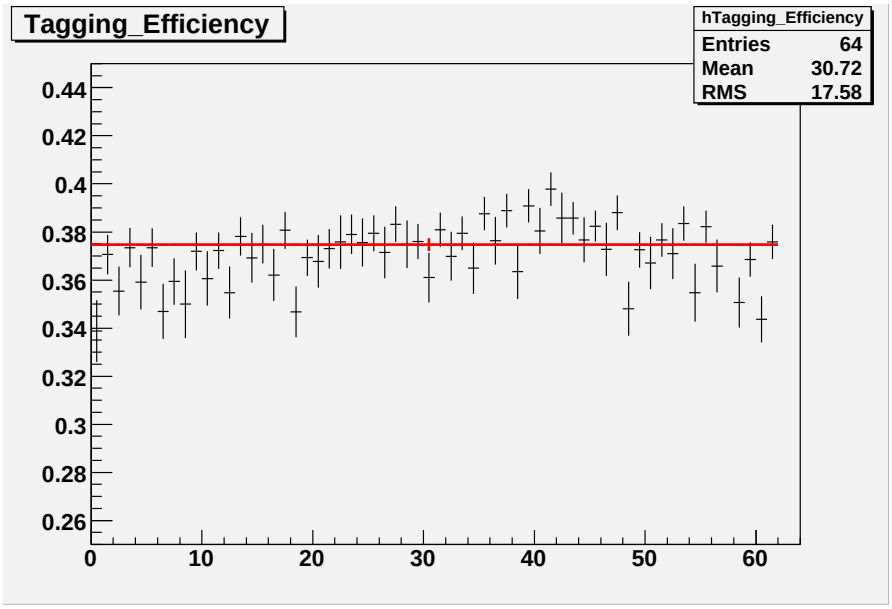

Figure 4.25: *The tagging efficiency for each of the channels for the reference measurement (black), and the weighted average (red). Note that the error bar on the average is much smaller than the individual errors.*

Also the uncertainty in the average was calculated using Eq. 4.4. The average tagging efficiency for the reference measurement is shown in Figure 4.25, together with the tagging efficiency for all the individual channels. The error bars of the average is reduced significantly due to the better statistics. For the measurements at higher intensities, where the statistics is very poor, it is necessary to consider the average instead of the individual channels in order to get reasonable uncertainties.

4.7 Correction for Ghost Events

The signals from the focal plane detectors are divided into three different types in Equation 2.6; electrons that have emitted bremsstrahlung, beam-related background that is proportional to the beam intensity, and background in the room. Actually, there is another source of "events" that was not mentioned before, namely the so called "ghost events". These "events" do not correspond to physical particles but are the result of the electronics of the setup. When two channels in the focal plane that are next neighbours are hit simultaneously, a signal will be produced also in the channel in between those. The number of those ghost events, N_{ghost} is approximately proportional to I^2 ($N_{ghost} = \alpha_{ghost} \cdot I^2$), which means that the tagging efficiency as a function of intensity is

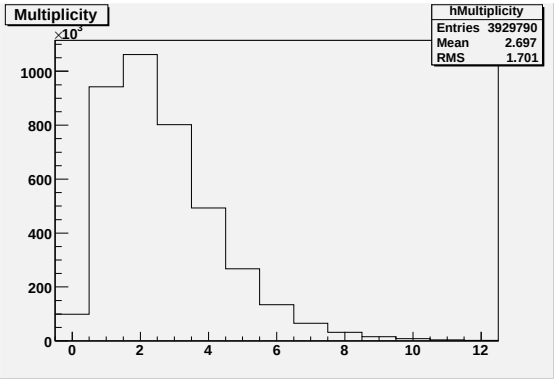

Figure 4.26: *The focal plane multiplicity for the measurement with the highest intensity. The multiplicity is considered being low enough to ignore the possible contribution from ghost events. The events that have zero multiplicity, i.e. no recorded hit in any TDC, which means that it should not have been accepted by the trigger system, are caused by the malfunctioning electronics of channel 57.*

$$\epsilon_{tag}(\bar{I}) = \frac{\alpha_{brems} + \frac{\alpha_{bcg,room,detector}}{\bar{I}}}{\alpha_{brems} + \alpha_{bcg,beam} + \frac{\alpha_{bcg,room}}{\bar{I}} + \alpha_{ghost} \cdot \bar{I}} \tag{4.6}$$

At low intensities, at which tagging efficiency measurements are usually made, the number of ghost events are virtually zero. For measurements at high intensities, the ghost events start to become an issue. However, even for the tagging efficiency measurements at high intensities presented here (that go up to approximately 4% of full intensity), the intensity was considered being low enough that the contribution from ghost events is small enough to be neglected. The motivation for this is the low *focal plane multiplicity*, which is the number of focal plane channels that recorded the presence of a particle, for each event that is read out. The distribution of the multiplicity for the measurement with 5 absorbers is shown in Figure 4.26. Most events have a multiplicity that is below 10. In order to create a ghost event, the events in the two next-neighbour channels must arrive within a time span of only 50 ns. This is just a small fraction of the full TDC-window (which is 1000 ns), and the chance for such coincidence to happen when the multiplicity for the entire TDC-window is below 10 is very small. Hence, no correction for ghost events was made in the tagging efficiency measurements.

However, when the measured tagging efficiency is used in order to calculate the number of photons that were incident on a target during an experiment made at high intensity, the ghost events need to be taken into account. The tagging efficiency is multiplied by the number of counts in every focal plane channel; $N_{photon} = N_{fp} \cdot \epsilon_{tag}$, and to get the correct number of photons, the number of counts in the focal plane channels must be corrected for ghost events.

4.8 Analysis of the Pb-glass Tagging Efficiency Measurements

In order to check the consistency of the measurements with the NaI(Tl) detector with the results from the standard procedure that is used to measure the tagging efficiency, the measurements done with the Pb-glass detector were also analysed. One of the measurement was done at normal tagging efficiency intensity and one was made at an even lower intensity. The standard tagging efficiency measurements are done using either signals from the in-beam detector or the focal plane as the trigger source. The measurements presented here were made with the same trigger system as the measurements with the NaI(Tl), so that the Pb-glass detector provided the triggers and only those events that contained a signal in both hodoscope and in-beam detector were read out.

The raw data from the in-beam detector is shown in Figures 4.27. The efficiency of the Pb-glass detector is good enough that any photon that would leave enough energy to give a signal in the 10"$\times$ 10" NaI(Tl) detector does so in the lead glass detector as well [15], but the resolution is very poor. Figure 4.27 shows the energy spectrum of the events that correspond to a hit in focal plane channel 0 and 61, respectively. The spectrum overflows at around channel 1250, and all events with energies higher than that end up in the same channel. The different positions of the peaks show that the response of the detector is different for photons of different energies, but there would be no possibility to separate the tagged photons from any background. However, this is not necessary since there is virtually no prompt background when the absorbers are not present and the intensity is low.

The only cut that was applied to the data is a restriction on the TDC-values. The TDC-peaks for the measurements with the Pb-glass detector are positioned somewhat differently from the ones from the NaI detector, due to the different delays in the cables from the in-beam detector and/or from the time it takes for the detector to produce a signal. These changes affect the time at which the trigger system opens the TDC gates, which in principle affects all focal plane channels in the same way. Nonetheless, the relative positions of the TDC peaks will change, due to the different conversion gains of the TDC:s. However, in this specific case it turned out that the difference in timing between the outputs of the trigger system for the two different detectors was small enough not to affect the relative positions very much. Therefore, the same offsets as for the measurements with the NaI(Tl) detector were be used in order to align the TDC:s. The only noticeably difference is that the summed peak is now in a different position compared to the NaI(Tl) measurements. The summed and aligned TDC-spectrum is shown in Figure 4.28.

In order to simplify the analysis, the same prompt area was used for all channels. The summed TDC spectrum is shown in Figure 4.28, and the prompt region is shown in red. The fraction of random events inside the prompt TDC peak were estimated using the random region as shown in blue in the figure. The fraction of the two numbers of events was found to be as small as 0.25%. Hence, no attempt to make any correction for random events was made.

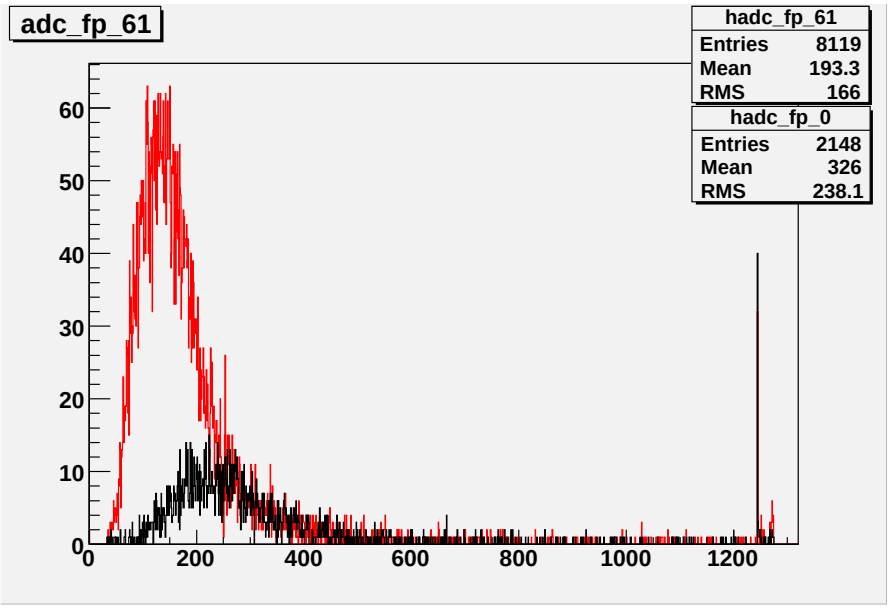

Figure 4.27: *Energy spectra from the Pb-glass detector from two focal plane channels; number 0 (black) and number 61 (red). The spectra show that the response of the detector is different for different energies, but the resolution is too poor to make any conclusion about the actual energy of the incoming events.*

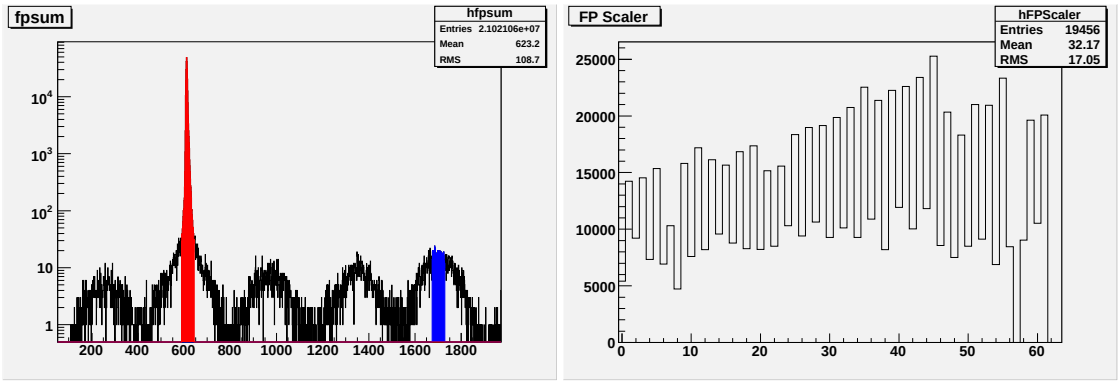

Figure 4.28: *Left: Summed and aligned TDC spectrum from all the channels. The chosen prompt region is shown in red, and the chosen region of random events is shown in blue. The same regions were used for all the channels. The fraction of random events inside the prompt peak was found by dividing the number of events in the random region with all those in the prompt region. This fraction was negligible and no subtraction of random events was made. Right: The number of counts in each of the focal plane scalers. The background in the room was subtracted from the scalers.*

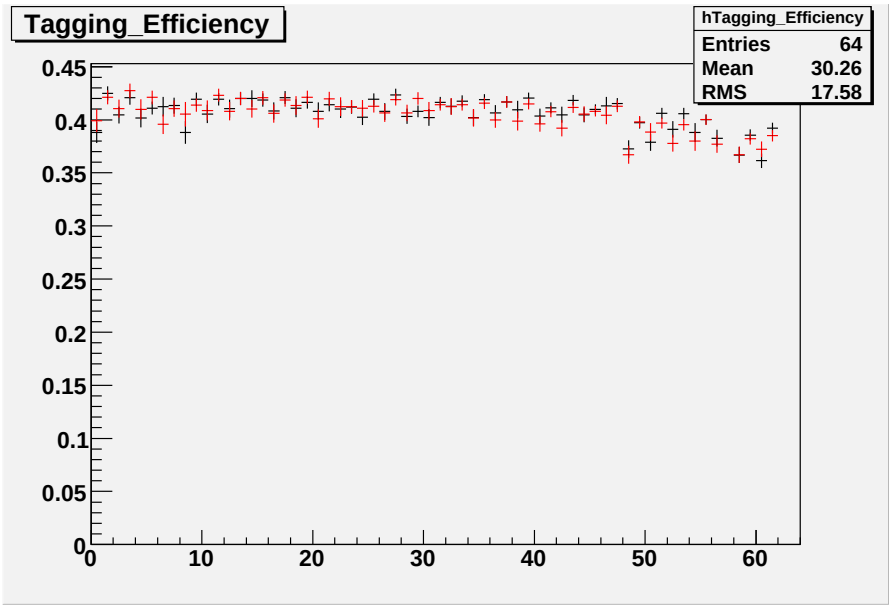

Figure 4.29: *The tagging efficiencies for each channel from the two measurements done with the Pb-glass detector. The black lines represent the measurement done at normal tagging efficiency intensities, while the red lines show the measurement done at a reduced intensity. The agreement between the two measurements is very good. The error bars consist of both statistical and systematic uncertainties.*

The number of counts in the focal planes scalers is shown in Figure 4.28. The background in the room, as seen by the focal plane detector, was measured and subtracted from the focal plane scalers in the same way as described for the NaI measurements. As there is no restriction on the energy of the events, the tagging efficiency is calculated by taking the number of prompt events divided by the number of events, corrected for the background, in the focal plane scalers. The final tagging efficiencies for the two measurements with the Pb-glass detector, the one at normal intensity and the one at reduced intensity, are shown in Figure 4.29.

The tagging efficiencies for the Pb-glass measurements take into account all the photons that reach the detector, whereas the calculations for the measurements with the NaI(Tl) are restricted to just a fraction of the photons. This fraction is a function of energy, and is thus not the same throughout the focal plane. The fraction was determined for each of the channels by dividing the number of events inside the chosen full-energy region with the total number of events recorded during the reference measurement. The tagging efficiency from each channel from the Pb-glass measurements was rescaled with the corresponding factor before the average tagging efficiency was calculated. In Figure 4.30, the rescaled average tagging efficiencies from the Pb-glass measurements are shown. The Pb-glass measurements agree very well. This shows that the tagging efficiency does not change over the factor of ten in intensity that differs between the measurements, which is a strong indication on the tagging efficiency not being intensity-dependent.

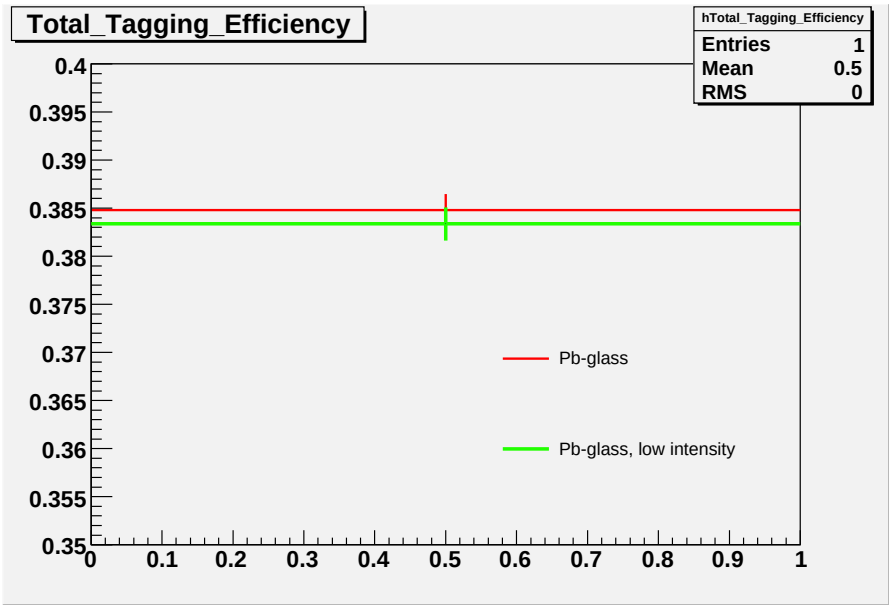

Figure 4.30: *The average tagging efficiencies from the two measurements made with the Pb-glass detector, rescaled so that they now represents the same fraction of the full tagging efficiency as was chosen for the measurements with the NaI(Tl) detector. The two Pb-glass detector measurements agree very well, which shows that the tagging efficiency does not change when the intensity is decreased by a factor of about ten from ordinary tagging efficiency intensities.*

Chapter 5

Results

Low-intensity measurements

The result of the analysis of all the tagging efficiency measurements made at low intensity and/or without any absorbers is shown in Figure 5.1. The data point showing the highest tagging efficiency is from the first measurement that was done with the NaI(Tl) detector. The analysis of this measurement suffered from some unexplained deviations as compared to the rest of the NaI measurements; both the TDC peak and the energy peak were positioned differently than the rest of the peaks. Therefore, this measurement will not be considered further.

The lowest tagging efficiency is from the low-intensity measurement that was done in the middle of the experiment, and that has been used throughout the analysis as the reference. This measurement was used when, for example, the limits for the prompt region and for the energy region were set. The measurement with the slightly higher tagging efficiency than the reference was made at the end of the experiment. The very small discrepancy between the two measurements, which is covered by the error bars, indicate that there was no deviation in the tagging efficiency between these two measurements. All the high-intensity measurements were done in conjunction with these two measurements, and therefore they will serve as the standard to which the other measurements will be compared.

The two measurements done with the Pb-glass detector show a very good agreement, which shows that the tagging efficiency does not vary over the factor of ten in intensity which separates the two measurements. This is in itself a clear indication on the tagging efficiency not being intensity dependent. These two measurements have tagging efficiencies that are somewhat higher than the ones from the NaI(Tl) measurements. A possible explanation for this could be that maybe the beam-induced background suffered from a small change at some point during the experiment. An indication for this is that a check on the beam-induced background (estimated from the count rates when the radiator is in and then it is taken out) that was made in the end of the experiment, gave a somewhat higher value than usual.

The measurement that gives a tagging efficiency that ends up in between the two references (shown in red) is made at ordinary tagging efficiency intensities, but with one absorber inserted. This measurement differs from the other two measurements only in that one absorber is present, and the fact that it coincides well with the other two indicates that the change in the setup does not have any unexpected impact on the

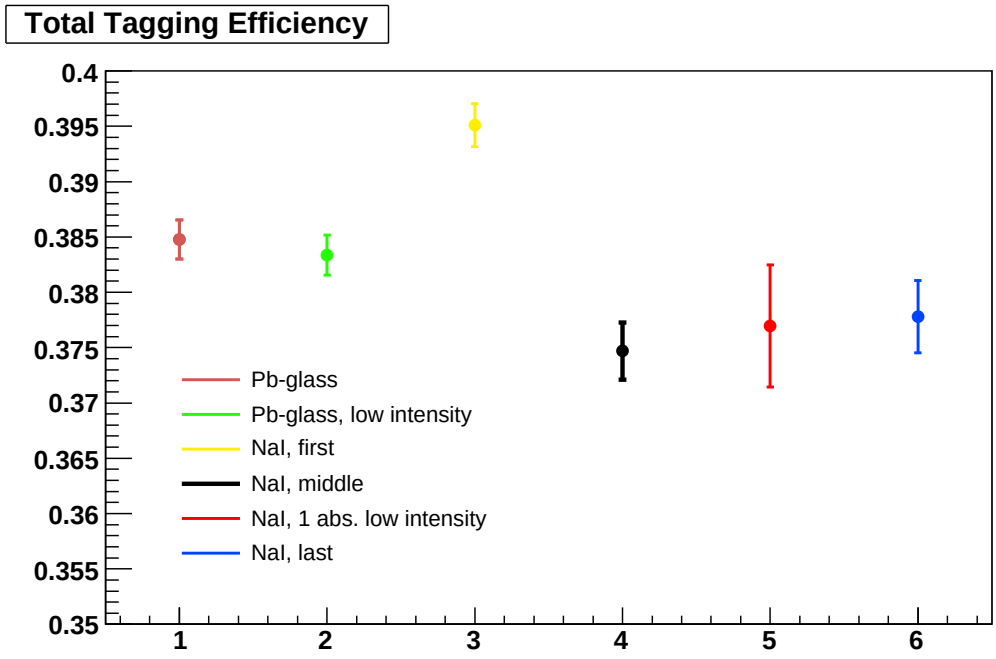

Figure 5.1: *Average tagging efficiencies for all the measurements done at low intensity and/or without absorbers. The measurements are presented in chronological order. The first NaI(Tl) reference measurement (red), which has a much larger tagging efficiency than the other ones, was discarded due to the strange features that were discovered during the analysis. The two other reference NaI(Tl) measurements agree well. The measurement with one absorber shows that the insertion of an absorber does not change the tagging efficiency or the experimental situation. The reason why the Pb-glass measurements do not agree with the ones from the NaI(Tl) could be due to a small variation in the beam-induced background.*

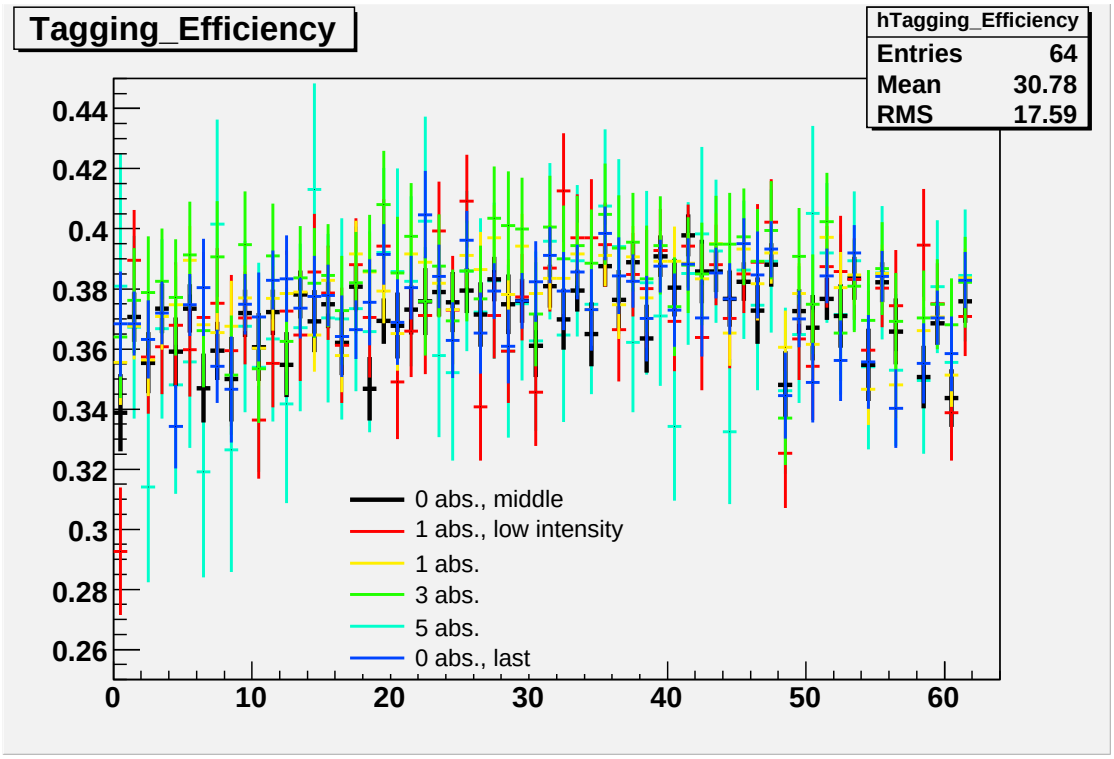

Figure 5.2: *The final tagging efficiencies for each of the focal plane channels for the measurements from the NaI(Tl) detector. The uncertainties are large due to the poor statistics. There is no clear trend to be seen in the figure, and all the values seem to be mixed without any order. This is very good, as the absence of any order implies that the tagging efficiency does not depend on the intensity.*

experimental situation.

Comparison of measurements done at various intensities

Figure 5.2 shows the tagging efficiencies for all focal plane channels for all the measurements done with the NaI(Tl) detector, except for the discarded low-intensity measurement. The figure shows that all the tagging efficiencies are in approximately the same region, and there is no indication of an intensity-dependent behaviour of the tagging efficiency. The only measurement which seems to differ is the one with 3 absorbers. The tagging efficiencies for this measurement seem to be a little higher than the rest of the measurements, which are mixed together seemingly without any specific order.

The general trend of the tagging efficiencies over the focal plane is a horisontal line, but there are local variations between the channels. These variations are to some extent a result of the poor statistics. The error bars are large, in particular for the measurements with the highest intensities. Especially the measurement done with 5 absorbers has tagging efficiencies that vary over a large region, which is a consequence of the low number of counts that the values are based on.

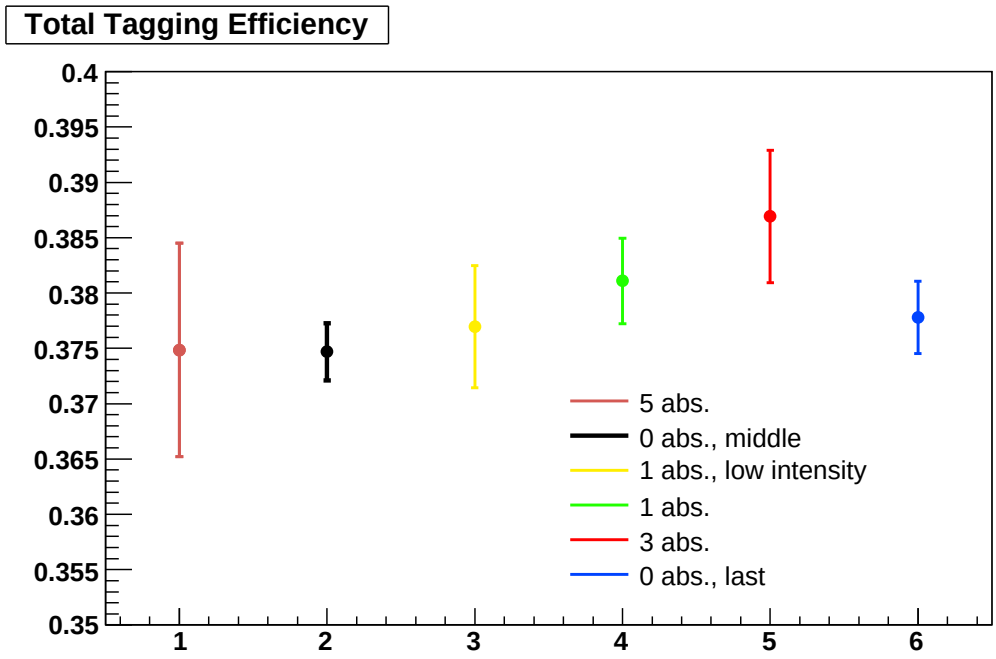

Figure 5.3: *Average tagging efficiencies for the same measurements as in the previous figure (5.2). The measurements are presented in chronological order. The statistic errors are much smaller than for the individual channels. Note that the scale is different from the previous figure. The fraction between the highest and lowest tagging efficiency is 1.03.*

Comparison of average tagging efficiencies for various intensities

In order to improve on the statistics, and to get a clearer picture, the weighted average tagging efficiency for each of the measurements was calculated, as well as the statistical and systematic errors for those values. The result is shown in Figure 5.3. As a consequence of the improved statistics, the error bars are also much smaller for the average values. The two measurements without absorbers define the standard to which the measurements at higher intensities should be compared. The measurement with the highest intensity falls between these two measurements, as well as the measurement done with one absorber, at ordinary tagging efficiency intensity. The measurement with three absorbers is a little too high, which could be seen already in the previous figure. The next measurement with 1 absorber also gives a tagging efficiency that is a little too high, but it agrees within error bars with both of the low-intensity measurements.

Even if the measurement with 3 absorbers gives a tagging efficiency that is a little higher than the other measurements, it still agrees within error bars with last reference measurement. Therefore the higher tagging efficiency for the measurement with 3 absorbers does not imply that the tagging efficiency varies with intensity. The most important indication on the tagging efficiency not depending on intensity is that the values for the measurement do not end up in an order that coincides with the increase in intensity. Starting from the three measurements done at ordinary intensity (the two

without absorbers, and the first one with 1 absorber), the tagging efficiency goes up a little with the first two increases and then down again for the measurement with the highest intensity.

The largest discrepancy between the average tagging efficiencies is between the reference measurement, made in the middle of the experiment, and the measurement with three absorbers. The fraction of the these two average tagging efficiencies is 1.03. The measurements presented here cover three orders of magnitude in intensity, ranging from ordinary tagging efficiency intensities up to 4% of full intensity, and there is no indication of an intensity dependence over this span. Therefore, it seems reasonable to conclude that the systematic uncertainty that should be ascribed to the tagging efficiency due to the extrapolation that is made when measuring the factor at low intensities and then using this to describe the high-intensity situation, is at most a few percent.

Chapter 6

Summary and Conclusions

The analysis of the experiment done in September 2007, which consisted of measuring the tagging efficiency at various intensities, shows that the tagging efficiency does not depend on the intensity of the electron beam. The measurements were done at intensities that cover more than three orders of magnitude. The first two were done with the Pb-glass detector that is commonly used for measuring the tagging efficiency at MAX-lab. The intensities that were examined with this detector included ordinary tagging efficiency intensities and about one tenth of this, and the results agreed well.

The NaI(Tl) was used to go in the other direction and increase the intensity. Measurements at intensities that cover three orders of magnitude, ranging up to $\sim$4% of full intensity, were made. The tagging efficiencies for these measurements contained large statistical errors and therefore large local variations over the focal plane, so the average tagging efficiencies were calculated in order to get values that are more reliable and easier to compare. All measurements but the one with three absorbers, agreed within error bars with both of the two reference measurements made at low intensity. The measurement with three absorbers agrees within error bars with one of the reference measurements. The largest discrepancy between the measured average tagging efficiencies was 3%.

The results imply that the tagging efficiency does not depend on the intensity of the electron beam, and that the upper limit to the systematic uncertainty in measuring the tagging efficiency at low intensities should be no more than a few percent. This is an important result for the MAX-lab photonuclear facility, since it means that that tagging efficiency can be measured at low intensities and extrapolated without introducing any large systematic uncertainties into the experiments. Since the absolute cross sections that are measured at the facility are directly proportional to the tagging efficiency, the total uncertainty can never be less than the uncertainty in this factor. Therefore, the uncertainty needs to be small, and a good estimate of the uncertainty is needed.

The fact that the tagging efficiency measurement can be done at low intensities also makes the experimental situation easier. Not only is it an easier process not having to insert the absorbers every time, but is also saves a lot of time. In order to get the wanted statistics, the measurements done at high intensity have to be run for a much longer time, and it would not be possible to use several hours per day to measure the tagging efficiency. Measuring the tagging efficiency at low intensity also allows for a much easier analysis; only the steps explained in section 4.8 need to be performed, as opposed to the entire analysis that is described in this thesis.

The largest problem in the measurements presented here is the poor statistics. With a larger number of counts, especially for the measurements at high intensities, the uncertainties would be smaller. Possibly, the discrepancy between the measurements could then have been determined to be even smaller than 3%. Another thing which could have been done differently would be to perform reference measurements between every high-intensity measurement. For this experiment, the first reference measurement had to be discarded, and it would have been good to have several reference measurements as a consistency check. The data set analysed here contained two more reference measurements, which made it possible to perform the analysis in a satisfactory way anyhow, but nonetheless it would be an improvement to have even more reference measurements.

Bibliography

[1] MAX-lab - the bright link to microcosm. MAX-lab.

[2] Bengt-Erik Andersson. *Experiments in Light Nuclei at $E_\gamma \simeq 60MeV$*. PhD thesis, Lund University, 1994.

[3] Kevin Fissum. *Inclusive Photoproduction of Positive Pions*. PhD thesis, University of Saskatchewan, 1993.

[4] D. Häger et al. Elastic scattering of 58 and 75 mev photons by ^{12}C and ^{16}O and electromagnetic polarizabilities of the bound nucleon. *Nuclear Physics A*, 595:287–306, 1995.

[5] Kurt Hansen. Private communication, November 2009.

[6] Anders Hansson. Deeply bound pionic atoms from the (γ, p) reaction. Master's thesis, Lund University, 2006.

[7] E. Hisdal. Bremsstrahlung spectra corrected for multiple scattering in the target. *Physical Review*, 105(6):1821–1826, March 1956.

[8] Lennart Isaksson. Private communication, January 2010.

[9] H. W Koch and J. W. Motz. Bremsstrahlung cross-section formulas and related data. *Reviews of Modern Physics*, 31(4):920–956, October 1959.

[10] Per Lilja. Private communication, November 2009.

[11] L.-J. Lindgren. Pulse stretcher upgrade. *Nuclear Instruments and Methods in Physics Research A*, 492:299–304, 2002.

[12] Magnus Lundin. *Compton Scattering from the Deuteron at Low Energies*. PhD thesis, Lund University, 2002.

[13] The Magnetic Spectrometer Workshop, Williamsburg, VA. *Photon Tagging - Present Practice and Future Prospect*, October 1983.

[14] J. L. Matthews and R. O. Owens. Accurate formulae for the calculation of high energy electron bremsstrahlung spectra. *Nuclear Instruments and Methods*, 111:157–168, 1973.

[15] Luke Myers. Private communication, December 2009.

[16] National Institute of Standards and Technology. www.nist.gov.

[17] William R.Leo. *Techniques for Nuclear and Particle Physics Experiments*. Springer-Verlag, second revised edition, 1994.

[18] root.cern.ch.

[19] A. Sirlin. Angular distribution of betatron target radiation. *The Physical Review*, 101(4):1219–1226, February 1956.

[20] J.M. Vogt et al. The photon tagging facility at the Saskatchewan Accelerator Laboratory. *Nuclear Instruments and Methods in Physics Research*, A324:198–208, 1993.

Appendix A

Attenuation Coefficients

Table A.1: *Photon energy and attenuation coefficient for each of the focal plane channels*

Focal plane channel	**Photon energy**	**Attenuation coefficient** ($\cdot 10^{-4} cm^2/g$)
1	84.32	903
2	83.89	902
3	83.46	901
4	83.02	900
5	82.59	899
6	82.14	898
7	81.70	897
8	81.26	896
9	80.81	895
10	80.36	894
11	79.91	893
12	79.45	892
13	78.99	891
14	78.53	890
15	78.07	889
16	77.61	888
17	77.14	887
18	76.68	886
19	76.20	885
20	75.73	884
21	75.26	883
22	74.78	881
23	74.30	880
24	73.82	879
25	73.33	878
26	72.84	877
27	72.35	876
28	71.86	874

Continued on next page

Table A.1 – continued from previous page

Focal plane channel	Photon energy	Attenuation coefficient ($\cdot 10^{-4} cm^2/g$)
29	71.37	873
30	70.87	872
31	70.38	870
32	69.88	869
33	69.37	868
34	68.87	867
35	68.36	865
36	67.85	864
37	67.34	862
38	66.83	861
39	66.32	860
40	65.80	858
41	65.28	857
42	64.77	855
43	64.24	854
44	63.72	852
45	63.20	851
46	62.68	849
47	62.15	847
48	61.62	846
49	61.10	844
50	60.57	843
51	60.04	841
52	59.51	839
53	58.98	838
54	58.45	836
55	57.92	834
56	57.39	832
57	56.86	831
58	56.33	829
59	55.80	827
60	55.28	825
61	54.75	823
62	54.22	821

Appendix B

Different Choices of Energy Region

To check if the limits that define the accepted energy region are chosen in a good way, two other regions were also defined in order to make a comparison. Figure B.1 shows the tagging efficiencies that result from the main analysis. Figure B.2 shows the tagging efficiencies that result from an energy region that is 300 channels wide, as compared to 250 which was used for the analysis. As expected, the tagging efficiencies are higher now, as there are more events in the larger region. An interesting feature of the picture is that the tagging efficiency of the measurement with 5 absorbers increases more than the rest of the measurements. This indicates that a fraction of the background events are included in this region, and this energy region is inappropriately large.

Figure B.3 shows the tagging efficiencies from an energy region that is 200 channels wide. The relative tagging efficiencies from this region are very similar to those from the region that is 250 channels wide. A change in the energy region of 50 channels would result in a change in the relative tagging efficiencies if either of the regions had extended into the background, since the background that is present only in the high-intensity measurement would cause a relative shift in the high intensity measurement compared to the measurements made at low intensities. The fact that the two different limits give relative tagging efficiencies that are very similar indicates that none, or at least only very little, of the low-energy background is included in any of these two regions. This means that the chosen energy region, with a width of 250 channels, is a good choice.

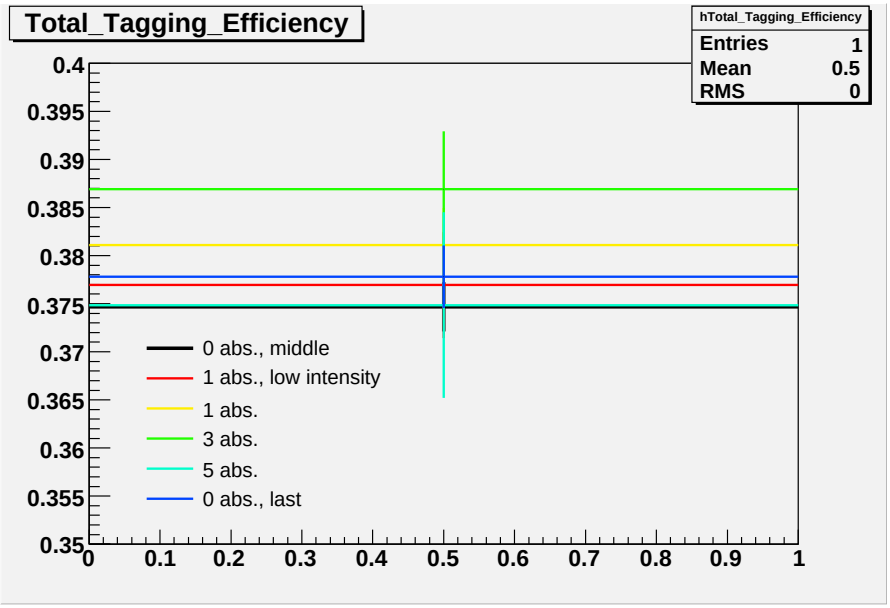

Figure B.1: *Average tagging efficiencies for the measurements made with the NaI(Tl) from the main analysis. The picture shows the same as Figure 5.3, just displayed differently. The widths of the individual full-energy regions are 250 channels.*

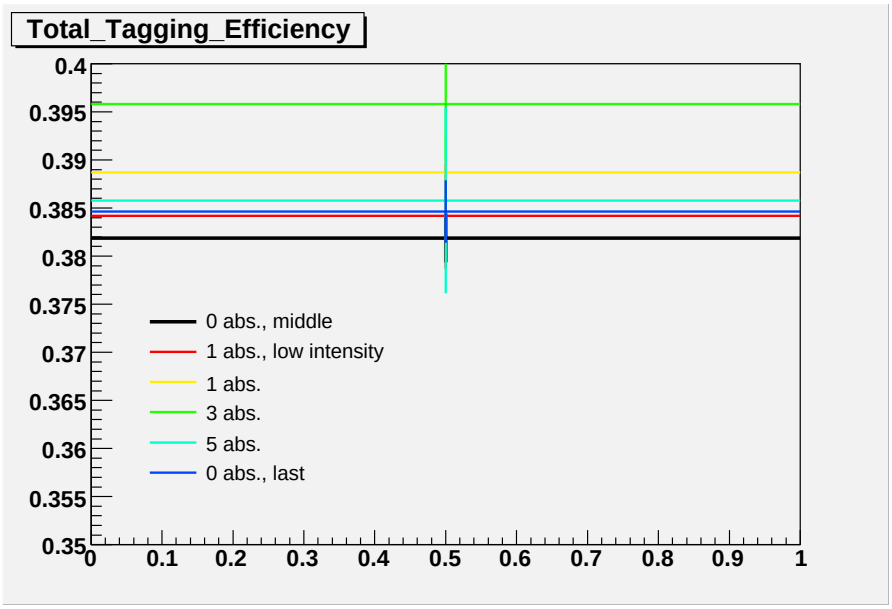

Figure B.2: *Average tagging efficiencies for the measurements made with the NaI(Tl). The energy region is set to be 300 channels wide instead of 250, as was chosen for the analysis. The relative position of the values is somewhat different from when a width of 250 channels is used. This indicates that the wider region stretches into the background.*

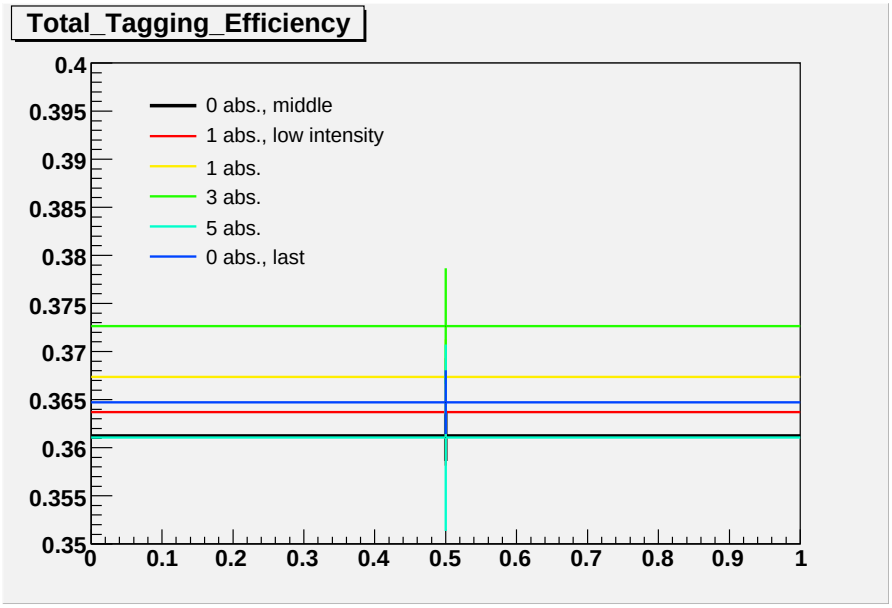

Figure B.3: *Average tagging efficiencies for the measurements with NaI(Tl), but with an energy region that is 200 channels. The relative positions of the values is the same as when a width of 250 channels is used. This shows that there is no, or very little, background included in any of the regions.*